Recent Advances in Green Synthesis, Chemical-Physics Characterizations, and Biological Adeptness of Selenium and Silver Nanoparticles for Medical Application

Iman Amer Mohammed Ali
Ali Ben Ahmed

DeepScience

Recent Advances in Green Synthesis, Chemical-Physics Characterizations, and Biological Adeptness of Selenium and Silver Nanoparticles for Medical Application

Iman Amer Mohammed Ali

Ministry of Higher Education and Scientific Research, Baghdad , Iraq

Ali Ben Ahmed

Higher Institute of Biotechnology of Sfax , Sfax ,Tunisia

DeepScience

Published, marketed, and distributed by:

Deep Science Publishing
USA | UK | India | Turkey
Reg. No. MH-33-0523625
www.deepscienceresearch.com
editor@deepscienceresearch.com
WhatsApp: +91 7977171947

ISBN: 978-93-49307-55-1

E-ISBN: 978-93-49307-47-6

https://doi.org/10.70593/978-93-49307-47-6

Citation: Ali, I. A. M., & Ben, A. A. (2025). *Recent Advances in Green Synthesis, Chemical-Physics Characterizations, and Biological Adeptness of Selenium and Silver Nanoparticles for Medical Application*. Deep Science Publishing. https://doi.org/10.70593/978-93-49307-47-6

Preface

This book offers a comprehensive exploration of the evolving landscape of the preparation and evaluation of stable selenium nanoparticles (Se NPs) and silver nanoparticles (Ag NPs). The synthesis was done using the fast green method, which is environmentally friendly, and the selected physical factors such as temperatures and by using an aqueous solution of Withenia somanifera roots and garlic fruits, respectively, as a reducing and stabilizing agent for nanoparticles. The studied evaluation was confirmed using different techniques including X-Ray Diffraction Studies, FESEM - EDS analysis, Transmission electron microscopy analysis, Atomic Force Microscope analysis, Dynamic Light Scattering, Zeta Potential Measurement, and Optical Properties.

In this study, the role of nanoparticles in Improvement of physiological characteristics on diabetic rats by streptozotocin. The results indicated the effective role of Se NPs and Ag NPs for diabetes patients through a significant decrease in the percentage of high and medium damage in the group treated with nanoparticles compared to the rest of the groups, with an increase in the number of healthy sperm and a decrease in the number of deaths resulting from abnormalities and weakness resulting from diabetes. It begins with a detailed overview of nanomaterials and their modern biomedical applications in Chapters 1–3. In chapter 4 a presentation and interpretations of the results obtained. This book ends with a general conclusion.

Dr. Iman Amer Mohammed Ali
Prof. Dr. Ali Ben Ahmed

Contents

List of Abbreviations

1D…….One Dimension
2D…….Two Dimension
3D…….Three Dimension
AFM….. Atomic Force Microscope
Ag NPs….. Silver Nanoparticles
ALP…… Alkaline phosphatase
ALT…… Alanine transaminase
AST…….. Aspartate transaminase
CNT…… Carbon Nano Tubes
CVD…… Chemical Vapor Deposition
DIW…… Deionized water
DLS…… Dynamic light scattering
DMA……. Differential Mobility Analysis
DNA….. Deoxyribonucleic acid
EDTA… Ethylene diamine tetra etic Acid
EDX….. Energy-dispersive X-ray
ELISA….. Enzyme-Linked Immunosorbent Assay
FE-SEM…… field emission scanning electron microscope
FT-IR….. Fourier infrared Spectroscopy
FWHM……. Full Width at Half Maximum
LH….. Luteinizing Hormone
MDA…… Malondialdehyde
MIU/ml….. Millie-international units per milliliter
Mg/dL. …… Milligrams per deciliter
µl….. Microliter
Ng/ml …….. Nano gram per Milliliter (mL)
NMR…… Nuclear Magnetic Resonance
No……. Number
OD……Zero Dimension
PBS …… Phosphate-Buffered Saline
Pg/ml ……. Pico gram per milliliter
RNA…….. Ribonucleic acid
Rpm…… Revolutions per minute
SCGE…… single-cell gel electrophoresis
SCGE……. Single Cell Gel Electrophoresis
Se NPs…. Selenium Nanoparticles AgNO3
SOD…….. Superoxide Dismutase's
STZ… Streptozotocin

TEM…… Transmission electron microscopy
U/L…… Units per litre
U/mg….. Unit per Milligram
UV …. UV-vis spectra analysis
XRD…… X-Ray Diffraction

Deep Science Publishing
https://doi.org/10.70593/978-93-49307-47-6

DeepScience
Open Access Books

Introduction

Nanotechnology is an important field that focuses on the precise arrangement of matter at a dimension less than micrometers (Stoimenov et al., 2002; Neuberger et al., 2005; Iqbal et al., 2019). Presented by Richard B. Feynman coined the term & quot; nanotechnology quot; through his famous speech " There is plenty of room at the bottom" (1959) (Szabó & Schlabach, 2014). The importance of nanotechnology arose from modifications in the chemical and physical properties of materials and their energy at the nanoscale (1-100 nanometers). Considering this, the discipline takes intoaccount the formation of new functional systems, materials, and devices at themolecular and atomic scales (Neuberger et al., 2005). Nanoparticles fall into several classes. Depending on the shape, nanoparticles can be 0D, 1D, 2D and 3D (Lv et al., 2021; Busatto & de Mello Donega, 2022). The researchers realized the importance of these nanoparticles when they discovered that size has an affect on the chemical and physical characteristics of materials, such as optical properties, morphology and shape of nanoparticles. These properties can classify nanoparticles into different classes and three layers. (Hano & Abbasi, 2021; Hu & Yang, 2022).

Some of the most important classes of nanoparticles are discussed every day, and new strategies are being developed for their creation (Gul et al., 2021). Biological methods, physical methods, and chemical methods are the three basic groups of these strategies. Physical and biological methods are ideal for nanoparticle production because they are simple, harmless and cost-effective, while chemical methods for nanoparticle production are used highly hazardous and toxic compounds which may cause various environmental and health damages. In addition, chemical procedures use expensive reducing or covering agents. The price is unlike other methods. As a result, the biophysical technique is the most preferred method for nanoparticle fabrication (Hano & Abbasi, 2021). Nanotechnology has been used for a wide range of applications and a variety of materials have been created. One of the greatest applications of nanotechnology is medicine. It helps in solving a variety of erectile dysfunction diseases prevalent in the world. At present, major causes of male infertility have been reported worldwide, including sperm defects and abnormalities, insufficient numbers caused by azoospermia or oligospermia, as well as poor motility and structure (abnormal morphology). (Abarikwu, 2013; Sengupta et al., 2017). Many Studies have shown a decrease in the number of sperm over the past decades (Sharma, 2017; Sharma, 2017).

which put the male factor as the main contributor to the increased prevalence of infertility worldwide (World Health Organization, 2021). In addition, male infertility has been described as a form of infertility that does not respond well to initial treatment. The World Health Organization has therefore worked to review standards for normal and abnormal sperm counts for use in andrology laboratories around the world (Ombelet & Van Robays, 2015)

Secondary measures, such as artificial insemination (Abdelkader & Yeh, 2009) intrauterine insemination (Iketubosin, 2018) in vitro fertilization and embryo transfer (Allouche, 2013) intracytoplasmic sperm transfer, a treatment for infertility. The environment and the use of less expensive treatments. A new technology has recently been developed focusing on metals where nanoparticles have been synthesized and low toxicity has been reported in. The resulting nanoparticles, a green synthesis technology (Singh et al., 2020). The green approach to the 12 synthesis of metal nanoparticles side by side is associated with the use of a several of natural plants. The obtained nanoparticles are environmentally friendly, biocompatible and harmless (Khan et al., 2019; Umar et al., 2019). Thesis the nanoparticles were prepared using the green synthesis method, and the important properties of nanoparticles and nano-phenomena were studied, which include quantum restriction, which in turn leads to new electromagnetic and optical phenomena of matter and surface plasmon resonance, and studying the toxicity of nanoparticles on living cells inside the body, and the effect of nanoparticles On diabetic organism (mice) sperm, and finally single-cell electrolyte (SCGE), called the comet assay, is a rapid and sensitive method that can be used to analyze the RNA damage that was first described. The fundamental idea is that during agarose gel electrolysis, DNA fragments of various lengths travel in distinct ways. It is a method for analyzing RNA damage that was initially described (Bouqellah et al., 2019; May et al., 2022). The basic premise is that in agarose gel electrolysis, DNA pieces of different lengths move differently (Khan et al., 2020; Tariq et al., 2022).

Deep Science Publishing
https://doi.org/10.70593/978-93-49307-47-6

Chapter 1

Literature review

Recently, metal nanoparticles have anti-impotence activities caused by diabetes and other diseases have been demonstrated in several studies. These studies were presented. The importance of nanoparticles through their large surface area, high surface-to-volume ratio and many other attractive features. Hence, recent developments of both Ag NPs and Se NPs nanoparticles for their therapeutic activity are reported in the following subsections.

1.1. Silver Nanoparticles (Ag NPs)

Bouqellah et al. 2019: Allium cepa and Allium sativa plants were utilized in this study to assess the potential synthesis of silver nanoparticles and their antibacterial impact on Streptococcus pneumoniae and Pseudomonas aeruginosa. The morphology of nanoparticles extracted from plant extracts was studied using transmission electron microscopy (TEM). Using energy-dispersive X-ray spectroscopy (EDX), they discovered the elemental sign of silver and the homogeneity of silver nanoparticles . The presence of diffraction in the structure of spherical and cubic shapes with varied levels ranging from (111) to (311) planes was also demonstrated in the study using X-ray analysis (XRD). Ag NPs have also been shown to have antibacterial properties against vaginal infections, Streptococcus pneumoniae, and Pseudomonas aeruginosa. This study found that the synthesis of Ag NPs from extracts of Allium cepa and Allium sativa is quick, ecologically friendly, and acceptable for biomedical applications (Kazmi et al., 2021).

Khan et al. 2020: Several methods were used to make gold (Au) and silver (Ag) nanoparticles (NPs) in this work. The researcher created gold (CI-Au) and silver (CI-Ag) capped with medicinally active functional groups of Clerodendrum inerme leaf extract (C. inerme) as a reducing and covering agent. The antibacterial and antifungal properties of the produced NPs were tested against a variety of harmful microorganisms (B. subtilis, S. aureus, Klebsiella, E. coli) and (A. niger, T. harzianum, A. flavus). In terms of percent DPPH scavenging, CI-Au and CI-Ag NPs were shown to have significantly more antioxidants (75.85 percent 0.67 percent and 78.87 percent 0.19

percent, respectively). When compared to commercial Au cells and Ag NPs working with dodecanethiol and PVP, they demonstrated superior antibacterial, antibacterial, biofilm, and cytotoxic performance against pathogenic germs and MCF-7 cells (Shehata et al., 2021)

Mazhir et al. 2021: Have been synthesized Silver nanoparticles (Ag NPs) by mixing Origanum Vulgar with silver nitrate ($AgNO_3$) A second extract that can be employed in therapy is part of the NPs of cold plasma. UV spectroscopy, FE-SEM, FT-IR, and AFM were used to investigate factors such as size and form characteristics, plasmodium surface, structure, and optical qualities. The average particle size distribution in $(Ag\ NPs)_1$ was (44.2 - 88.1) nm, while the average particle size distribution in $(Ag\ NPs)_2$ was (44.2 - 86.1) nm. In the presence of NPs, the results demonstrated that NPs were efficient in suppressing human pathogens1. Because of a combination in the chemical after exposure to plasma energy, the inhibitory efficacy of $(NPs)_1$ was determined to be superior than $(NPs)_2$. The results also revealed that NPs responded differently depending on the dosage concentration applied to L20B tumor cell lines. Antioxidants were discovered in all cell types. In addition, the damage rate in the DNA of L20B tumor cells was measured. After exposure, the rate of DNA damage in cancer cells rose. The findings revealed that NPs placed on live cell lines produced superior results than the control group (Bruna et al., 2021).

Shafea et al. 2021: Have been successfully a green synthesis silver nanoparticles, Ag NPs, using *garlic* extract. Absorption spectroscopy, the Fourier Transform Infrared Spectrometry (FTIR) and X-ray Diffraction (X-Ray) tests have been used to study the characteristics of silver nanoparticles. The antibacterial properties of the produced nanoparticles were studied. It was discovered that the *garlic* extract inhibits the growth of three bacteria (Micrococcus sp. eruginosa and Candida albicans). This preparation was found to be safe, quick, and effective against germs and fungus (Shantkriti et al., 2023).

Kazmi et al. 2021: Have been established, the antagonistic efficacy of minocycline-modified silver nanoparticles (Mino/Ag NPs) against alloxan-induced diabetic mice. The antioxidant capacity of the newly synthesized Mino/Ag NPs was determined using the 2,2-diphenyl-1-picrylhydrazyl free free radical scavenging assay. In comparison to minocycline (IC = 26.0 g/ml) and ascorbic acid (IC = 25.2 g/ml), Mino/Ag NPs values demonstrated stronger radical scavenging activity (IC = 19.7 g/ml). Mino/Ag NPs have also been utilized to test their anti-diabetic potential in diabetic mice caused by alloxan. In comparison to the untreated diabetic group, mice treated with Mino/Ag NPs demonstrated a significant reduction in fasting blood glucose and lipid profile (Fadl et al., 2023).

Shehata et al. 2021: Have been investigated the negative impacts of Ag-NPs (50 nm) on the male reproductive system, as well as the beneficial benefits of Zn-NPs (100 nm) on these negative effects. For 90 days, Ag-NPs (50 mg/kg) and/or Zn-NPs (30 mg/kg) were given orally. The findings revealed that Ag-NPs had a deleterious impact on sperm motility, oxidative stress, and lipid peroxidation. in the tissue of the testes Exposure to Ag-NPs resulted in lower levels of FSH, LH, and testosterone in the blood. DNA degradation was discovered in the testicular tissues of mice exposed to Ag-NPs in a comet study experiment. Histological alterations in the testes of mice infused with Ag-NPs were discovered through several histopathological examinations (Vahdati & Tohidi Moghadam, 2020).

Bruna et al. 2021: Have been studied, the parameters influencing silver nanoparticles' antibacterial and cytotoxic effects were discovered, and the benefits of combining Ag NPs with antibiotics as a new antibacterial agent were also shown. (Ag NPs) has been hypothesized as an effective antimicrobial agent capable of fighting bacteria that cause inflammation in vitro and the living organism. Both Gram-negative and Gram-positive bacteria, including multidrug-resistant strains, are susceptible to Ag NPs' antibacterial properties. When combined with other antibacterial agents such as chemical compounds or antibiotics, Ag NPs have demonstrated a synergistic impact against harmful bacteria including Escherichia coli and Staphylococcus aureus. Due to their ability to effectively treat or prevent infections, silver nanoparticles are well-suited for use in medical and healthcare products. A new generation of potent antibacterial medications is urgently needed (Pyrzynska & Sentkowska, 2021)

Shantkriti, S., et al. 2023: Have been created Silver nanoparticles from the aqueous extract of microalgae of the type Dunaliclla Salina, and spectroscopy UV-Vis was used to analyze and characterize the silver nanoparticles, where the absorption peak was at a wavelength of 454 nm, and using SEM-EDX, to verfy the existence of nanoparticles and the size of 35 nm, and an XRD and FTIR examinations were carried out to study the functional aggregates that were synthesized. It was found that the silver nanoparticles synthesized from microalgae have an effective antibacterial role (Khanna et al., 2022).

Fadl, et al. 2023: Have been evaluated, silver nanoparticles on the fertility of male albino mice. They delivered silver nanoparticles orally for 35 days at doses of 62.5 mg/kg/d and 125 mg/kg/d, respectively. The results confirmed the toxic effect of silver nanoparticles on male mice, which led to Infertility by reducing the number of sperms and increasing abnormalities and abnormalities in the group of other sperms (Othman et al., 2022).

1.2. Selenium Nanoparticles (Se NPs)

(Vahdati et al.,2020) : The antibacterial activity of selenium nanoparticles and lysozyme is reported in this study. While very high protein concentrations are required to stop individual bacterial growth, selenium nanoparticles have a significant effect in preventing bacterial growth at very low protein concentrations. The antibacterial property of selenium nanoparticles, on the other hand, was greatly influenced by lysozyme and resulted in 100% inhibition of each component at relatively low concentrations. The nanohybrid system experienced a biological reaction as a result of the coexistence of biological and nano isotopes. The Se NPs were well-stabilized in both their complete and complex forms in the historical samples. The outcomes of this endeavor include the development of nanohybrid systems with complementary antibacterial capabilities to combat the emergence of antibiotic resistance as well as to uncover useful applications in (Alhazza et al., 2022).

Pyrzynska et al. 2021: In this review They were illustrated that the recent research reports explaining the ability of different plant active substances to biosynthesis of Se NPs are presented. The most important conditions or factors involved in the synthesis were discussed, including temperature, time, selenium precursors, the concentration of the plant extract used and others. This is in conjunction with the most important characteristics that characterize the product obtained from composition, size, shape, and stability. The Medical application of synthesized selenium nanoparticles is briefly presented (Shahbaz et al., 2023).

Khanna et al. 2022: In this study, discussed the many synthetic processes used to prepare Se NPs as well as their applications in the biomedical area, such as the treatment of fungal, bacterial, and parasite infections, cancer, and diabetes. Nanoparticles have also been employed as chemoprevention, anti-inflammatory, and antioxidant agents (Salem, 2022).

Othman et al. 2022: In this study, Se NPs-Ber treatment resulted in a higher survival rate, as well as a reduction in body weight and tumor volume, when compared to the EST group. Se NPs-Ber was also discovered to diminish oxidative stress in tumor tissues. Se NPs-Ber also stimulated the apoptotic cascade in cancer cells by lowering B-cell lymphoma 2 (Bcl-2) expression and modulating Bcl-2-related X protein and caspase-3 production rates in cancer cells. In comparison to the EST group, Se NPs -Ber considerably improved histological alterations in advanced tumor tissues (Shahbaz et al., 2023).

Alhazza et al. 2022: In this study, the effects of Se NPs on kidney injury in streptococcus-induced diabetic mellitus in pregnant (DDP) mice were examined in this work. In

comparison to control mice, diabetic mice had more frequent urination, a lower body weight, a delayed pregnancy, and a pregnancy success rate of only 40%. In diabetic females, Se NPs reduced the frequency of urine, expedited the beginning of pregnancy, and raised the rate of successful pregnancy. In this study, diabetic mice had significantly higher levels of urea, creatinine, MDA, and glucose, but their GSH levels were significantly lower than controls. The current study was considered to be directly related to GDM because it shows that Se NPs protect kidney structure and function in vivo (Abdallah et al., 2023).

Khazaei et al. 2022: This study is the impact of Trifolium pratense extract on blood antioxidant status, sperm characteristics, testicular tissue alterations, and testosterone levels in diabetic mice was investigated. A streptozotocin injection into the peritoneal cavity was used to cause diabetes. Total antioxidant capacity (TAC) and testicular tissue were assessed. Compared to untreated diabetic mice, sperm motility, number, and viability, as well as TAC and testosterone, were dramatically enhanced in diabetic mice treated with T. pratense extract, whereas serum NO, bcl-2, and p53 expression were significantly decreased. T. pratense extract was found to prevent diabetes-related testicular tissue damage (Jadoun et al., 2021) .

Salem et al. 2022: Have been used a green, cost-effective, and environmentally friendly method to biosynthesize Se NPs using baker's yeast extract (Saccharomyces cerevisiae). UV-VIS, XRD, FTIR, DLS, and TEM were used to characterize the biosynthesized Se NPs. With sizes ranging from 4 to 51 nm, the particles had a spherical shape. FTIR analyses of NPs revealed functional groups that relate to metabolites (proteins), which decrease and stabilize the nanoparticle. Biosynthesized Se NPs' antimicrobial potency against food-borne microorganisms was evaluated. With a minimal inhibitory concentration (MIC) of 62.5, 125, 250, and 500 g/mL against Staphylococcus aureus, Escherichia coli, Aspergillus fumigatus, and Aspergillus niger, respectively, Se NPs demonstrated promising antimicrobial action against food-borne pathogens (Escherichia coli, Staphylococcus aureus, Aspergillus fumigatus, as a result, the biosynthesized Se NPs made from baker's yeast extract show promise as a secure antibacterial agent against food pathogens. Due to their antibacterial properties, the biosynthesized Se NPs made from baker's yeast extract have potential use in the medical and food industries (Chulakham, 2021).

Shahbaz et al. 2023: In this study, selenium nanoparticles were synthesized using Melia azedarach plant extract, and the Properties of selenium nanoparticles were studied using SEM, UV, XRD, EDX, FTIR. The study also showed that Se NPs reduced biological stress by enhancing enzymatic and non-enzymatic activities, and it was concluded that Se NPs have an effective role in both physiological and biochemical aspects (Bayda et al., 2019).

Abdallah, et al. 2023: Showed the effect of Se NPs on androgen and its action in polycystic ovaries and the resulting effect on the ovary and its effectiveness, where the mice were divided into groups and one of the groups was given to the mice orally in daily doses of 0.1 and 0.2 mg / kg of the weight of the mice and within 14 days. It was noted in this study that Se NPs have a role in restoring estrous cyclicity, low testosterone and insulin resistance. Se NPs proved their importance as an antioxidant and anti-inflammatory, so they were considered a source for the treatment of polycystic ovaries, through the treatment of endocrine glands, abnormalities and reproductive imbalances (Lawson, 2021).

1.3. Research Objectives

1. To investigate the structural, morphological, and optical properties of Ag NPs and Se NPs prepared using the green synthesis approach.
2. To study the relationship between the anti-free radical activity and impaired spermatogenesis in diabetic patients with inhibition of malformations and increased sexual activity of the organism from Ag NPs and Se NPs prepared.
3. To study the relationship between the side effects of liver and kidney enzymes.
4. Examination of glucose and insulin levels after treatment of diabetic rats induced with STZ.

1.4. Thesis layout

A basic book structure includes the following sections:

- The chapter one of this book includes a general introduction to nanoparticles, how to make them, and a study of their properties, as well as a brief introduction to diabetes.
- The II chapter presents the theoretical notion of the approach utilized in this study.
- The third chapter describes the experimental work that was done in the preparation of nanomaterials and living cells, as well as the different tests that were conducted.
- The fourth chapter covers the experimental aspect, which includes tables and Figures that explain the results by calculating the statistical benefit of blocking free radicals caused by diabetes and boosting the effectiveness of living cells in diabetic patients. The rate of DNA damage, sperm damage and abnormalities, antioxidants. Conclusions and future action plans are finaly presented.

Deep Science Publishing
https://doi.org/10.70593/978-93-49307-47-6

Chapter 2

Theoretical Concepts

2.1. Introduction

Nanotechnologies, nanoparticles and nanomaterials, which are part of everyday life today, are the subject of intense research activities and a certain amount of media coverage. In this chapter, the concepts of nanoparticles are defined. Nanoparticles are tiny, made of carbon, metal, metal oxides, or organic compounds, particles with a diameter of 1 to 100 nanometers (Szabó & Schlabach, 2014; Oktaviani, 2021). Nanoparticles differ from their larger counterparts in terms of their physical, chemical, and biological characteristics. This is due to enhanced mechanical strength, increased reactivity or stability in a chemical process, increased surface area per volume, and other considerations (Hu & Yang, 2022). Due to the characteristics of nanoparticles, they are used in many different applications. There are numerous shapes, sizes, and diameters for nanoparticles (Gul et al., 2021). Nanoparticles can be one-dimensional, with only one parameter, like graphene, two dimensional, with length and width, like carbon nanotubes, or three-dimensional, with all three parameters, like length, width, and height, like gold nanoparticles. Nanoparticles can also be zero-dimensional, with length, width, and height specified at a single point, like in the case of Nano. Form, size, and structure are what separate nanoparticles from other particles. They range in size from 1 to 100 nanometers and can be spherical, cylindrical, tubular, conical, hollow, flat, or irregular. The surface may become more or less uniform or uneven as it changes. Some nanoparticles are solitary or polycrystalline, lose or agglomerated, and crystalline or amorphous (Lv et al., 2021: Busatto & de Mello Donega, 2022).

To improve attributes and lower manufacturing costs, several synthesis processes are being developed or improved. Some procedures are tweaked to improve the optical, mechanical, physical, and chemical characteristics of particular nanoparticles (Hano & Abbasi, 2021). The characterization of nanoparticles and their subsequent use have improved as a result of the tremendous advancement in device technology. Nanoparticles are presently employed in a multitude of uses, such as kitchenware, electronics, renewable energy, and aerospace. Nanoparticles can also be utilized to cure a variety of ailments, as well as to transport pharmaceuticals and improve the qualities of materials. The secret to a future that is both sustainable and clean lies in nanotechnology

2.2.The nanoparticles

2.2.1. History of nanoparticles

A nanoparticle is a small particle that ranges between 1 to 100 nanometres in size. Undetectable by the human eye, nanoparticles can exhibit significantly different physical and chemical properties to their larger material counterparts . Although nanoparticles are considered a discovery of modern science, they have a long history (Ijaz et al., 2020; Baig et al., 2021). The ancients have used nanotechnology for thousands of years. However, it is not clear when they first started using the benefits of nanoparticles in various fields (Singh et al., 2019)

Optical properties are one of the most fundamental properties that can be used to detect nanoparticles. Example: Ag NPs are yellowish-gray. Au NPs have the standard red color (Tahir et al., 2021). Platinum and palladium NPs are black.

Prior to the fourth century AD, Since nanoparticles have good optical qualities, they were used in drawing. The Lycurgus Cup is the most notable illustration. The British Museum in London has this cup on display. This beautiful mug is a prime illustration from the past. It is made from a rare type of glass called dichroic glass. The color may change when exposed to light. When the light hits the mug at a 90-degree angle, the opaque green of the mug turns into a bright translucent color. This shave has a molar ratio of 1:14 and is made up of incredibly minute amounts of gold and silver crystals (Baig et al., 2021). It has unique optical qualities because of these mineral crystals. Due to the presence of these nanocrystals, this Lycurgus Cup has a unique tint. In the 17th century, a dye called "Cassius Purple" made from gold and tin dioxide particles was used on glass. Several academic papers have been written about the synthesis, assembly, and manipulation of metal nanoparticles (Khalid et al., 2020). Metallic NPs are used as a variety of solvents and other substrates. Evidence of nanotechnology is readily available in many ancient churches (Desai et al., 2021). A characteristic use of early nanotechnology was ruby. Used in stained glass windows in the middle Ages, medieval artisans were unaware that they were using nanotechnology (Kuznetsova & Timerbaev, 2022). Jin and his collaborators have identified specific techniques for producing very beautiful color effects. The correlation between the size and form of NPs and the color of stained glass is summarized in this paragraph. Faraday made the first gold nanoparticles. These gold particles were stored at the Royal Institute in London. Gustav Mie explains in the German journal Annalen der Physik (1908) "how the color of glass changes with the size of the mineral" (Desai et al., 2021) (Desai et al., 2021).

2.2.2: Classification of nanoparticles

2.2.2.1: Classification based on nature of nanoparticles

Nanoparticles are classified according to their nature into organic, inorganic and carbon nanoparticles see Figure (2_1) (Mohammapdour & Ghandehari, 2022).

A. Organic nanoparticles

Organic nanoparticles or polymers are generally known as dendrimers, micelles, liposomes, and ferritin, among others. These nanoparticles are biodegradable, non-toxic, and some feature a hollow core, (Desai et al., 2021) sometimes referred to as nanocapsules, which are sensitive to electromagnetic radiation and thermal radiation like light. Because of their distinct properties, they are an excellent alternative for medication delivery. Apart from their usual properties like size, composition, surface shape, etc., Their field of use and efficacy is determined by their drug-carrying capacity, stability, and delivery systems, whether an entrapped drug or adsorbed drug system. Organic nanoparticles are frequently utilized in biomedical fields, such as medication delivery systems, since they are efficient and can be injected into particular regions of the body, a process known as targeted drug delivery (Adil et al., 2022)

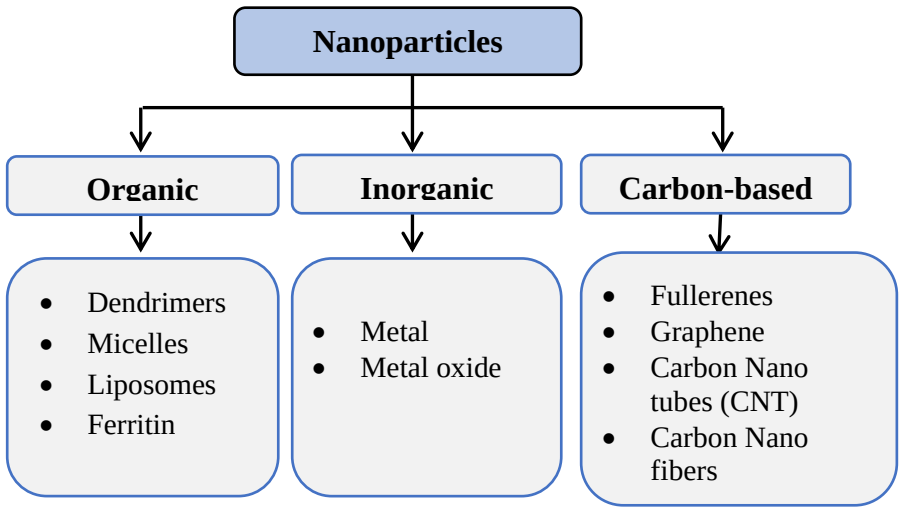

Fig (2-1). Classification based on nature of nanoparticles

B. Inorganic nanoparticles

Inorganic nanoparticles are non-toxic, hydrophilic, biocompatible and highly stable compared to organic materials.

Mainly semiconductor quantum dots, gold nanoparticles, and magnetic nanoparticles—have been widely explored forbiomedical application, diagnosis and imaging. Their unique electro, chemical, and magnetic properties make them highly efficient for imaging and diagnosis. Inorganic nanoparticles have a wide range of uses in medicine. Nanoparticles' appealing characteristics, including as biocompatibility, adjustable size, and unique physicochemical properties, make them appropriate for a variety of biomedical applications. The produced nanoparticle must be inert, stable under physiological circumstances, and have a surface that can be readily conjugated to the metal in order to travel freely through the body. The most efficient treatments technique is injecting nanoparticles with encapsulated cargo or magnetic capabilities, and surface targeting ligands assist nanoparticles in delivering to target locations without generating significant harm. Natural and inorganic NPs can be utilized to target the lung in order to counteract the side effects of conventional organization's high serum groupings. Carbon-based NPs, metal oxides (Fe2O3, TiO2, ZnO2,) and transition metal NPs (Ag, Cu, Zn) exhibit inherent antipathogenic properties by interfering with at least one viral life-cycle phase (Georgakilas et al., 2015; Adil et al., 2022).

1) Metal based.

Metal based nanoparticles are nanoparticles that are synthesized from metals to nonmetric sizes using destructive or constructive processes. Almost all metals have nanoparticles that can be synthesized. Aluminum (Al), cadmium (Cd), cobalt (Co), copper (Cu), gold (Au), iron (Fe), lead (Pb), silver (Ag), and zinc are the most widely employed metals for nanoparticle production (Zn). Nanoparticles have unique characteristics such as sizes ranging from 10 to 100nm, surface characteristics such as high surface area to volume ratio, pore size, surface charge and surface charge density, crystalline and amorphous structures, spherical and cylindrical shapes, and color, as well as reactivity and sensitivity to environmental factors such as air, moisture, heat, and sunlight (Chamoli et al., 2020).

2) Metal oxides based

Metal oxide-based nanoparticles are synthesized to alter the characteristics of their respective metal-based nanoparticles. For example, iron nanoparticles (Fe) rapidly oxidize to iron oxide (Fe_2O_3) in the presence of oxygen at ambient temperature, increasing their reactivity. The improved reactivity and efficiency of metal oxide nanoparticles are the fundamental reasons for their creation. Aluminum oxide (Al_2O_3), Cerium oxide (CeO_2), Iron oxide (Fe_2O_3), Magnetite (Fe_3O_4), Silicon dioxide (SiO_2), Titanium oxide (TiO_2), and Zinc oxide (ZnO) are the most typically synthesized. When compared to their metal counterparts, these nanoparticles have a unique feature (Taufiq Musa et al., 2021).

3) Carbon based

Carbon-based nanoparticles are those that are entirely formed of carbon. They are divided into fullerenes, graphene, carbon nanotubes (CNT), carbon nanofibers, carbon black, and occasionally activated carbon in Nano size (Saleh, 2022).

a. Fullerenes.

Fullerenes (C60) are spherical carbon molecules composed of carbon atoms that are held together and bonded together by sp2 hybridization. It is a cage consisting of 60 carbon atoms linked together by single or double bonds to form a hollow ball with 20 hexagonal faces and 12 pentagonal faces, with diameters ranging from 8.2 nanometers for the individual layers to 4 to 36 nm for the multilayer fullerenes and named after this buckyball Attributed to the world Buckminter Fuller (Khan, 2020).

b. Graphene.

Graphene is an allotrope of carbon. Graphene is a two-dimensional planar hexagonal honeycomb lattice composed of carbon atoms. Usually, the thickness of the graphene sheet is about 1 nanometer, it has a high conductivity of heat and electricity due to the presence of p-electrons and has a strength that is higher than that of steel (Singh et al., 2020; Saleh, 2022).

c. Carbon Nano Tubes (CNT).

A graphene Nano sheet with a honeycomb lattice of carbon atoms is coiled into hollow cylinders to generate carbon nanotubes with diameters as small as 0.7 nm for single-layered CNTs and 100 nm for multi-layered CNTs, and lengths ranging from a few micrometers to several millimeters. The ends might be empty or half fullerene molecules can close them It has high thermal and electrical conductivity (Abid et al., 2021)

d. Carbon Nanofiber.

Carbon nanofiber is made from the same graphene Nano foils as CNT, but it is coiled into a cone or cup form rather than a conventional cylindrical tube (Abid et al., 2021)

e. Carbon black.

Carbon-based amorphous material with diameters ranging from 20 to 70 nanometers with a usually spherical form. The particles' interactions are so strong that they form agglomerates of roughly 500 nanometers in size (Abid et al., 2021).

f. Nano cones.

Are conical structures made of carbon, having at least one dimension and a length of some micrometers or less, obtained from rolled graphene sheets (Poh et al., 2018).

2.2.2.2: Classification based on size of nanoparticles

Nanoparticles can be divided into four categories according to size, which are 0D, 1D, 2D and 3D see Figure (2_2) (Dolez, 2015).

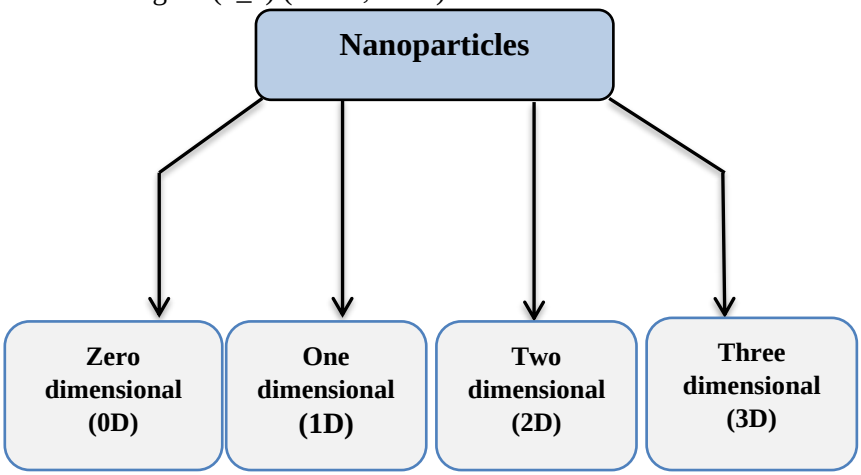

Fig (2-2). Classification based on size of nanoparticles

Zero-dimensional nanomaterials (0-D): They are materials whose dimensions (X, Y, Z) are within the nanoscale (less than 100 nanometers) and are called nanoparticles with dimensions or quantum dots, and their dimensions are less than 20 nanometers, and an example of these materials are nanoclusters and nanospheres (Daraio & Jin, 2012).

One-dimensional nanomaterials (1-D): They are nanomaterials that have two dimensions within the nanoscale and a third dimension outside the nanoscale. They are called one-dimensional nanoparticles. An example of these materials are nanotubes, nanowires, and others (Bokov et al., 2021).

Two-dimensional nanomaterials (2-D): They are nanomaterials that have one dimension within the nanoscale and the other two dimensions outside the nanoscale, and they are called two-dimensional nanoparticles An example of these materials is nano-layers, nano-membranes (Malik et al., 2012).

Three-dimensional nanomaterials (3-D): They are nanomaterials whose dimensions are outside the nanoscale (above 100 nanometers) and are called three-dimensional nanoparticles. They consist of multiple arrangement of 0D, 1D and 2D nanomaterials in different directions. An example of these materials is nanotubes and nanowires bundle (Richard et al., 2017).

2.2.3: Synthesis of nanoparticles

Nanoparticle synthesis refers to methods for creating nanoparticles.There are numerous methods used to create nanoparticles, which can be categorized as bottom-up or top-down. The procedure is depicted in a simple manner see Figure (2-3) (Oktaviani, 2021; Hu & Yang, 2022).

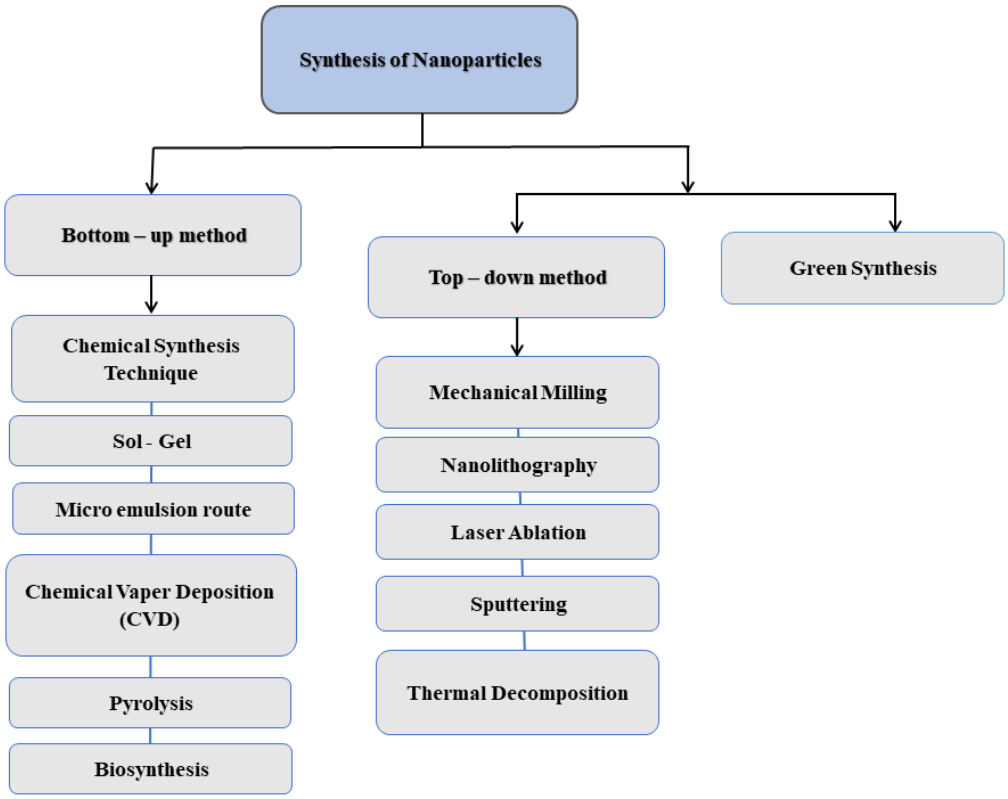

Fig (2-3). Procedure of synthesis of nanoparticles

2.2.3.1: Bottom-up method

Nanoparticles can be derived from larger molecules, or synthesized by "bottom–up" methods that, for example, nucleate and grow particles from fine molecular distributions in liquid or vapor phase .The accumulation of material from atoms to clusters to nanoparticles is known as the upward or constructive process. These materials are in their infancy in the gaseous or liquid state and bottom-up processing is required in our lives as this technology allows for smaller geometries than optical lithography. Also, using a bottom-up process, some structures such as carbon nanotubes and nanowires are grown. New technologies such as organic semiconductors also use bottom-up processes for their design. This technique is more economical than descending because it does not waste material in drilling (Oktaviani, 2021; Sun et al., 2021).

2.2.3.1.1 Chemical synthesis technique

A: Sol-gel.

A colloidal solution of particles floating in the liquid phase is known as a colloidal solution. A large, solid molecule immersed in a solvent is called a gel. Due to its simplicity and the fact that most nanoparticles can be synthesized using this process, sol-gel is the most widely used bottom-up method. It is a wet chemical process that uses either a chemical solution as a precursor to a separate particle system or colloidal particles to produce a gel. In the sol-gel method, metal oxides and metal chlorides are commonly used as typical precursors. Vibration, ripple, or sonication is used to diffuse the feedstock into a colloidal host fluid, this produces a system with a liquid and solid (gel) phase. The nanoparticles are recovered by a number of procedures, including as sedimentation, filtering, and centrifugation, after which the moisture is eliminated through drying (Bruna et al., 2021; Stodt et al., 2021).

B: Microemulsion route

This technique is an example of self-assembly that achieves a limited degree of control over both organization and composition, and it thermodynamically disperses oil, water, and all surface tension materials, producing the growth of quantum dots. Microemulsions act as hypotensive and can be described as oil-in-water (O/W) or water-in-oil (W/O) any continuous binary system. (Gour & Jain, 2019; Song et al., 2021)

C: CVD, or chemical vapor deposition.

Chemical vapor deposition is the process of depositing a thin layer of gaseous reactants on a substrate. Gas molecules are mixed at room temperature in a reaction chamber to create the deposition. When the mixed gas interacts with a heated substrate, a chemical reaction occurs. A thin product coating is left on the surface of the substrate as a result of this reaction, which can be removed and reused. The substrate's temperature is a deciding factor in CVD. Extremely pure, uniform, robust, and hard nanoparticles are created using CVD. The need for specialized equipment and the extremely poisonous gaseous byproducts are two drawbacks of CVD (El-Eskandarany et al., 2021).

D: Pyrolysis

Pyrolysis is the most widely utilized method in industry for producing nanoparticles on a big scale. It entails the use of flame to burn a precursor. The precursor is either a liquid or a gas that is introduced into the furnace under high pressure through a tiny opening and burns. To recover the nanoparticles, the combustion or by-product gases are air categorized. To reach high temperatures for simple evaporation, some furnaces employ laser and plasma instead of flame. Pyrolysis has the benefits of being a simple, efficient, cost-effective, and continuous process with a high yield (Yadav et al., 2012).

2.2.2.1.2. Biosynthesis

Making nontoxic and biodegradable nanoparticles using biosynthesis is a sustainable, green process. To create nanoparticles for bio reduction and capping, biosynthesis uses bacteria, plant extracts, fungi, and other precursors in place of traditional chemicals. Biosynthesized nanoparticles are ideal for biological applications due to their distinctive and improved characteristics (Subhan et al., 2021).

2.2.3.2: Top-down method

Attrition is a mechanical method for creating certain types of nanoparticles. The macro or small-scale particles are ground in a ball mill, planetary ball mill or other machinery to reduce the size. The resulting particles are separated by filters and recovered. Particle sizes range from tens to hundreds of nanometers. It is generally considered energy-intensive (Modena et al., 2019) (Subhan et al., 2021).

2.2.3.2.1. Mechanical milling.

Mechanical milling is the top-down technique that most usually results in a diversity of nanoparticles. The constituent components are processed in an inert environment using mechanical grinding and post-annealing during the synthesis of nanoparticles. Mechanical grinding is influenced by a number of elements, including plastic deformation, which affects particle shape, fracture, which affects particle size, and cold welding, which affects particle size growth. Hollow steel containing tungsten balls and a solid precursor rotating around its central axis. The particle size is reduced by brittle crushing resulting from ball and ball wall collision. The grinding process is carried out in an inert gas atmosphere to reduce pollution. (Rasmussen et al., 2020; Włodarczyk & Kwarciak-Kozłowska, 2021)

2.2.3.2.2. Nanolithography.

Lithography is a process that uses focused radiant energy and chemical films to create precise patterns in silicon wafers or other materials. Nanolithography is the process of creating non-metric scale structures with at least one dimension between 1 and 100 nanometers. Among the nano-lithography techniques are photolithography, electron-beam, photon multiplexing, nano-fingerprinting, and scanning lithography. Lithography, in general, is a method of selectively removing a portion of a photosensitive material to produce the required shape and structure before printing it in the appropriate location on the material. It is therefore a technique for adding or removing material from a specific area. The main benefits of nanolithography include the ability to generate anything from a single nanoparticle to a cluster of the desired shape and size. The downsides include the need for complex equipment and the attendant cost Lithographic techniques include mobile phase lithography, electron beam lithography, focused ion beam lithography, neutral atomic beam lithography, Nano processing, nanolithography, scanning tunneling

microscopy, atomic force microscopy, and others (Subhan et al., 2021; Salvioni et al., 2021)

2.2.3.2.3. Laser ablation.

LASIS (Laser Ablation Synthesis in Solution) is a physical method for creating nanoparticles in a liquid environment. This top-down technique employs well-known laser-based technologies to generate additive-free nanocolloids that are less harmful and more ecologically friendly. When a metal is exposed to a laser beam while submerged in a liquid solutionthe plasma plume that the laser beam condenses into nanoparticles. For the production of metal-based nanoparticles, it is a trustworthy top-down strategy as an alternative to conventional chemical reduction. It is a "green" method since Lassis enables stable nanoparticle synthesis in organic solvents and water without the use of chemicals or stabilizing agents (Salvioni et al., 2021).

2.2.3.2.4. Sputtering.

Sputter deposition onto a low volatile liquid matrix is a recently developed green synthesis method for metal/metal oxide nanoparticles (NPs). The sputtering process is a physical vapor deposition (PVD) process that deposits materials onto a particular surface by ejecting atoms from that material and condenses ejected atoms onto the surface when a high vacuum environment is maintained (Salvioni et al., 2021). Nanoparticles prepared by the direct sputtering into liquid medium .usually contains fewer impurities than those which were prepared by chemical synthesis. And these nanoparticles are often also very stable for a long time.

2.2.3.2.5. Thermal decomposition.

When heat is used to break down chemical bonds in a substance, thermal decomposition an endothermic chemical breakdown occurs. The decomposition temperature is the temperature at which an element begins to chemically decompose. By allowing metal to break down at a certain temperature, secondary compounds are created chemically, creating the nanoparticles (Subhan et al., 2021)

2.2.4: Properties of nanoparticles

Physical and chemical characteristics of nanoparticles are the most common classifications. A few common nanoparticles' qualities are listed.

2.2.4.1: Physical

Among the physical characteristics of a nanoparticle are its optical characteristics, including color, light absorption, reflection, and UV absorption and reflection properties in a solution or when deposited on a surface. It also comprises mechanical qualities like elastic, ductile, and tensile strengths, as well as flexibility, which are important in their

application. Many contemporary things now include additional properties like hydrophilicity, hydrophobicity, suspension, diffusion, and settling characteristics. Due to their magnetic and electrical properties, including conductivity, semiconductivity, and resistance, nanoparticles are used in modern electronics and thermal conductivity in renewable energy applications (May et al., 2022).

2.2.4.2: Chemical

Its uses are determined by chemical features such as the nanoparticles' reactivity with the target, as well as their stability and susceptibility to elements such as moisture, environment, heat, and light. The nanoparticles' antibacterial, antifungal, disinfection, and toxicological capabilities make them appropriate for biomedical and environmental use. The oxidation, reduction, flammability, anti-corrosive, and corrosive properties of the nanoparticles determine their usage (May et al., 2022).

2.2.5: Characterization

A nanoparticle's potential and applicability are determined by its distinct properties. The characterization of nanoparticles is carried out using a variety of measuring techniques (Birla et al., 2022; Nzereogu et al., 2022).

2.2.5.1: Size

The size effects (quantum effects) of nanoparticles introduces many size-dependent phenomena such as chemical, electronic, magnetic and mechanical properties. For example, the melting point of nanoparticles is evidently decreased when the size is reached to the nanometer scale. The particle size plays a crucial role in nanoparticle properties and therefore an essential task in property characterization of nanoparticles is particle sizing . The particle size and size distribution of nanoparticles can be determined using numerous commercially available instruments. Instruments can be used for the analysis of dry powders and powders dispersed in suspension. The most widely used technique for determining particle size and dispersion are Scanning Electron Microscope (SEM) and Transmission Electron Microscope (TEM). Laser diffraction techniques are used to measure bulk materials in solid phase, while pictures from TEM and SEM are used to identify particles and clusters. Photon correlation spectroscopy and centrifugation are employed to measure the particles in the liquid phase. The usage of a Scanning Mobility Particle Sizer (SMPS), which provides quick and accurate readings when compared to other techniques, is made possible by the challenging and irreversible nature of imaging operations for particles in the gaseous phase (Birla et al., 2022).

2.2.5.2: Surface Area

One of the first indicators to identify whether a material or product contains NANO – and thus is potentially entitled as a nanomaterial – is its specific surface area. Since

nanoparticles are very small particles their surface-to-volume ratio is very high and therefore nanoparticles also exhibit a relatively high surface area per unit mass compared to micrometer-sized particles. The ratio of a nanoparticle's surface area to volume significantly affects both its characteristics and performance. The most used technique for figuring out the surface area is Brunauer-Emmett-Teller (BET) surface area analysis. Simple titrations work well to estimate the surface area of particles in liquid phase, but they take a long time. Nuclear Magnetic Resonance (NMR) spectroscopy is used as a result. A modified Scanning Mobility Particle Size Spectrometer (SMPS) and Differential Mobility Analysis (DMA) are used to calculate the surface area of nanoparticles in the gaseous phase. Urban ultrafine atmospheric aerosol and particle emissions from combustion sources such as diesel engines are typically low fractal dimension aggregates ($D \leq 2$) composed of spherical primary particles with diameter 5 to 50 nm (Nzereogu et al., 2022; Birla et al., 2022).

2.2.5.3: Composition

A nanoparticle's chemical or elemental make-up determines its purity and functionality. A nanoparticle's effectiveness can be lowered by having more secondary or unwanted components in it, which can also lead to contamination and secondary reactions. To ascertain composition, X-ray Photoelectron Spectroscopy (XPS) is frequently utilized. Some of the techniques utilized include chemically dissolving the particles, Wet chemical analysis is next using techniques including mass spectrometry, atomic emission spectroscopy, and ion chromatography. The analysis is carried out using spectrometric or wet chemical techniques, and the particles in the gaseous phase are collected either by filtering or electrostatically (Nzereogu et al., 2022).

2.2.5.4: Surface Morphology

Utilizing the properties of nanoparticles requires understanding their shapes and surface textures. Spherical, flat, cylindrical, tubular, conical, and irregular forms with flawless or imperfect crystalline or amorphous surfaces are some of the shapes. To determine the surface, electron microscopy imaging techniques like SEM and TEM are frequently utilized. While gaseous particles are electrostatically or filtered out for electron microscope imaging, liquid particles are deposition on a surface and examined (Nzereogu et al., 2022).

2.2.5.5: Surface Charge

The interactions of a nanoparticle with the target are controlled by its surface charge. Surface charges and their overall dispersion stability in a solution are measured using a zeta potentiometer. Using a Differential Mobility Analyzer (DMA), it is possible to determine the charge of nanoparticles in the gaseous phase (Nzereogu et al., 2022; Birla et al., 2022).

2.2.5.6: Crystallography

Crystallography is the study of the configuration of atoms and molecules in crystal solids. The structural organization of nanoparticles is studied using powder X-ray, electron, or neutron diffraction (Poh et al., 2018).

2.2.5.7. Concentration

The volume of air or gas required for the operation is calculated by counting the number of nanoparticles present in the gaseous phase. The concentration of a substance determines a system's effectiveness or efficiency, size, and dispersion of nanoparticles in a unit volume of air or gas. A Condensation Particle Counter is commonly used to quantify concentrations (CPC) (Birla et al., 2022).

2.2.6: Applications of the nanoparticles

Some of the most important applications of nanoparticles are listed below.

2.2.6.1: Cosmetics and Sunscreens

Nanotechnology has been shown to improve cosmetic performance in a variety of ways, including: 1) increasing the confining efficiency and skin penetration of the active ingredient, 2) controlling drug release, 3) improving physical stability, 4) improving moisturizing power, and 5) providing better UV protection. The influence of nanoparticles in semi-solid formulations on skin penetration issues is given special consideration. Traditional UV-protective sunscreens, for example, do not have long-term stability when used due to developing concerns regarding nanoparticle toxicity. Nanoparticles are used in sunscreen. Some sunscreens include titanium oxide and zinc oxide nanoparticles because of their UV-protective qualities, which include transparency to visible light while absorbing and reflecting UV radiation. Iron oxide nanoparticles are used in some lipsticks as a pigment. (Astruc, 2020; Damodharan, 2021)

2.2.6.2: Electronics

The growing demand for big-screen, brilliant displays in computer monitors and televisions in recent years has prompted the usage of nanoparticles in display technologies. Nanocrystal line lead telluride, cadmium sulphide, zinc selenide, and sulphide, for example, are utilized in contemporary displays' light emitting diodes (LED) [84]. The rise of portable consumer devices such as cell phones and laptop computers has resulted in a huge need for small, lightweight, high-capacity batteries. Separator plates in batteries should be made of nanoparticles. Because of its foam-like (aerogel) shape, they can store far more energy than regular batteries. Because of their enormous surface area, batteries built of nanocrystal line nickel and metal hydrides require less recharging and last longer [84]. Nanoparticles with increased electrical conductivity are utilized to detect gases like NO2 and NH3. The pores of nanoparticles expand owing to

charge transfer from nanoparticles to NO2 when gas molecules bind them together, giving them a superior gas sensor (Nile et al., 2020).

2.2.6.3: Catalysis

Nanoparticles have a large surface area, which means they have more catalytic activity. Nanoparticles are effective catalysts in the synthesis of chemicals because of their exceptionally large surface to volume ratio (Shantkriti et al., 2023). using platinum nanoparticles in catalytic converters for vehicles is one of the most important applications because they minimize the quantity of platinum required due to the nanoparticles' large surface area, lowering the cost and enhancing efficiency. Nanoparticles are used in several chemical processes, such as the reduction of nickel oxide to metal nickel (Ni) (Shafiq et al., 2020).

2.2.6.4: Medicine

The use of nanoparticles in medication delivery has benefited the medical profession thanks to nanotechnology. Nanoparticles can be used to deliver the medicine to particular cells. By putting the medicine in the desired location and in the needed dosage, the overall drug intake and adverse effects are considerably reduced. This approach is less expensive and has fewer adverse effects. Nanotechnology can aid in tissue engineering, which is the replication and repair of damaged tissue (Mohajerani et al., 2019). Tissue engineering can be used to replace traditional therapies like artificial implants and organ transplants. The development of carbon nanotube scaffolds in bones is one such example. Gold has long been used in medicine. Gold is employed in numerous activities in Ayurveda, an Indian medicinal system. The use of gold for memory improvement is a typical prescription. Gold is used in certain medicinal treatments to improve a baby's mental fitness (Astruc, 2020; Santhosh & Nayaka, 2022).

2.2.6.5: Food

Incorporating nanotechnology into food manufacturing, processing, protection, and packaging improves the quality of the product. For example, in the food packaging process, a nanocomposite coating can directly incorporate antimicrobial chemicals onto the coated film surface (Saleem et al., 2021). Nano drops, an additive meant to transmit vitamins and minerals in food, are used in the manufacturing of canola oil, for example (Durgalakshmi et al., 2020)

2.2.6.6: Construction

Construction processes have been enhanced by nanotechnology, which has made them faster, less costly, and safer. When Nano silica (SiO_2) is blended with regular concrete, for example, the nanoparticles can increase the mechanical qualities as well as the durability (Manikandan et al., 2022). The inclusion of hematite (Fe_2O_3) nanoparticles to

the concrete improves its strength. In the building sector, steel is the most extensively accessible and utilized material. The qualities of steel may be enhanced by the use of nanotechnology in steel. For example, using Nano size steel in bridge building results in stronger steel cables (Kuhn et al., 2022). Glass is another major building element. The use of nanotechnology in building glass is the subject of much investigation. Titanium dioxide (TiO2) nanoparticles are utilized to cover glazing because they have sterilizing and anti-fouling capabilities and catalyze intense chemical reactions that break down volatile organic compounds (VOV) and organic contaminants. The use of nanotechnology allows for more effective light and heat blocking via the windows. By incorporating nanoparticles into paints, self-healing, corrosion resistance, and insulating properties can be achieved. These paints' hydrophobic properties repel water; therefore, They can be utilized to cover metal pipes to shield them from harm from salt water. Nanoparticles in paints increase performance by making them lighter with improved qualities (Sapra et al., 2021) thus when used on airplanes, for example, it may lower total weight and the amount of paint necessary, which is good for the environment as well as the company's bottom line.

2.2.6.7: Environmental Cleanup and the use of Renewable Energy

Due to their distinct physical and chemical properties, nanoparticles have emerged as a viable alternative for environmental remediation and performance enhancement in the field of renewable energy (Göğebakan & Şah, 2021). There are nanoparticles in nature, and some of them have been found to be environmentally beneficial. cleaning up the environment with nanoparticles, or "Nano remediation," has been successfully used for more than ten years to clean or disinfect the air, water, and soil (Falcone et al., 2021). Because in-situ treatment is offered by nano remediation, there is no longer a need to pump ground water out for treatment or excavate to get to the desired site, making it one of the most effective solutions. By immobilizing contaminants, To purify the water, the nanoparticles are placed in the right place and moved by the groundwater flow. Redox reactions are the primary decontamination method. Surface water is cleaned, disinfected, and desalinated using nanoparticles. The three most likely contaminants are heavy metals, viruses, and organic pollutants. It has proven to be successful, eliminating the need for chemicals that could produce unwanted byproducts of the process. Oil spills are one of the world's most serious hazards because they may spread across large areas. Cleaning those using traditional ways is tough and time-consuming, which exacerbates the problem by allowing it to spread further. Nanoparticles have also been employed to clean up oil spills and have shown to be an effective strategy. Nanoparticles are primarily used to clean municipal and industrial wastewater, as well as the resulting sludge. Nanoparticles are replacing traditional chemicals because they are less expensive, more efficient, and need less treatment volume. Nano filtration is a relatively new membrane filtration technique for water purification that has found widespread application in the

food and dairy sectors. Contamination of the soil is also becoming more of a worry. For heavy metal pollution, hazardous industrial waste, and other contaminants, nanoparticles are injected into precise target sites and cleaned or treated. Certain nanoparticles with a greater surface area have been employed as a Nano catalyst in gaseous processes. The most often utilized area is in industrial stacks to lower pollutant levels to set limits or to totally eliminate them, hence reducing air pollution. The use of nanoparticles for renewable energy is the subject of extensive investigation. higher absorption of light and UV, as well as extremely low reflection coatings, have considerably improved the efficiency of solar cells. Because some nanoparticles are hydrophobic, self-cleaning solar cells have been created. Boilers and solar concentrators are covered with specific nanoparticles with high thermal conductivity and heat absorption capacity to boost their thermal efficiency (Li et al., 2019).

2.3: Diabetes Mellitus (DM)

In developing nations, One of the most important health risks is diabetes, social, and economic issues. Diabetes occurs when the pancreas is unable to produce enough insulin, or when the body is unable to effectively use the insulin it produces. Unfortunately, diabetes can affect people of any age, race, or sex, and it can affect people with any lifestyle. The underlying cause of diabetes varies by type. But, no matter what type of diabetes you have, it can lead to an increase in your blood sugar. Having too much sugar in the blood can lead to serious health problems. Before we get to the heart of the topic of diabetes and sex, we mention some important things for diabetic men and women (Barron et al., 2020).

2.3.1: Diabetes symptoms in women and men include:

Depending on how high your blood sugar is, your diabetes symptoms will vary. Some patients, particularly those with prediabetes or type 2 diabetes, may not have any symptoms at all. Symptoms of type 1 diabetes tend to appear rapidly and are more severe (Barron et al., 2020; DiMeglio et al., 2018).

1. A strong desire to drink
2. Urinating on a regular basis
3. being really hungry
4. Weight loss or growth that isn't explained
5. Ketones present in the urine (ketones are a byproduct of the breakdown of muscle and fat that occurs when there is not enough insulin available) (83).
6. Nausea and fatigue
7. Arousal comfort
8. Eyesight is hazy (blurred vision)

9. Chronic sores and wounds that take a long time to cure (84).
10. Infections that occur frequently, such as skin infections or vaginal infections (Syed, 2022).
11. Loss of sensation in the hands or feet (Ernst, 2021).

Many persons with type 2 diabetes do not experience all of these symptoms at the same time. The most prevalent kind of diabetes, type 2, can strike at any age, though it is more frequent in those over the age of 40. Type 1 diabetes can strike at any age, although it is more common in childhood and adolescence (Galicia-Garcia et al., 2020).

2.3.2: Classification of diabetes mellitus

Diabetes can be classified into three types by age group and cause. People can discover diabetes at any age. That diabetes or diabetes can affect both women and men, according to the source (Shafiq et al., 2020).

2.3.2.1. Type one diabetes

Type 1 diabetes (this type of disease is called diabetes dependent on insulin and affects this type of diabetes, children). A condition in which the body has a very small amount of insulin or may not be available insulin in the body at all and this type of the disease is prevalent in approximately 10% of diabetics worldwide and is due to the demolition of beta-β cells found in the pancreas, which are considered as a source of insulin in the body. This leads to a lack of absolute insulin, in which case patients rely entirely on the supply of external insulin to prevent ketosis and thus maintain the continuity of life (Agbaje et al., 2022). Diabetes is the first type of autoimmune disease often; in which case the immune system of the body decreases and the damage in the DNA begins to attack healthy tissues. In this type of disease, the disease attacks the immune system by mistake, causing the breakdown of cells producing insulin, known as pancreatic beta cells. Researchers have discovered a variety of genetic, environmental, and other environmental factors that can boost the immune system's vulnerability to destroying these cells. About 20 genes for the first type of diabetes have been discovered so far through research. Particularly among those who already have a genetic susceptibility to the disease, environmental factors and particular viruses may contribute to the spread of the illness. Surgery for surgical pancreatic resection can also result in type 1 diabetes (Songisepp et al., 2022).

2.3.2.2. Type two diabetes

Type two diabetes is a heterogeneous, insulin-follow diabetes that affects most adults. It has been found that about 85% of people develop this type of diabetes around the world. This type of diabetes is caused by insulin resistance to the cells of the body

(Lancherhans) and thus the occurrence of insulin deficiency. The causes of type 2 diabetes are multifactorial and include both hereditary and non-genetic factors (Northcott, 2020). The reason why tissues are not fully responsive to insulin in most cases is that they cause insulin receptors present in cell membranes. Type 2 diabetes in its early stages, there is a decrease in the susceptibility of the dominant cells to the sensitivity of insulin, which leads to the production of high levels of insulin in the blood. At this stage acts contrary to high blood sugar with a variety of measures and drugs that increase and make the sensitivity of insulin better and therefore decrease in the production of glucose from the liver (Gál et al., 2021). As the disease progresses, insulin deficiency decreases, and glucose increases. The use of insulin replacement therapy often becomes mandatory. This type of diabetes usually increases as people age, and in general, research found that about 80% are overweight and are most likely to suffer from type 2 diabetes, where about 90-95% of people with type two diabetes were observed (Kalra & Khandelwal, 2018). This pointing that this type of sugar is the most common among older people and obese, and the cause of the gene history of diabetes has the effect of diabetes mellitus. There are a number of underlying causes associated with type two diabetes. The increased the risk of type two diabetes, the more likely these factors are and the risk factors that an individual carry. There are many theories about the precise and automatic cause of type 2 diabetes. The concentration of obesity around the waist for abdominal organs is due to the release of a group of hormones called adipokines but not subcutaneous fat. This is commonplace for individuals to resist insulin. It may reduce glucose tolerance (Roep et al., 2021). Obesity was found in about 55% of people with type two diabetes. This type of disease is more common in those with relatives who have type 2 diabetes (McIntyre et al., 2019).

2.3.2.3. Other specific types of diabetes

1. Pancreatic ailment (e.g., pancreatitis, cystic fibrosis and hemochromatosis (Sweeting et al., 2022)
2. Endocrine brokenness (e.g., Cushing's disorder, furthest point limits, Vero chromosome (Burgner & McCall, 2022).
3. Incited drugs (e.g., glucocorticoid, antipsychotics, alpha, interferon, pentamidine) .
4. Genetic imperfections of cell work (e.g., MODY MODELS).
5. Genetic imperfections of insulin work .
6. Other hereditary disorders that can be related with diabetes .
7. Inflammation.
8. Rare types of immune system safe sclerosis (Layden & Bhaskar, 2022) (Layden & Bhaskar, 2022).

2.3.2.4. Pregnancy diabetes

This type of gestational diabetes is a diabetes that is detected and monitored during pregnancy, as well as diabetes and diabetes that are before and which increases during

pregnancy. This type of diabetes is due to a group of relatively inadequate insulin secretion and response that can be found in about 2% -5% of all pregnancies, and that the characteristic of this type of diabetes that it can improve or disappear after birth. During pregnancy, the patient must be under strict medical supervision for the treatment of gestational diabetes (Márquez-Pardo et al., 2020). About 20% to 50% of women develop type 2 diabetes in their later years. Despite the possibility that it will pass quickly, the risk of this sort of untreated diabetes is harmful to the mother's or the fetus's health. The risk to the child may be high birth weight, muscle and skeletal abnormalities and possible cardiac and congenital anomalies of the central nervous system (Alahmar, 2019).

2.3.3: What effect does diabetes have on your fertility?

Diabetes has a severe impact on fertility, and as the prevalence of type 2 diabetes is increasing year after year, infertility specialists are considering diabetes as a primary cause of some unexplained infertility in couples. Unfortunately, diabetes interferes with the appropriate placement of the embryo in the uterus, leading to miscarriage before the woman even recognizes she is pregnant (Glazyrine et al., 2022). This illness does not prohibit pregnancy in this situation, but it does impact the pregnancy's continuance till delivery. In addition to the aforementioned, dangerously high blood sugar levels can impact hormone levels in the body, including estrogen, progesterone, and testosterone, all of which are required for pregnancy (Buzea et al., 2007). As a result, maintaining a healthy blood sugar level is critical to your fertility. There are further hazards to consider even if the embryo is placed in the womb, including:

A higher risk of birth abnormalities as a result of genetic cell damage caused by high blood sugar levels. The baby's big size necessitates a cesarean section, which raises the fetus's risk of infection (Alahmar, 2019). Increased risk of gestational diabetes, which can lead to a variety of serious health issues for both the mother and the child. Diabetes does not just influence women's fertility; it can also cause males to become infertile as a result of excessive blood sugar levels. Those with diabetes had greater damage to their sperm DNA than men without the condition, according to researchers (Vijayakumar et al., 2022). DNA damage, according to scientists, can influence a man's fertility. Men with diabetes who do not regulate their blood sugar levels have a decreased probability of fertilizing an egg with sperm, and if fertilization does occur, the risk of miscarriage and birth defects is higher. Lower fetal quality, lower implantation rates, greater miscarriage rates, and the occurrence of several significant childhood disorders, including some childhood malignancies, are all known to be linked to sperm DNA quality (Rai et al., 2021). While we are aware of the dangers of high blood sugar and its impact on fertility, we must equally be aware that merely regulating the sugar level and achieving or maintaining a normal level would limit the incidence of the aforementioned hazards and allow for a healthy pregnancy and childbirth. Healthy. The key to success

in this matter is, of course, communication with the reproductive endocrinologist and obstetrician-gynecologist to ensure that blood sugar levels remain stable months before trying to conceive as well as during pregnancy, in addition to following some habits such as eating healthy and maintaining good health. You will then have a higher chance of getting pregnant and giving birth, even if you have diabetes. The final picture resembles a "comet," complete with a distinct head and tail. The head is made up of intact DNA, whereas the tail is made up of broken or damaged DNA (single-strand or double-strand breaks). While the Comet Assay has mostly been used to investigate animal eukaryotes, there have been instances of it being used to examine plant cells successfully (Castillo-Henríquez et al., 2020).

2.4: Toxicity in Nanoparticles

The rapid emergence and extensive use of nanoparticles of all kinds in various life applications raise some questions about the safety of these particles, and whether nanoparticles are toxic or not. Nature, it is either produced naturally in the environment and can exist anywhere that has been exposed to physical, biological and chemical phenomena from the impact of nature and an example of this type of natural nanoparticles is inorganic particles that have a mineral basis, for example particles Silver nanoparticles and another type of viral nanoparticles. As for the other type, it is incidental nanoparticles, which are unintentionally produced in nature. They are secondary particles that result from industrial processes such as combustion, corrosion, oxidation and other external factors. For example, for this type of nanoparticles is carbon and others (Anjum et al., 2016). The last type of nanoparticles is engineering, which resulted intentionally and with human intervention, as he is responsible for manufacturing them to benefit from them in various applications, such as the manufacture of nanoparticles of selenium, Nano silver, or zinc oxide and others. The first and second types of nanoparticles are widely available in the environment, they also tend to have heterogeneous chemical and physical properties, and this is due to the way they are formed in nature, unlike engineering nanoparticles. Because of this constant exposure, it has become important to understand the potential harmful and toxic effects that these particles may cause to humans (Sharma et al., 2009).

2.4.1: Toxicity in Silver Nanoparticles

Silver nanoparticles are generally used in many medical, agricultural and other applications (Singh et al., 2018). Therefore, scientists have made, and the research is still ongoing, and with very great efforts in the synthesis of homogeneous silver nanoparticles, using physical, chemical properties and environmentally friendly biological methods to overcome some of the restrictions that hinder the use of Nano silver in treatment and in the manufacture of food products for its effective effect as an

antibacterial and to enhance the shelf life (El-Ramady et al., 2015). Silver nanoparticles can also be used in the medical fields and various pharmaceutical sciences, as it is used in the manufacture of sunscreen, cosmetics, medical devices, and in the treatment of burns and trophic ulcers and others. In addition to the above, it was discovered through laboratory materials that there are some silver nanoparticles in the environment that have an unacceptable toxic effect on human health. As zero valence silver nanoparticles can generate highly reactive oxygen species and thus lead to the production of free radicals. Which can lead to DNA damage in addition to changes in the permeability of the early cell membrane and has a little role on the male reproductive system if nanoparticles can be deposited in the testicles and cause harmful effects in sperm (Hosnedlova et al., 2018). There are studies that have reported on Green composition and environmentally friendly biological methods that can be used in the manufacture of silver nanoparticles, as the green synthesis has a significant role in reducing the toxicity in nanoparticles and then it can be used in medical applications safely, and as such there is a need for more studies to evaluate the toxicity of silver nanoparticles (Dosay-Akbulut, 2020; Hasanuzzaman et al., 2020).

2.4.2: Toxicity in Selenium Nanoparticles

Selenium is a nutritional component necessary for human health and is found in nature mainly in the form of selenite, as well as selenide and biologically inert selenium, which is safe, non-toxic and insoluble in water. Nano-selenium directly depends on the physical and chemical properties of the constituent molecules For this ingredient and through many experiments, it was found that the dose, duration and high concentrations can affect the living systems and the possibility of toxicity is more likely, so it cannot exceed the specified dose (2 mg/kg) as it negatively affects ROS, LDH and MDA with this still More experiments are necessary to get a clear idea of the mechanism of toxicity (Karbaschi et al., 2019; Ge et al., 2021)

On the other hand, it was found that selenium is one of the rare minerals that helps maintain plant physiology and also has an important role in sustainable development and effectively affects production. Also, Nano-selenium has attracted great importance as a nutritional supplement and as a therapeutic agent that has no harmful side effects (Shahabadi et al., 2021)

2.5: Comet Assay

The Comet Assay, commonly known as single cell gel electrophoresis (SCGE), is a sensitive and quick way to measure and analyze DNA damage in individual cells. As a result, this is one of the methodologies used in cancer research to evaluate genotoxicity and chemoprevention efficacy. This approach was invented in 1984 by Swedish

academics Staling & Johansson. 1 Singh et al. eventually renamed this procedure the Alkaline Comet Assay in 1988 (Shar et al., 2019). On a microscope slide, individual cells are embedded in a thin agarose gel. The cells are then lysed to eliminate all cellular proteins. Under alkaline/neutral circumstances, the DNA is permitted to unravel. After unwinding, the DNA is electrophoresed, which allows broken or damaged DNA pieces to move out from the nucleus. After staining the gel with a DNA-specific fluorescent dye like ethidium bromide or propidium iodide, the quantity of fluorescence in the head and tail, as well as the length of the tail, are measured. The quantity of DNA that is freed from the comet's head is proportional to the degree of DNA damage (Ramamurthy et al., 2013). DNA damage produced by double strand breaks, single strand breaks, alkali labile sites, oxidative base damage, and DNA cross-linking with DNA or protein may all be detected with the Comet Assay. The Comet Assay is also used to track living cell DNA repair (Rahmah & Garallah, 2022).

Deep Science Publishing
https://doi.org/10.70593/978-93-49307-47-6

Chapter 3

Experimental part

3.1: Introduction

In this chapter, reference is made to how to prepare nanoparticles using different methods and materials, where active plant components such as flavonoids, enzymes, allicin, carbohydrates, polyphenols and other materials are used as reducing agents for silver salts and stabilizing agents for single bonds during producing silver nanoparticles. Aqueous fresh *garlic* extract was used in the current study as a reducing agent and stabilizer, while silver nitrate solution was used to synthesize silver nanoparticles utilizing physics. Due to its bright future in many contemporary domains, selenium nanoparticles have grown in significance in the contemporary field of medicine. *Withania Somnifer* plant and chemicals were used in this work to create selenium nanoparticles, and the impact of these particles on living cells was investigated. The use of SPSS Veirsion18 is to study the significant differences between the results obtained from live cell extracts. Conducting various assays to detect the toxicity of nano-preparations and study the activity and activity of NPs on the amount of damage in sperm and antioxidants of living cell lines in diabetic white mice. See Figures (3-1) shows the flow diagram of our work steps.

3.2: Materials and methods

3.2.1: Instruments and equipment's

In this work, all equipment and instruments used are included in Table (3-1).

Table (3-1): List of equipment and instruments used

Equipment's	Company/Origin
Autoclave	Webeco Gmbh/ Germany
Electric balance	Sartorius/ Germany
Centrifuge	Hattic/ Germany
Eppendorf Centrifuge	5417R/ Germany
Light microscopy	Olympus/ Japan
Water bath	Grant/ England
Electric oven	Memmert/ Germany
ELISA reader	Human Reader HS/ Germany
UV/visible spectrophotometer	Shimadzu- 2450/ Japan
FTIR	Shimadzu FTIR-8400/ Japan
FESEM	EDS-Mapping-Line-EBSD / Germany
AFM	DualScope TM DS/ USA
TEM	ZEISS LEO 912 AB/ Germany
XRD	Panalytical XPert Pr/ UK
DLS/Zeta	Malvern Zetasizer/ Germany
Hood	Bio Meraux/ France
Hot plate with magnetic stirrer	Spin mix/ England
Incubator	Gerhardt/ Germany
Microscope	Motic/ Japan
Water bath	Gallenkamp/ England
Filter paper	Macklin/ Chania

3.2.2: Chemical compounds and kit

The chemical materials and their manufacture used in this study are listed in Table (3-2), and Table (3-3).

Table (3-2). List of chemical compounds used

Materials	Company / Origin
Agarose	Cambrex/bioscience/USA
Ethylene Diamine Tetra Acetic Acid Disodium (EDTA)	Sigma/Aldrich/USA
Ethanol	Duksan/
RBC buffer	Qian/Germany
Silver nitrate (AgNO3)	Sigma/USA
Methyl Thiazolyl Tetrazolium (MTT)	Bio-world/USA
Trypsin Versene	Capricorn –scientific/Germany
Ficoll solution	Capricorn-scientific/Germany
Phosphate-Buffered Saline (PBS)	Sigma/USA
Streptozotocin	Sigma/USA
Alloxan	Sigma/Aldrich/USA
Insulin syringes	China
Selenous acid (H2SeO3)	K International"/USSR
Ascorbic acid (C6H8O6)	Sigma/USA
Withania somnifera plant	Local made/Iraq
Garlic plant	Local made/Iraq

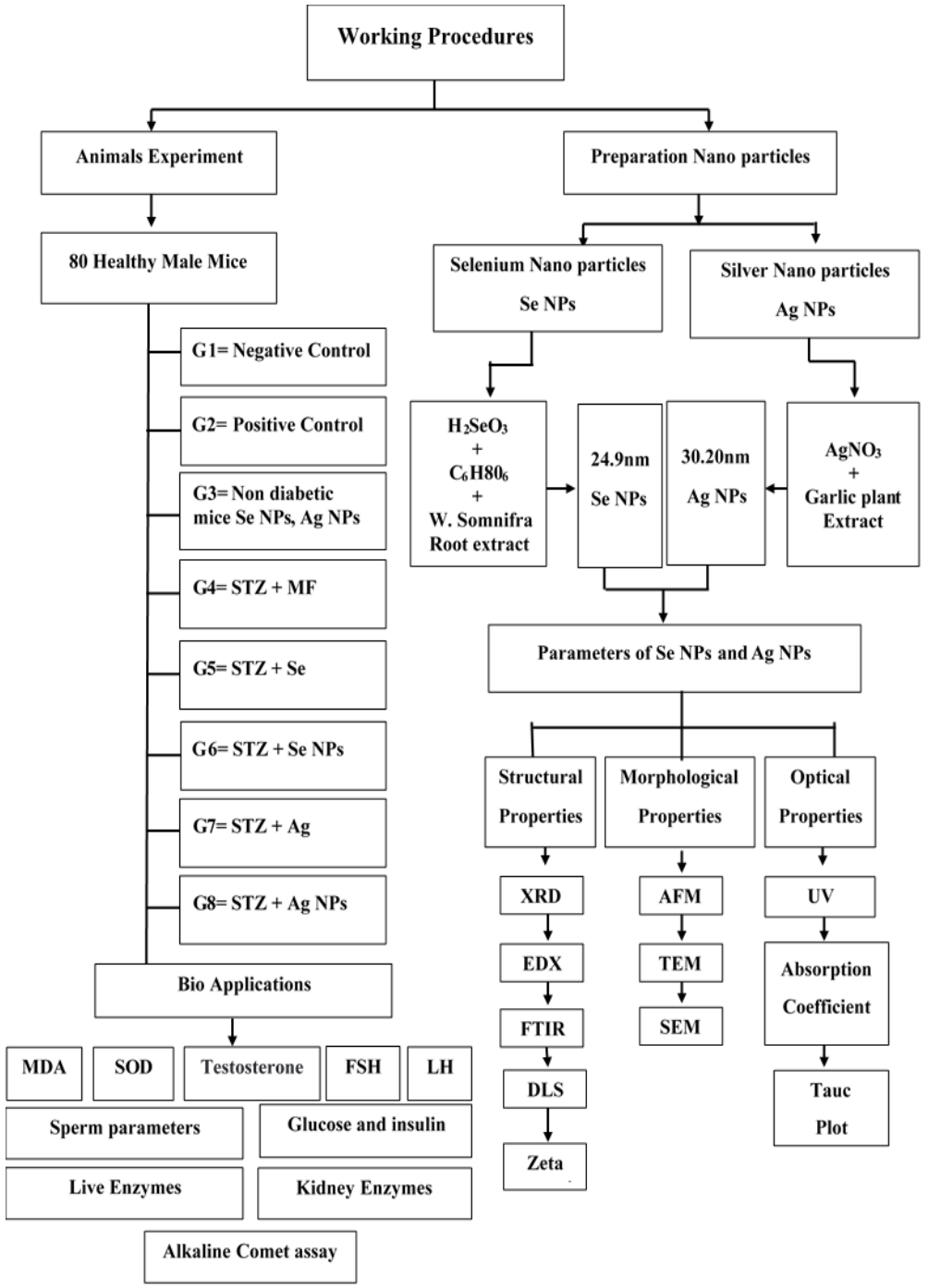

Fig (3-1). Schematic working Procedures

Table (3-3). Kit used in the study with their countries

Kit	Company / Origin
Comet Assay Kit	Cell Bio labs, ISN/USA
Cholesterol kit	Agape/India
Glucose kit	Agape/India
Insulin kit	Fine Test/China
MDA Kit	Cohesion/China
TAC Kit	Cohesion/China
SOD	Cohesion/China

3.3: Nanomaterial preparation

3.3.1: Synthesis of selenium nanoparticle

3.3.1.1 Withania somnifera

We bought *withania somnifera* from Baghdad market. The herbalist classified it in the Department of Life Sciences / College of Science / University of Baghdad, confirming that it is from the Solanaceae family.

3.3.1.2 Preparation of aqueous extract of Withania somnifera medicinal plant

The plant's roots After the plant's roots had been washed many times with distilled water and dried for 24 h, they were then processed in a standard mill to make *withania somnifera* extract. 10 g of ground plant roots were taken and 100 mL of deionized water was added, which is of very high purity so it has been used for its great advantages in various fields. The contents were mixed by stirring for 10 min at a temperature of 40-45 °C and then left to cool at a temperature the room. The aqueous extract of the plant was filtered using Whatman no. 1 filter paper and then centrifuge for 15 min. By removing only the supernatant, it was filtered. Figure (3-2) show the *withania somnifera* extracts.

3.3.1.3 Green synthesis of selenium nanoparticles from *withania somnifera* solution

The procedure of preparation was carried out in accordance with (Xue et al., 2007; Von White et al., 2012) with a few changes (Lenzen, 2008; Xue et al., 2007; Von White et al., 2012). 10% plant extract, 10 mL was mixed with 0.14 g of 100 mL of splenius acid as a solution, 15 min at 40-45 °C with constant stirring and a magnetic stirrer (600 rpm). at a moderate temperature, at the same time it was taken with 50 mg of ascorbic acid powder and dissolved in 50 mL of deionized water ions. Ascorbic acid (10 mL) was added to the mixture. Pipette for 30 min at 40-45 °C until the solution turns reddish-orange in color.

Fig (3-2). Withania somnifera extracts

The latter was used as an initiator for the reduction reaction. A little amount (1 mL) of the solution is added after it has had time to cool is used to be examined using ultraviolet rays. After a 24-h incubation period for the nano-solution, the solution was centrifuged at 10,000 rpm for 20 min. The precipitate was taken and the granules washed with distilled water and then absolute ethanol was applied several times until the granules were dried for 4 h in a 100°C oven. To keep the red Se NPs particles safe until use, PBS solution was used to suspend them See Figure (3-3).

3.3.2: Synthesis of silver nanoparticles

3.3.2.1 Garlic Plant

Fresh garlic was obtained from the supermarket. An herbalist at the College of Science/University of Baghdad identified the plant as being a member of the Amaryllidaceae family and Allium sativum L. Plant sample .

Fig (3-3). Selenium nanoparticles formation

3.3.2.2. Preparation of aqueous extract of medicinal *garlic*

Fresh *garlic* after washing was used The plant was washed multiple times with deionized water (DIW) to get rid of the dust, and after that it was allowed to air dry to get rid of any remaining moisture. An ordinary grinder was used to grind the dry *garlic*. A magnetic stirrer was used to mix 15 g of finely ground *garlic* powder into 500 mL of very pure DIW for 30 min when the temperature was 100 °C. The solution was then purified by filtering it through filter paper and centrifuging it for 30 min at 4000 rpm to get rid of any contaminants. To prepare silver nanoparticles later, the extract is refrigerated in the refrigerator (Anderson et al., 2018) See Figure (3-4).

3.3.2.3 Green synthesis of silver nanoparticles from medicinal *garlic* solution

Commercially purchased silver nitrate (molecular weight 169.87) was used to prepare a 1 mM concentration of silver nitrate solution. The preparation was done in line with (Payton et al., 2017; Kim et al., 2021) with a few changes. A magnetic stirrer running at 600 rpm for 30 min was used to dissolve 2 g of silver nitrate powder in 25 mL of distilled water. This procedure was carried out following the addition of 25 mL of garlic extract progressively to the silver nitrate solution while it was continuously magnetically stirred for an hour at 80 °C. After then, the solution turns black and takes the form of a

precipitate. The solution was allowed to stand for a whole night before the precipitate was separated by a centrifuge and repeatedly rinsed with ethanol and water. The precipitate was dried for 4 h in an oven at 85 °C. See Figure (3-5).

Fig (3-4). Garlic extract

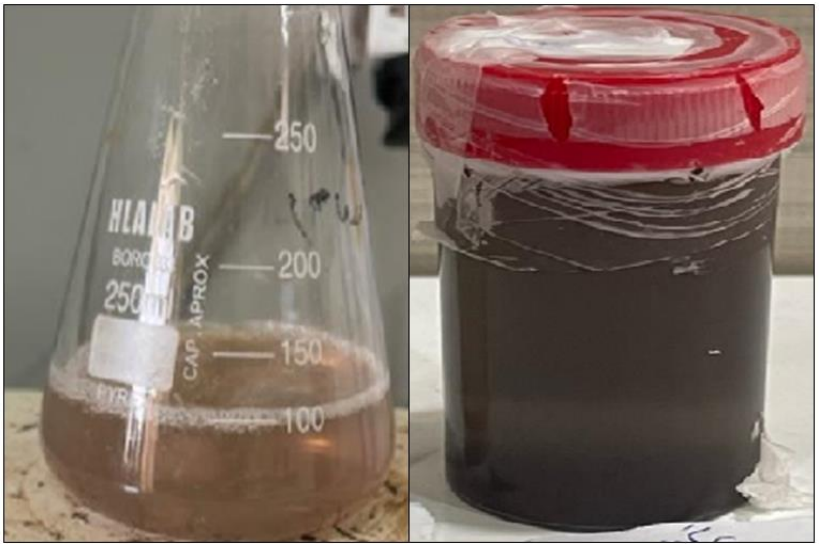

Fig (3-5). Silver Nanoparticles

3.4. Characterization of selenium and silver, nanoparticles

In order to comprehend the morphology, structure, and optical characteristics of aggregated nanoparticles as well as to establish the dimensions of nanoparticles and classify them accordingly. The following is a summary of the many measures that were employed.

3.4.1: (XRD) X-Ray diffraction analysis

The XRD measurements of reduced performance Ag NPs and Se NPs were recorded on an X-ray diffractometer instrument operated at a voltage of 40 kV and a current of 30 mA with CuK (α) radiation for crystal phase determination and material identification. The sample was examined by placing the sample in a centrifuge at 10,000 rpm for 15 min. The precipitate was collected and the resulting granules were dried at 50 °C in an oven. The samples were taken in coverslips and placed under an instrument for analysis. The generator voltage and current were set at 40 kV and 30 mA, respectively. Nanoparticles were scanned in the 2° range from 15 to 70 °C in continuous scanning mode. The scan rate was 0.04°/sec. Phases in the sample were determined using the search matching tool available with the Philips X'pert High Score software.

3.4.2: Field Emission Scanning Electron Microscopes (FE-SEM)

Field emission scanning electron microscopes were used for the analysis. This test was performed to characterize and determine the morphology and shape of the formed nanoparticles. This assay is very effective in finding accurate analysis of solid inorganic samples and determining the shape of nanoparticles. Using a scanning electron microscope (EDS-Mapping-Line-EBSD) made in Germany. The assay was performed after placing the sample in a centrifuge with a spin speed of 10,000 rpm for 15 min, after which the sample was washed with distilled water and dried at 50°C. The sample was placed on a platinum grid covered with palladium, and the sample was analyzed by the radiation passing through the sample and analyzed by the enlarged image resulting from the electronic radiation passing through the sample. A structural analysis of the sample was performed. The particle size distribution and stability of the nanoparticles were measured by preparing a thin film of NPs powder. The energy of the electron beam ranges from 10 keV to 30 keV and is focused into a beam with a very small spot size by two condensing lenses.

3.4.3: Measurements for Transmission Electron Microscopy (TEM)

It is a very powerful technique in materials science that can be described by a beam of high-energy electrons passing through very thin samples. Samples were prepared for TEM analysis using an Instrument ZEISS LE0912 AB/Germany, an analytical

microscope used to characterize various materials. Some nanoparticle droplets were applied to form a partially transparent layer on carbon-coated TEM copper grids. The sample is covered by the electron beam's shadow after drying for 1 min is shown and recorded digitally (Khan et al., 2019; Khan et al., 2020).

3.4.4: Atomic Force Microscopy (AFM) analysis

The surface morphology of the nanoparticles was visualized by atomic force microscopy contact mode, under a normal atmosphere Circumstances. AFM analysis was performed using AA3000 stent microscopy. A small drop of this sample was placed on a glass slide (2 x 1 cm) to dry. Then the slide was placed on the AFM sample stage.AFM micrographs could provide 3-D and 2-D image information for all studied samples, ruggedness and grain size.

3.4.5: Dynamic light scattering (DLS) Analysis

Average dimension of complex AgNPs and SeNPs. Malvern Zeta sizer from Origin/Germany was utilized to determine it using dynamic light scattering (DLS) and its multiple scattering laser diffraction method.

3.4.6: Zeta Potential Measurement

The surface charge of Ag NPs and Se NPs was determined by measurement of the potential of Zeta. Zeta potentials were determined using a 300 HAS. Zetaser Based on photon correlation spectroscopy. The analysis time was 60 seconds, average Zeta potential has been determined. Zeta potentials of both Ag NPs and Se NPs. The dispersion was determined as such without dilution.

3.4.7: UV-visible absorption spectrophotometer

Absorption spectra were measured by dual-beam spectrophotometer utilizing a Japanese-made Shimadzu UV-Visible spectrometer. All spectra were measured at room temperature in a quartz cell with a resolution of 1 nm in 2 mL and an optical path of 1 cm. Distilled, deionized water was used absorbances were taken from 300-800 nm at 475 nm/min scanning speed. UV-visible absorbance spectra of all samples were recorded using “UV Winlab” software for recording and data analysis. Base correction was performed for a spectrophotometer using a reference blank. The digital data were recorded using a Shimadzu UV-Visible spectrometer.

3.4.8: Energy-dispersive X-ray (EDX) spectroscopy

The energy dispersive X-ray (EDX) spectroscopy can provide information on the chemical composition, the detection of particular elements and the relative proportions of a sample.

3.5: Biological activity testing of Se NPs and Ag NPs

3.5.1: Animals experiment

Eighty healthy male albino mice weighing have the rang about 30 ± 5 g used in the experiment were purchased from Biotechnology Research Center/Al-Nahrain University. All animals were kept in standard conditions of 22 ± 3 °C with a constant 12 h dark and 12 h light exposure cycle, and in a controlled environment at an equilibrium humidity of 50 ± 5%. The animals were left for a week to acclimatize to the experimental conditions while being provided with the standard healthy diet of food and water. The experiment was conducted in the animal house of Al-Nahrain University.

3.5.2: Stimulating experimental diabetes mellitus in albino mice

Diabetes mellitus was induced in all male albino mice, except for the healthy control group, by giving them a single dose of fresh streptozotocin after dissolving it in saline in an amount (200 mg/kg) of body weight. This dose stimulated diabetes mellitus in male mice, where hyperglycemia was measured by measuring blood glucose 3-6 days after streptozotocin administration. Using a glucose meter, blood was drawn from the tail vein of mice, white mice that showed a blood glucose level above 245 mg/dL were taken, and with this methodology these animals alone were selected for the current study [139, 140].

3.5.3: Experimental design

Eighty male mice were randomly divided into eight groups (ten mice for each group) as follows: The first group (G-1) As mice were given Normal Saline by IP for 35 days, this group acted as a negative control; the second group (G-2) This group served as a STZ (50 mg/kg body weight/day) positive control; Group III (G-3) healthy, non-diabetic mice were treated intraperitoneally (IP) with the studied daily dose (nanoparticles, Se NPs, Ag or Ag NPs at a high dose of (10 mg/kg) for 35 days; group IV (G-4) This group's diabetic mice received oral administration of conventional metformin (200 mg/kg) for 35 days; group V (G-5) treated with Se by intraperitoneal injection of (200 mg/kg) Se for 35 days; group VI (G-6)) treated with Se NPs once daily at (2 mg/kg) for 35 days; the seventh (G-7) was treated with Ag once daily at a dose of (200 mg/kg) for 35 days; and the eighth (G-8) was treated with Ag NPs (2 mg/kg) for 35 days, Table (3-4).

Table (3-4). Groups of mice used *in vivo* study

Groups	No. of infected mice	Treatment
G1	10	uninfected &untreated.
G2	10	Infected &untreated.
G3	10	uninfected &treated with (IP, Se, Se NPs, Ag or Ag NPs).
G4	10	Infected &treated with dose of metformin (200) mg/kg.
G5	10	Infected &treated with dose of Se (200) mg/kg.
G6	10	Infected &treated with dose of Se NPs (2) mg/kg.
G7	10	Infected &treated with dose of Ag (200) mg/kg.
G8	10	Infected &treated with dose of Ag NPs (2) mg/kg.

3.5.4: blood collection method

Blood samples were collected from direct cardiac puncture. Finally, the blood sample was shaken slightly and then placed in a centrifuge at 3000 rpm for 5 min to obtain blood serum samples. The serum was kept in the freezer at -21°C until used See Figure (3-6).

3.5.5: The method of isolating cells

An easy method was used to isolate semen from testes of male mice using spinal dislocation method. Mice were sacrificed using the method indicated in (Tice et al., 2000). The mice were fixed on a dissection board and the animal's abdomen was washed with ethanol. A central and vertical incision was made using forceps and scissors. The caudal epididymis was cut and placed in a small container containing 2 mL of PBS and carefully mashed using laboratory scissors. A drop of semen was taken and placed on a clean, dry slide, See Figure (3-7) , then 3 drops of eosin spot were mixed and spread with another slide and left until microscopy (Burlinson, 2012).

Fig (3-6). Blood collection from direct cardiac puncture

Fig (3-7). The method of isolating cells

3.5.6: Sample preparation for comet assay

24 h before removal, slides were prepared. After being dissolved in Eppendorf at a temperature of 100 °C and then transferred to a water bath at a more moderate temperature of 37 °C, $250\mu l$ of US-made LM agarose wax from Cambrex/Bioscienc. A sample of $10\mu l$ of sperm cells was put to the agarose wax. On the glass slides, $50\mu l$ of the combination (cells plus agarose) was applied. To prevent the agarose from breaking while raising the lid, slides are set on ice. Slides were submerged with Complication G (cell lysis) and Solution 2. It is the arrangement that analyzes and breaks down cells, killing layers and proteins bound to DNA at a pH of more prominent than 13 (kept in for

at least 24 h). The slides were then pulled out and sequentially dipped into the second solution, which draws a comet indicative of a pH more than 13, which is made by the American company Sigma/Aldrich (200 mM NaOH, 1 mM EDTA). At 40 V and 60 min, the transfer of the harmed DNA starts and moves toward the anode See Figure (3-8). One possible indicator of the degree of DNA damage is the distance between the organism's head and tail (Walsh & Kato, 2022; Zhang et al., 2023). Utilizing the comet scoring tool, DNA migration and picture drawing were evaluated, as well as tail length (px), tail DNA (%), and tail mean moment (Qiao et al., 2023; Paradizo et al., 2023).

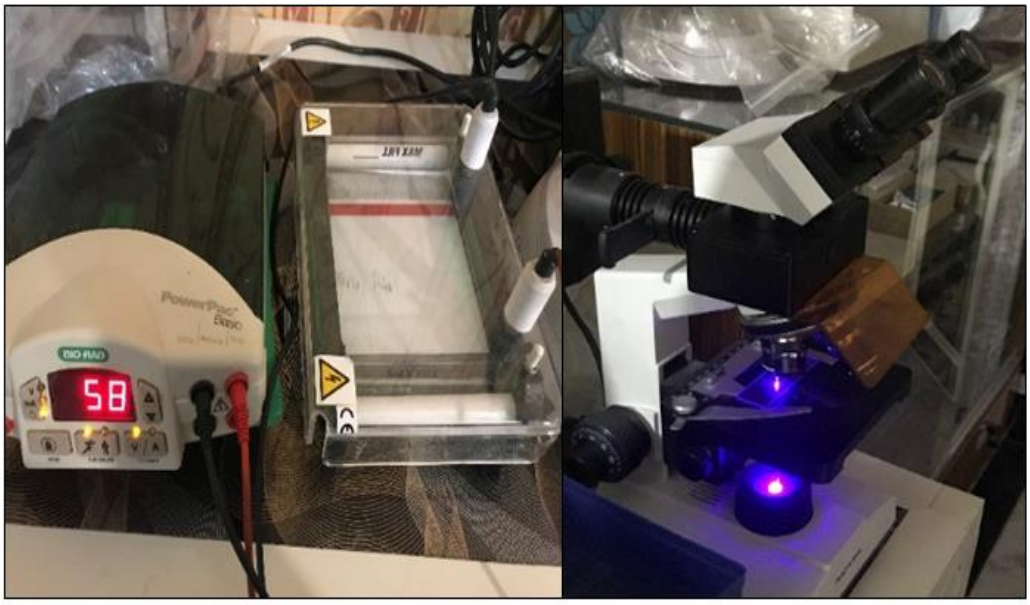

Fig (3-8). Gel electrophoresis

3.6: Biochemical measurements

3.6.1: Comet assay

DNA damage was assessed using the comet test. The experiment was carried out using an Oxiselect Comet Assay Kit (She et al., 2023).

- **Prepare the Reagent**

Asterisk-denoted reagents must be prepared right away before use. When handling any chemical chemicals, put on gloves, a lab coat, and goggles for protection.

- **1X PBS, Ca^{++} and Mg^{++} free**

10X Phosphate-Buffered Saline (PBS) was diluted with deionized water to prepared 1X PBS and stored at room temperature (10X PBS is available from Trevigen).

- **Lysis Solution**

For up to 10 slides (2 samples per slide) were prepared:

1. Lysis Solution 40 mL
2. Dimethyl Sulfoxide (DMSO) (optional) 4 mL

Must be kept on ice or at a temperature of 4°C for at least 20 min before to usage. Only samples containing heme, such as blood cells or tissue samples, must also contain DMSO; adding it is optional. The buffer's composition is secret.

- **200 mM NaOH, 1 mM EDTA Alkaline Unwinding Solution, pH > 13**

When making and handling the Alkaline Unwinding Solution, gloves should be worn. To make 50 mL of alkaline solution, combine:

1. NaOH Pellets 0.4 mg
2. 200 mM EDTA 250 μL
3. dH2O 49.75 mL

It should be stirred until fully dissolved. The solution should warm during preparation. The solution was allowed to cool at room temperature before use.

- **Solution for SYBR Green Staining**

When kept at 4°C and kept in the dark, the diluted stock is stable for a few weeks.
10,000X SYBR Green in DMSO 1 μL

- **Comet LM Agarose**

The Comet LM Agarose was used once molten. The cap was loosed to allow for expansion then heat the bottle in a 90–100 °C water bath for 5 min, or until the agarose is molten (Caution: Microwaving is not recommended). Place the bottle was placed in a 37 °C water bath for at least 20 min to cool. The LM Agarose should remain molten at 37 °C for sample preparation indefinitely. The LMA agarose formulation is proprietary.

- **Alkaline Unwinding Solution, pH>13 (200 mM NaOH, 1 mM EDTA) for the Comet Assay ES system:**

Prepared was a stock solution containing 500 mM EDTA. For 1 liter of the electrophoresis mixture:

- **NaOH pellets 8 gm**
- **500 mM EDTA**
- **dH2O (after NaOH is dissolved) added to: 1 liter**

Freshly made solution is recommended for use. Cool at 4°C.

Assay Protocol

The sensitivity of the assay is dependent on the electrophoresis parameters utilized. The Alkaline Comet Assay detects single and double-stranded DNA breaks, the majority of basic sites, and alkali labile DNA adducts (such as phosphoglycols and phosphotriesters), while the Neutral Comet Assay only detects double-stranded DNA breaks.

Alkaline comet assay

1. Before use, the lysis solution was produced and allowed to chill at 4 °C for at least 20 min.
2. With the cap looseened, LM Agarose was melted in a beaker of hot water for 5 min. For at least 20 min, a bottle was immersed in a bath of 37 °C water to chill.
3. Cells were mixed at a 1:10 (v/v) ratio with molten LM Agarose (at 37 °C) and pipetted $50\mu l$ onto Comet Slide right away. To achieve comprehensive covering of the sample area, agarose/cells were spread over it as needed using the side of the pipette tip. Before applying the sample, the slide will be warmed at 37 °C if it is not spreading evenly.
4. Flat Slides were left at 4 °C in the dark for 10 min (for example, in a refrigerator). At the margin of the Comet Slide area, a 0.5 mm transparent ring can be seen. In situations with high humidity, improving sample adhesion requires increasing the gelling time to 30 min.
5. For 30 to 60 min, slides were submerged in 4 °C Lysis Solution. It should be incubated at 4 °C for the entire night in order to increase sensitivity or for convenience.
6. Extra buffer was removed from slides before they were dipped into freshly made Alkaline Unwinding Solution, pH>13. When preparing or handling this solution, gloves should be worn.
7. In the dark, Alkaline Unwinding Solution was submerged in Comet Slide for 20 min at ambient temperature or for an hour at 4 °C.
8. Slides were placed in an electrophoresis slide tray with labels next to the black cathode and coated with Slide Tray Overlay for the Comet Assay electrophoresis (ES-unit). Approximately 850 mL of 4 °C Alkaline Electrophoresis Solution was also added. The voltage was applied for 30 min with the power supply set to 21 volts.

9. Extra electrophoresis solution was gently drained and submerged twice for 5 min each in dH2O before being submerged in 70% ethanol for 5 min.
10. Samples were dried for 10 to 15 min at 37 °C. Drying arranges all of the cells into a flat plane to make observation easier. Before scoring at this point, samples must be held at room temperature with desiccant.
11. Stained each dried agarose circle with $100\mu l$ of diluted SYBR Green for 30 min. at room temperature and in the dark. Slide was briefly rinsed in water after being gently tapped to remove any surplus SYBR solution. At 37 °C, the slides were totally dry.
12. Fluorescence microscopy was used to examine the slides. (The highest excitation/emission for SYBR Green is 496 nm/522 nm. Fluorescein filter works well.

For each sample, 50 randomly chosen cells were counted in order to determine the comet cell's size. The Comet Index (CI) was calculated using the ratio of the L/W comet., the scoring ranges from 1.2 to 2 for low DNA damage (LD), 2.1 to 3 for medium DNA damage (MD), and up to 3 for significant DNA damage (HD).Three parameters were estimated to indicate DNA migration using image analysis software, including tail length (the distance from the head center to the end of the tail), mean tail moment (the product of the tail DNA/total DNA by the tail center of gravity), and tail DNA%=100X Tail DNA Intensity/Cell DNA Intensity.

3.6.2. Sperm parameter

3.6.2.1. Sperm motility

The epididymis was separated, and its two tails were used to harvest spermatozoa. They were cut into small pieces with a sharp knife and forceps, added to a petri dish with 1 mL PBS (Ph 7.4), and then incubated at 37 °C for 30 min. To analyze sperm motility, pipette drops of the solution should be applied to glass slides and covered with a cover slide. The motility was determined using (Shiragannavar et al., 2023) by using the following formula:

$$\text{Motility (\%)} = \frac{\text{No. of motile sperms}}{\text{Total No. of sperms}} \times 100 \qquad (3.1)$$

3.6.2.2. Sperm viability percent

The following percentages of living sperms were calculated using the method described by (Shiragannavar et al., 2023). A drop of the sperm suspension was applied to the slide, followed by a drop of the eosin stain, which was mixed with the sperm suspension drop before being spread out and allowed to dry. After counting 100 sperms, it was noted that

the red-stained spermatozoa, which are alive spermatozoa, can be separated from the unstained spermatozoa, which are dead spermatozoa. The following equations were used to determine the proportion of viable sperm.

$$\text{Viability (\%)} = \frac{No.of\ Living\ sperms}{Total\ No.of\ sperms} \times 100 \qquad (3.2)$$

3.6.2.3. Abnormal sperm morphology percent

The defective sperm morphologies displayed a deformed head, tail, or both, and were distinct from the normal sperm shapes. Use the same slide that was used to determine sperm viability to determine the sperm abnormalities, suggests (Shiragannavar et al., 2023) formula:

$$\text{Abnormality (\%)} = \frac{No.of\ abnormal\ sperms}{Total\ No.of\ sperms} \times 100 \qquad (3.3)$$

3.6.3. Luteinizing hormone, follicle-stimulating hormone and testosterone level

3.6.3.1. Testosterone Test System

The Quantitative Determination of Total Testosterone Concentration in Human Serum or Plasma by a Microplate Enzyme Immunoassay

- **Principle**

Competitive Enzyme Immunoassay (TYPE 7): The essential reagents required for an enzyme immunoassay include antibody, enzyme-antigen conjugate and native antigen. Upon mixing biotinylated antibody, enzyme-antigen conjugate and a serum containing the native antigen, a competition reaction results between the native antigen and the enzyme-antigen conjugate for a limited number of antibody binding sites. The interaction is illustrated by the followed equation (Hartmann et al., 2022).

A simultaneous reaction between the biotin attached to the antibody and the streptavidin immobilized on the microwell occurs. This effect the separation of the antibody bound fraction after decantation or aspiration. $AgAb_{Btn}$ + $^{Enz}AgAb_{Btn}$ + $Streptavidin_{CW}$ ⇒ immobilized complex $Streptavidin_{CW}$ = Streptavidin immobilized on well Immobilized complex = sandwich complex bound to the solid surface.

The enzyme activity in the antibody bound fraction is inversely proportional to the native antigen concentration. By utilizing several different serum references of known antigen concentration, a dose response curve can be generated from which the antigen concentration of an unknown can be ascertained.

$$^{Enz}Ag + Ag + Ab_{Btn} + \underset{k_{-a}}{\overset{k_a}{\rightleftharpoons}} A\,Ab_{bin} + {}^{Enz}AgAb_{bin} \quad (3.4)$$

^{Enz}Ag: Enzyme Aantigen Conjugate (Constant Quantity)
Ag : Native Antigen (Variable Quantity)
Ab_{Btn} : Biotinylated Antibody (Constant Quantity)
$AgAb_{Btn}$=Antigen-Antibody Complex
^{Enz}Ag Ab_{Btn}=Enzyme Antigen Conjugate-Antibody Complex
K_a=Rate Constant of Association
K_{-a}=Rate Constant of Disassociation
K=K_a/K_{-a}=Equilibrium Constant

- **Calculation of Results**

To determine the testosterone content in unidentified specimens, a dosage response curve is employed.

1. The absorbance determined from the microplate reader's printout.

2. On a piece of linear graph paper, plot the absorbance for every duplicate serum reference against the matching Testosterone concentration in ng/ml (do not average the duplicate serum references prior to plotting).

3. Use a best-fit curve to join the points together.

4. To find the intersection point on the curve and read the concentration (in ng/ml) from the horizontal axis of the graph, find the average absorbance of the duplicates for each unknown on the vertical axis of the graph. The duplicates of the unknown may be averaged as indicated. The average absorbance (1.764) in the example below crosses the dosage response curve at (0.57 μg/ml). concentration of testosterone .

3.6.3.2. Follicle Stimulating Hormone (FSH) test system

The Microplate Immunoenzymometric Assay for the Quantitative Determination of Follicle Stimulating Hormone Concentration in Human Serum (IEMA/ ELISA).

Principle

Immunoenzymometric assay (TYPE 3) PRINCIPLES High affinity and specificity antibodies (enzyme and immobilized), with various and diverse epitope recognition, in excess, and native antigen are necessary reagents for an immunoenzymometric assay. In

this approach, the streptavidin coating on the well and the exogenously added biotinylated monoclonal anti-FSH antibody interact to immobilize the sample during the experiment at the surface of a microplate well. Native antigen reacts with the antibodies without competition or steric hindrance to produce a soluble sandwich complex when a monoclonal biotinylated antibody, an enzyme labeled antibody, and a serum containing the antigen are combined. The following equation serves as an example of the interaction. [(Ponzano et al., 2023):

$$^{Enz}Ab_{(p)} + Ag_{FSH} + {}^{Btn}Ab_{(m)} \underset{k_{-a}}{\overset{k_a}{\rightleftharpoons}} {}^{Enz}Ab_{(p)} - Ag_{FSH} - {}^{Btn}Ab_{(m)} \qquad (3.5)$$

$^{Btn}\mathbf{Ab_{(m)}}$ =Biotinylated Monoclonal Antibody (Excess Quantity)
$\mathbf{Ag_{FSH}}$ =Native Antigen (Variable Quantity)
$^{Enz}\mathbf{Ab_{(p)}}$ =Enzyme Lebed Antibody (Excise Quantity)
$^{Enz}\mathbf{Ab_{(p)}}\mathbf{-Ag_{FSH}-}\,^{Btn}\mathbf{Ab_{(m)}}$ =Antigen-Antibodies Sandwich Complex
$\mathbf{K_a}$=Rate Constant of Association
$\mathbf{K_{-a}}$=Rate Constant of Disassociation

high affinity reaction of streptavidin and biotinylated antibody. This interaction is illustrated below: $^{Enz}Ab_{(p)}\text{-}Ag_{FSH}\text{-}^{Btn}Ab_{(m)}$+$Streptavidin_{C.W.}$ ⇒ Immobilized complex $Streptavidin_{C.W.}$ = Streptavidin immobolized on well Immobilized complex = sandwich complex bound to the solid surface

After equilibrium is attained, the antibody-bound fraction is separated from unbound antigen by decantation or aspiration. The enzyme activity in the antibody-bound fraction is directly proportional to the native antigen concentration. By utilizing several different serum references of known antigen values, a dose response curve can be generated from which the antigen concentration of an unknown can be ascertained.

- **Preparation:**

The specimens shall be blood, serum in type and the usual precautions in the collection of venipuncture samples should be observed. For accurate comparison to established normal values, a fasting morning serum sample should be obtained. The blood should be collected in a plain redtop venipuncture tube without additives or anti-coagulants. Allow the blood to clot. Centrifuge the specimen to separate the serum from the cells. Samples may be refrigerated at 2-8 ^{o}C for a maximum period of 5 days. If the specimen(s) cannot be assayed within this time, the sample(s) may be stored at temperatures of -20 ^{o}C for up to 30 days. Avoid use of contaminated devices. Avoid repetitive freezing and thawing. When assayed in duplicate 0.100 mL of the specimen is required.

➢ **Calculation of results**

A dose response curve is used to ascertain the concentration of follicle stimulating hormone in unknown specimens.

1. Record the absorbance obtained from the printout of the microplate reader.
2. Plot the absorbance for each duplicate serum reference versus the corresponding FSH concentration in mIU/ml on linear graph paper (do not average the duplicates of the serum references before plotting).
3. Draw the best-fit curve through the plotted points.
4. To determine the concentration of FSH for an unknown, locate the average absorbance of the duplicates for each unknown on the vertical axis of the graph, find the intersecting point on the curve, and read the concentration (in mIU/ml) from the horizontal axis of the graph (the duplicates of the unknown may be averaged as indicated). In the following example, the average absorbance (1.214) intersects the dose response curve at (43.2 mIU/ml) FSH concentration .

3.6.3.3 Luteinizing Hormone (LH) test system

The Quantitative Determination of Luteinizing Hormone Concentration in Human Serum by a Microplate Enzyme Immunoassay, Colorimetric.

➢ **Principle**

Immunoenzymometric assay (TYPE 3): High affinity and specificity antibodies (enzyme and immobilized), with varied and distinct epitope recognition, in excess, and native antigen are the essential reagents needed for an immunoenzymometric assay. The streptavidin coating on the well and the exogenously added biotinylated monoclonal anti-LH antibody interact in this approach to immobilize the sample during the experiment at the surface of a microplate well. The native antigen reacts with the biotinylated monoclonal antibody, the enzyme-labeled antibody, and a serum carrying the native antigen without competition or steric hindrance to produce a soluble sandwich complex. The following equation serves as an example of the interaction. (Rashid et al., 2021)

$$^{Enz}\square Ab_{(p)} + Ag_{LH} + {}^{Btn}\square Ab_{(m)} \underset{k_{-a}}{\overset{k_a}{\rightleftharpoons}} {}^{Enz}\square Ab_{(p)} - Ag_{LH} - + {}^{Bth}\square Ab_{m} \qquad (3.6)$$

$^{Btn}Ab_{(m)}$ =Biotinylated Monoclonal Antibody (Excess Quantity)
Ag_{LH} =Native Antigen (Variable Quantity)
$^{Enz}Ab_{(p)}$ =Enzyme labeled Antibody (Excess Quantity)
$^{Enz}Ab_{(p)} - Ag_{LH} - {}^{Btn}Ab_{(m)}$ =Antigen-Antibodies Sandwich Complex
Ka =Rate Constant of Association

$\mathbf{K_{-a}}$ =Rate Constant of Dissociation

Through a simultaneous high affinity process involving streptavidin and a biotinylated antibody, the complex is deposited into the well. Below is an illustration of this interaction:

$^{Enz}Ab_{(p)}$ -Ag_{LH} - $^{Btn}Ab_{(m)}$ + $Streptavidin_{C.W.}$ ⇒ Immobilized complex $Streptavidin_{C.W.}$ = Streptavidin immobolized on well Immobilized complex = Antibodies-Antigen sandwich bound. After equilibrium is attained, the antibody-bound fraction is separated from unbound antigen by decantation or aspiration. The enzyme activity in the antibody-bound fraction is directly proportional to the native antigen concentration. A dosage response curve can be produced and used to determine the antigen concentration of an unknown by using many different serum standards for known antigen values.

- **Preparation**

1. Clean Buffer Fill a suitable storage container halfway with distilled or deionized water, then add the contents of the wash concentrate. Store for up to 60 days at 2-30 °C.
2. Solution for Working Substrate Solution 'A' from the amber vial should be added to Solution 'B' in the clear vial. To make the clear vial easier to identify, put the yellow cap on it. Mix and label as necessary. Store between 2 and 8 °C.

- **Calculation of results**

A dose response curve is used to ascertain the concentration of luteinizing hormone (LH) in unknown specimens.

1. Record the absorbance obtained from the printout of the microplate reader as outlined.
2. Plot the absorbance for each duplicate serum reference versus the corresponding LH concentration in mIU/ml on linear graph paper (do not average the duplicates of the serum references before plotting).
3. Draw the best-fit curve through the plotted points.
4. To determine the concentration of LH for an unknown, locate the average absorbance of the duplicates for each unknown on the vertical axis of the graph, find the intersecting point on the curve, and read the concentration (in mIU/ml) from the horizontal axis of the graph (the duplicates of the unknown may be averaged as indicated). In the following example, the average absorbance (1.005) intersects the dose response curve at 42.7 mIU/ml LH concentration.

3.6.4: Malondialdehyde (MDA) and Super Oxide Dismutase (SOD) level on control and treated groups

3.6.4.1. Superoxide Dismutase's Activity (SOD ELISA Kit)

Superoxide Dismutase (SOD) catalyze the dismutation of the superoxide radical (O_2) into hydrogen peroxide (H_2O_2) and elemental oxygen (O_2), and as such, provides an important defense against the toxicity of superoxide radical. SOD1 and SOD2 - deficient mice spontaneously develop liver cancer and are prone to develop tumors, whereas over expression of SOD protects tumor cells from apoptosis. Superoxide Dismutase Microplate Assay Kit, ions generated from the conversion of xanthine to uric acid, and hydrogen peroxide by xanthine oxidase (XOD), convert NBT to NBT-diformazan. NBT-diformazan absorbs light at 560 nm. SODs reduce superoxide ion concentrations and thereby lower the rate of NBT-diformazan formation. The extent of reduction in the appearance of NBT-diformazan is a measure of SOD activity present in experimental samples(Cittrarasu et al., 2021).

- **Sample preparation**

  From serum or plasma samples Detect directly.

- **Procedure:**

Reagent	Sample	Standard	Blank
Reaction Buffer	30 μL	30 μL	30 μL
Substrate	100 μL	100 μL	100 μL
Enzyme	1 μL	1 μL	1 μL
Sample	19 μL	--	--
Standard	--	19 μL	--
Distilled water	--	--	19 μL
Dye Reagent	50 μL	50 μL	50 μL

- **Calculation**

According to the quantity of cells or bacteria

$SOD\ (U/104) = (C_{Standard} \times V_{Standard}) \times (OD_{Blank} - OD_{Sample}) / (OD_{Blank} - OD_{Standard}) / (V_{Sample} \times N / VAssay) = 30 \times (OD_{Blank} - OD_{Sample}) / (OD_{Blank} - OD_{Standard}) / N$

$C_{Protein}$: the protein concentration, mg/ml;

$C_{Standard}$: the standard activity, 30 U/ml;

W: the weight of sample, g;

$V_{Standard}$: the volume of standard, 0.019 ml;

V_{Sample}: the volume of sample, 0.019 ml;

V_{Assay}: the volume of Assay buffer, 1 ml;

N: the quantity of cell or bacteria, $N \times 10^4$.

3.6.4.2. Measurement of Malondialdehyde (MDA ELISA Kit)

Quantification of lipid peroxidation is essential to assess oxidative stress in pathophysiological processes. Lipid peroxidation forms Malondialdehyde (MDA) and 4-hydroxynonenal (4-HNE), as natural bi-products. Measuring the end products of lipid peroxidation is one of the most widely accepted assays for oxidative damage. MDA Microplate Assay Kit provides a convenient tool for sensitive detection of the MDA in a variety of samples. The MDA in the sample is reacted with Thiobarbituric Acid (TBA) to generate the MDA-TBA adduct. The MDA-TBA adduct can be easily quantified calorimetrically (λ = 532 nm) (Cittrarasu et al., 2021).

- **Sample preparation**

From serum or plasma samples Detect directly.

- **Procedure:**

Reagent	Sample
Sample	100 μL
Dye Reagent	200 μL
Mix, put it in the oven, 90 °C for 30 min, then put it on ice, centrifuged at 10000 g, 25 °C for 10 min. Add the supernatant into the microplate.	
The supernatant	200 μL
Record absorbance measured at 532 nm, 600 nm.	

Add following reagents in the micro centrifuge tubes:

- **Calculation**

According to the volume of serum or plasma MDA
(n mol/ml) = $[(OD_{532} - OD_{600}) \times V_{Total} / (\varepsilon \times d) \times 10^9] / V_{Sample} = 32.25 \times (OD\ 532 - OD\ 600)$

ε: molar extinction coefficient of MDA, 155×10^3L/mol/cm;

d: the well diameter of 96-Well microplate, 0.6 cm;
$C_{Protein}$: the protein concentration, mg/ml;
W: the weight of sample, g;
V_{Total}: the total volume of the enzymatic reaction, 0.3 ml;
V_{Sample}: the volume of sample, 0.1 ml;
V_{Assay}: the volume of Assay buffer, 1 ml;
N: the quantity of cell or bacteria, $N \times 10^4$.

3.6.5: Liver enzymes assay

This assay involved the evaluation of the activity of liver enzymes (ALT, AST).

3.6.5.1: Alanine aminotransferase (ALT)

The activity of this enzymes was evaluated in blood serum depending on colorimetric method by using enzyme kit produced from (Agape company) according to (Rahmah et al., 2021).

- **Procedure:**

Working reagent 1000 µL

Sample 100 µL

Mix and incubate at 37 °C for 1 min. Measure the change in absorbance per minute (ΔOD/min) during 3 min.

- **High Linearity Procedure**

Mix and incubate for 1 min at 37 °C. Read the change in absorbance per 20 sec during 1 min.

- **Calculation:**

$$\text{ALT activity (U/L)} = (\Delta OD/min) \times 1745$$

ΔOD = Change in optical density.

3.6.5.2: Aspartate aminotransferase (AST)

The AST enzyme activity was evaluated in mouse serum by using enzymatic colorimetric kit method according to [155].

- **Procedure:**

Working reagent 1000 µL

Sample 100 µL

Mix and incubate at 37 °C for1 minute. Measure the change in absorbance per minute (ΔOD/min) during 3 min.

- **High Linearity Procedure:**

Mix and incubate at for 1 min 37 °C. The change in absorbance read per 20 sec, during 1 minute.

- **Calculation:**

AST activity (U/L) = (ΔOD/min) x 1745

3.6.5.3: Alkaline phosphatase (ALP)

This was intended for in vitro quantitative determination of Alkaline Phosphatase in serum or plasma according to (Abbas et al., 2023)

- **Procedure:**

Working reagent 1000 µL

Sample 20 µL

Mix and incubate at 37 °C for one minute. The change in absorbance measure per minute (ΔOD/min) during 3 min.

- **Calculation:**

$$\text{ALP Activity (U/L)} = (\Delta OD / \text{min.}) \times 2750$$

3.6.6: Kidney enzymes

3.6.6.1. UREA U.V (S.L)

This reagent is intended for in vitro quantitative determination of urea in serum, plasma & urine. Proteins should be broken down in excess since the human body cannot store them. Ammonia is produced when amino acids, which are building blocks of proteins, break down. This is hazardous, therefore a series of chemical processes (referred to as the urea cycle) produce nontoxic urea, which is then released into the blood, filtered in the kidneys, and eliminated in the urine. Increased protein breakdown, dehydration, vomiting, and diarrhea are associated with elevated levels. Also present in any form of nephrotic syndrome, chronic nephritis, or glomerular nephritis. Low amounts are seen in pregnancy and liver failure.

- **Procedure**

	Standard	Sample
Working Reagent	1000 µL	1000 µL
Standard	10 µL	-
Sample	-	10 µL

Mix and read the optical density (T1) 30 seconds after the sample or standard addition. Take second reading (T2) exactly 60 seconds after the first reading.

- **Calculation**

$$\text{Urea Conc.}\left(\frac{\text{mg}}{\text{dL}}\right) = \frac{(T1 - T2)of\ sample}{(T1 - T2)of\ Standard} \times 50 \qquad (3.7)$$

$$\text{Urea BUN Conc.}\left(\frac{\text{mg}}{\text{dL}}\right) = \frac{(T1 - T2)of\ sample}{(T1 - T2)of\ Standard} \times 23.4 \qquad (3.8)$$

3.6.6.2: Albumin &Total Protein

This reagent is intended for *in vitro* quantitative determination of albumin in serum or plasma. Albumin synthesized in the liver makes up a large part of the total proteins in the body, the other part being globulins, and they make up the bulk of the solutes in the plasma. Albumin functions include extracellular fluid distribution, regulation of osmotic pressure, and acts as a transport agent for a variety of substances such as hormones, lipids, vitamins etc. Higher levels are noted in drought. Decreased levels are observed in liver diseases (hepatitis, cirrhosis), malnutrition, kidney disorders, increased fluid loss during severe burns, and malabsorption.

- **Procedure**

	Blank	Standard	Sample
Reagent	1000 µL	1000 µL	1000 µL
Standard	-	10 µL	-
Sample	-	-	10 µL

Mix and incubate for 1 minute. Measure absorbance of standard & sample against the reagent blank.

➢ **Calculation**

$$\text{Albumin Con. } \left(\frac{\text{g}}{\text{dL}}\right) = \frac{Absorbance\ of\ sample}{Absorbance\ of\ Standard} \times 3 \qquad (3.9)$$

3.6.6.3: Enzymatic creatinine

This reagent is intended for *in vitro* quantitative determination creatinine in serum or urine. Creatinine is formed in muscles from phosphocreatine. It is an important form of energy by being a store of high energy phosphate. Creatinine determinations have one advantage over urea determination that it is not affected by a high protein diet. Serum creatinine is more specific & sensitive indicator of renal function. Simultaneous estimations of serum urea & creatinine provides better information. Serum urea nitrogen & creatinine ratio is > 15 in prerenal failure & < 10 in renal failure. Decreased levels are found in muscle dystrophy.

➢ **Procedure**

	Blank	**Calibrator**	**Sample**
Reagent 1	450 µL	450 µL	450 µL
Calib./Std	-	10 µL	-
Sample	-	-	10 µL
	Mix and incubate for 5 min at 37 °C then add,		
Reagent 2	150 µL	150 µL	150 µL
Mix and incubate for 5 min at 37 °C. Measure the absorbance of sample and the standard against the reagent blank.			

➢ **Calculation**

$$\text{Creatinine Conc } \left(\frac{\text{mg}}{\text{dL}}\right) = \frac{Absorbance\ of\ sample}{Absorbance\ of\ Standard} \times standard\ conc \qquad (3.10)$$

3.6.7. Glucose and insulin concentration

3.6.7.1: Determination of serum glucose concentration

➢ **Procedure**

The Procedure is accorded to Dingeon *et al*. 1975 as follow:

1. Reagents (Tris Buffer in pH= 7.40 + 4- Amino phenazone + Glucose Oxidase + Phenol) and samples were brought to room temperature.

2. Reagents and samples were pipette into labeled tubes as follows:

Tubes	Blank	Sample	Standard
Working Reagent	1.0 mL	1.0 mL	1.0 mL
Sample		10 μL	
Standard			10 μL

3. The tubes were mixed and let stand 10 min at 5 min at 37 °C.

4. The absorbance (A) of the samples and the standard were red at 505 nm against the reagent blank.

The color was stable for about 2 h while protected from light.

- **Calculations:**

The sample is diluted with normal saline, the assay is repeated, and the result is multiplied by the dilution factor if the concentration is higher than linearity (600 mg/dL).

3.6.7.2 Determination of serum insulin

The Reagents (Lyophilized Standard+ Sample / Standard dilution buffer+ Biotin-detection antibody + Antibody dilution buffer+ HRP-Streptavidin Conjugate+ SABC dilution buffer+ TMB substrate+ Stop solution+ Wash buffer).

- **Procedure**

Equilibrate the SABC working solution and TMB substrate for at least 30 min at room temperature (37 °C) before adding to the wells. Samples and reagents must be thoroughly and uniformly mixed before being diluted. Plotting a standard curve for each test is advised.

1. Following the establishment of the standard, the positions of the tested sample and control (zero) wells on the pre-coated plate were recorded. It is advised to take duplicate measurements of each standard and sample. Before adding the standard, sample, and control (zero) wells, wash the plate twice.

2. Standard solutions at concentrations of 5000 pg/mL, 2500 pg/mL, 1250 pg/mL, 625 pg/mL, 312.5 pg/mL, 156.25 pg/mL, and 78.125 pg/mL were added to the standard wells.

3. The control (zero) well received 0.1 mL of Sample / Standard dilution buffer.

4. The test sample wells were filled with the 0.1 mL of adequately diluted sample (Rat serum, plasma, tissue homogenates, and other biological fluids).

5. The plate was covered and incubated for 90 min at 37 °C.

6. The plate's cover was taken off, and the contents were thrown away after being placed on absorbent filter papers or another absorbent substance. At no point did the wells dry out. The plate was not washed, either.

7. The standard, test sample, and zero wells were filled with the 0.1 mL of Biotin-detection antibody working solution. Each well's bottom was filled with the solution, but the side walls were left untouched.

8. The plate was covered and incubated for 60 min at 37 °C.

9. The lid was taken off, and a wash buffer was used to wash the plate three times.

10. Each well received 0.1 mL of the SABC working solution, and the plate was covered and incubated at 37 °C for 30 min.

11. The plate was washed five times with wash buffer, each time letting the wash buffer sit in the wells for 1-2 min after removing the cover.

12. Each well received 90 μL of TMB substrate before the plate was covered and incubated at 37 °C in the dark for 15–30 min. The first three to four wells (which contain the most concentrated INS standard solutions) exhibit shades of blue; the remaining wells lack any discernible color.

13. Each well received 50 μL of the Stop solution, which was added and properly mixed. The color immediately turns yellow.

14. After adding the stop solution, the O.D. was read in a microplate reader using absorbance at 450 nm.

3.7: Statistical analysis

The comes about were subjected to factual examination to recognize the contrasts between the diverse comes about of each of the silver and selenium nanoparticles. Sample methods were evaluated using ANOVA and the mean (Mean ± SD) was found. P values of 0.05 were considered statistically significant.

1. Using the statistical program 2010 SPSS and excel application to find the result and draw shapes with some effect.

Deep Science Publishing
https://doi.org/10.70593/978-93-49307-47-6

Chapter 4

Results and discussion

4.1: Results and discussion

This chapter includes the results and discussion of the structural, morphological and optical properties and biological activity of Ag NPs at (2 mg/kg body weight/day) concentration and Se NPs at (2 mg/kg body weight/day) concentration prepared from aqueous extract of *garlic* roots and *Withania somnifera* directly.

4.2: Parameters of selenium and silver nanoparticles

4.2.1: X-Ray Diffraction Studies (XRD)

The nuclear course of action, cross section characteristics and crystalline measure can all be decided utilizing the significant strategy of X-ray diffraction [157].Figure (4-1), appear the XRD design of the amalgamation of selenium nanoparticles (Se NPs); the XRD design appears multi peaks with distinctive intensities at 23.4º, 29.6 º, 41.2º, 43.5º, 45.3º, 51.6º, 55.8º, 61.5, 65.1, which correspond to planes (100), (101), (110), (102), (111), (201), (003), 022) and (210), respectively. This behavior refers to Se NPs and full agreement with JCPDS (01-073-0465); our result is in great assention with the distributed result by Cittrarasu et al. in 2021[44, 158]. The high crystallinity is exceptionally clear and the phase structure of nanoparticles could be a hexagonal. D is The average crystalline size of Se NPs was calculated from Bragg reflections of full width at half maximum (FWHM) by Debye–Scherrer condition [159]:

$$D = \frac{0.9\lambda}{\beta\cos\theta} \qquad (4.1)$$

Where λ= 1.5406 Aº is the wavelength of the X-ray, β is the complete width half greatest (FWHM) of the peak in radians, and θ is the Bragg angle. The normal crystallite measure

of nanoparticles (D) is break even with to 24.97 nm. The crystallite estimate of Se NPs is appeared in Table (4-1).

Table (4-1). The crystallite size of Se NPs

Sample	2θ (°)	hkl	β (°)	θ (Rad)	β (Rad)	D (nm)
Se NPs	23.4289	(100)	0.2362	0.204	0.004	34.336
	29.6254	(101)	0.1968	0.259	0.003	41.739
	41.2558	(110)	0.3149	0.360	0.005	26.946
	43.5642	(102)	0.2362	0.380	0.004	36.206
	45.3221	(111)	0.3936	0.396	0.007	21.864
	51.6654	(201)	0.3149	0.451	0.005	28.018
	55.8639	(003)	0.9446	0.488	0.016	9.515
	61.5571	(022)	0.9446	0.537	0.016	9.785
	65.1915	(210)	0.576	0.569	0.010	16.364
		Average crystallite size (nm)				24.97

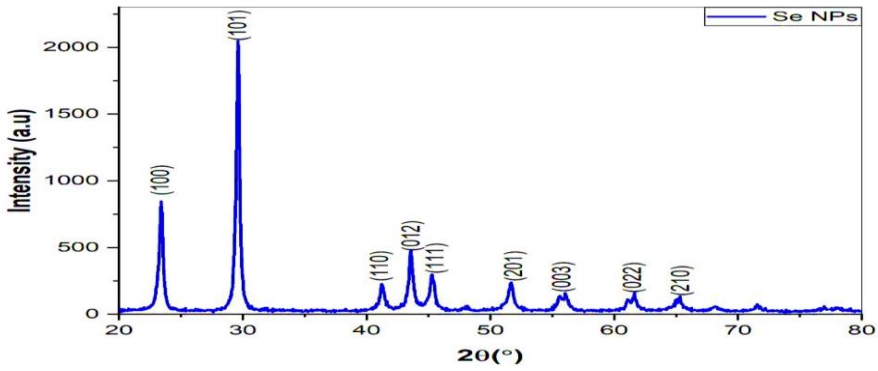

Fig (4-1). XRD pattern of synthesized Se NPs

Figure (4_2) demonstrates the pattern of Ag/Ago NPs made using the biosynthetic technique. Eight peaks are displayed, each with a distinct intensity. The diffraction

angles at 27.9º, 32.2º, and 54.72º confirm the behavior of Ago NPs and agreement with JCPDS (01-076-1489), and relate to planes (100), (111), and (220), respectively while, the diffraction angles at 38.2º and 46.3º, 34.74º, 77.23º, and 81.82º equivalent to planes (111), (200), (220), (311), and (222) respectively. These outcomes demonstrated the preparation of the Ag NPs and their agreement with the JCPDS (00-001-1167) [35]. Ag/Ago NPs' crystallite size was computed by using eq. (1), Nanoparticles (D) have an average crystallite size of 30.20 nm. Table (4-2) displays the Ag/Ago NPs' crystallite size.

Table (4-2). The crystallite size of Ag/Ago NPs

Sample	2θ (°)	hkl	β (°)	θ (Rad)	β (Rad)	D (nm)
Ag/Ago* NPs	27.96	(100) *	0.590	0.243	0.010	13.88
	32.28	(111) *	0.590	0.281	0.010	14.02
	38.20	(111)	0.590	0.333	0.010	14.25
	46.31	(200)	0.590	0.403	0.010	14.65
	54.72	(220) *	0.095	0.477	0.001	94.19
	34.74	(220)	0.095	0.303	0.001	87.65
	77.23	(311)	0.092	0.673	0.001	110.55
	81.82	(222)	0.090	0.713	0.001	116.84
	Average Crystallite Size (nm)				30.20	

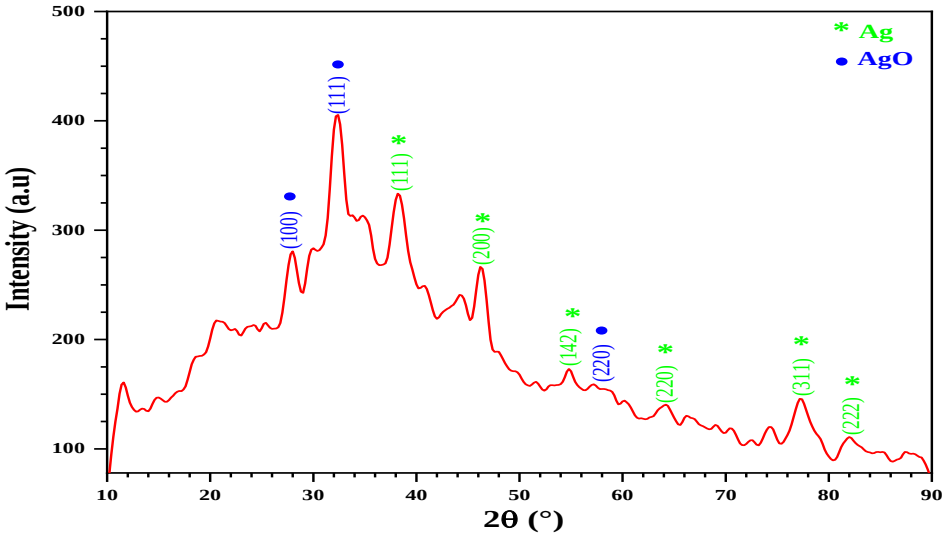

Fig (4-2). XRD pattern of Ag/Ago NPs

4.2.2: FESEM-EDS analysis

The field emission scanning electron microscope (FESESM) makes it possible to examine the topography of nanomaterials' surfaces and assess how well they may be used in various contexts. Figure (4-3) demonstrates the morphology of the Se NPs' production. From the figure, the results conirm the presence of clumps of nanoparticles, which form what looks like a porous structure. It is well known that spherical nanoparticles exhibit a distinctive optical absorption peak of 1.5 keV due to surface plasmon resonance. Alagesan et al. published a similar finding in 2019 (Shnoudeh et al., 2019)

The morphological pictures of the biosynthesized Ag/Ago NPs are displayed in Figure (4-4). The results show the existence of spherical nanoparticles with various nanodiameters that mimic clusters of spherical nanoparticles (Ahmed et al., 2020).

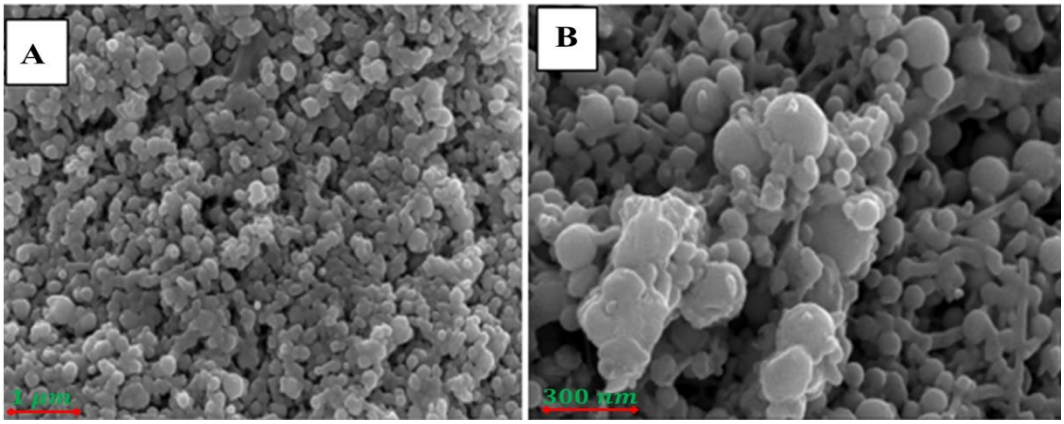

Fig (4-3). FESEM images of Se NPs at (A) 1µm and (B) 300 nm

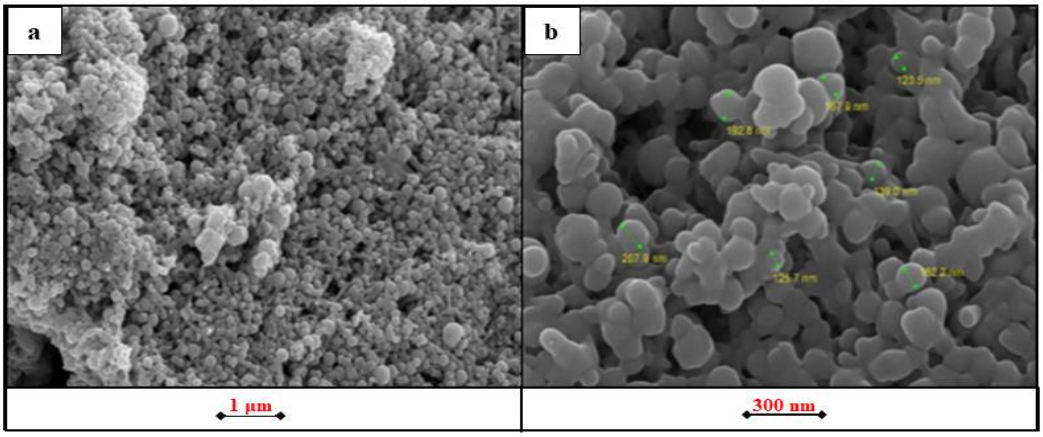

Fig (4-4). FESEM images of Ag NPs at (a) 1µm and (b) 300 nm

EDS was used to analyze the chemical composition of the elements. Figure (4-5) shows the presence of Se and its crystal structure using EDS analysis with a percentage of 99.2% with an O presence of 0.8%. It is widely known that surface plasmon resonance causes Se nanoparticles to have a characteristic optical absorption peak of about 1.4 keV. Figure (4-5) showed the absorption peak in the region of 1.4 keV, which indicates that the NPs are made of crystalline selenium. The current findings support the findings of the study (Pouri et al., 2018).

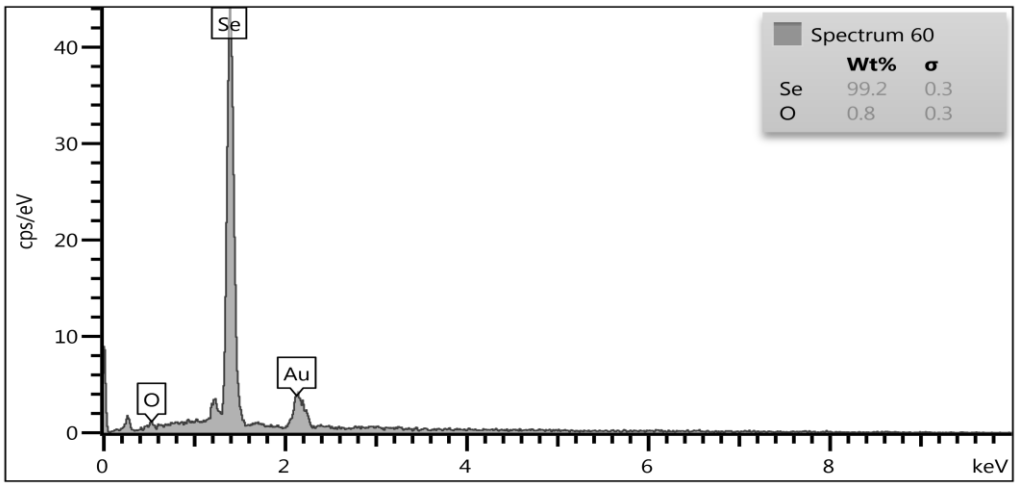

Fig (4-5). EDS of Se NPs

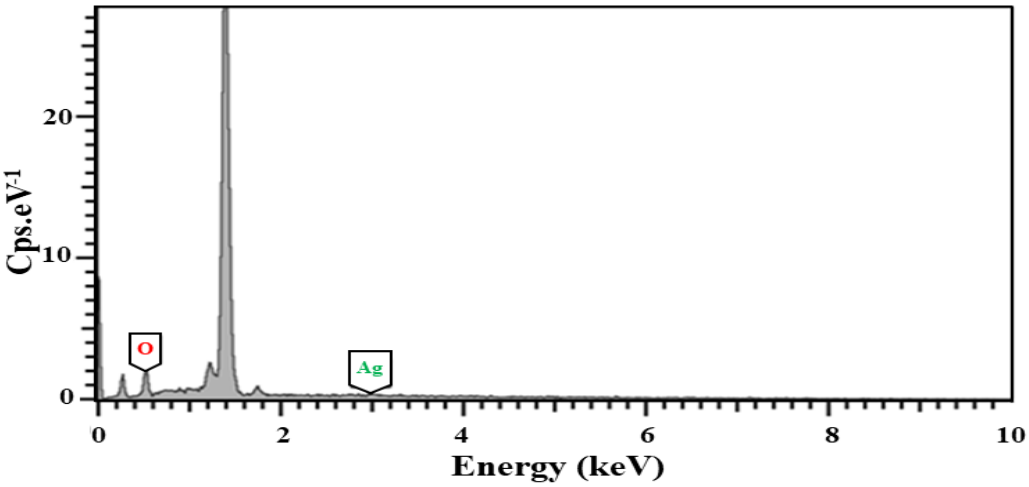

Fig (4-6). EDS of Ag/Ago NPs

Ag NPs' existence and crystalline structure were study by using EDS analysis. It is widely known that surface Plasmon resonance causes Ag spherical nanoparticles to have a characteristic optical absorption peak about 3 keV. Figure (4-6) displayed the absorption peak in the 3 keV area, demonstrating that NPs were made of crystalline silver. The presence of a high content of oxygen may be attributed to the presence of silver oxides in the prepared sample, these results are consistent with the results of XRD analysis. The present results are consistent with the results of the work (Pouri et al., 2018).

4.2.3. Transmission electron microscopy (TEM) analysis

One of the most advanced analytical measurement techniques for analyzing nanoparticles' size and form is the TEM (Lenzen, 2008). Figure (4-7) show the TEM Image of Se NPs prepared by the green synthesis method. The images show nanoparticles are an excellent uniform spherical shape of Se NPs and the distribution behavior with less aggregation, therefore, shown as an individual particle. Figure (4-7) (C) explained the histogram size distribution on Se- NPs and the average size of about 22 nm. This result is in good agreement with the crystallite size determined from XRD analysis. A similar result is published by Galić et al. in 2022(Feng et al., 2022).

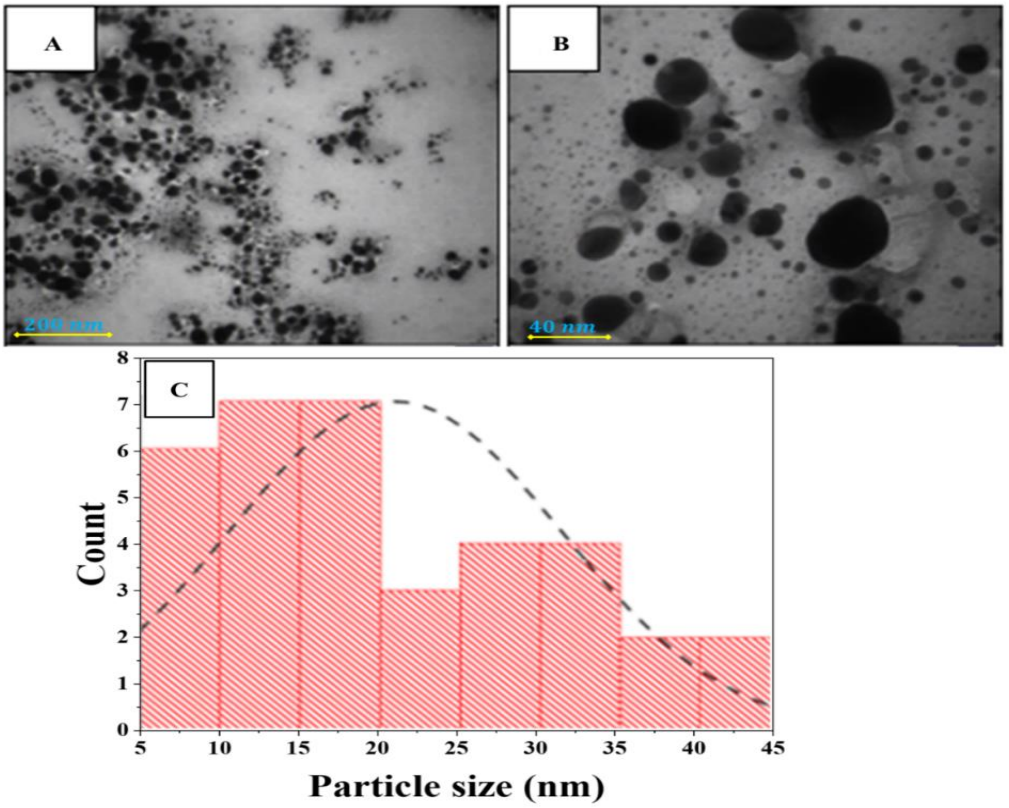

Fig (4-7). TEM pictures of Se nanoparticles created using extract from Withania somnifera are shown in (A) 200 nm magnification, (B) 40 nm magnification, and (C) the histogram size distribution.

Figure (4-8) TEM images of Ag/Ago NPs made using the biosynthetic process should be displayed. The findings demonstrate that, in comparison to Se NPs, the nanoparticles have a spherical form and exhibit some aggregation. Figure (4_8) (C) explains the Ag/Ag

O NPs' histogram size distribution, which shows particles with sizes between 50 and 350 nm.

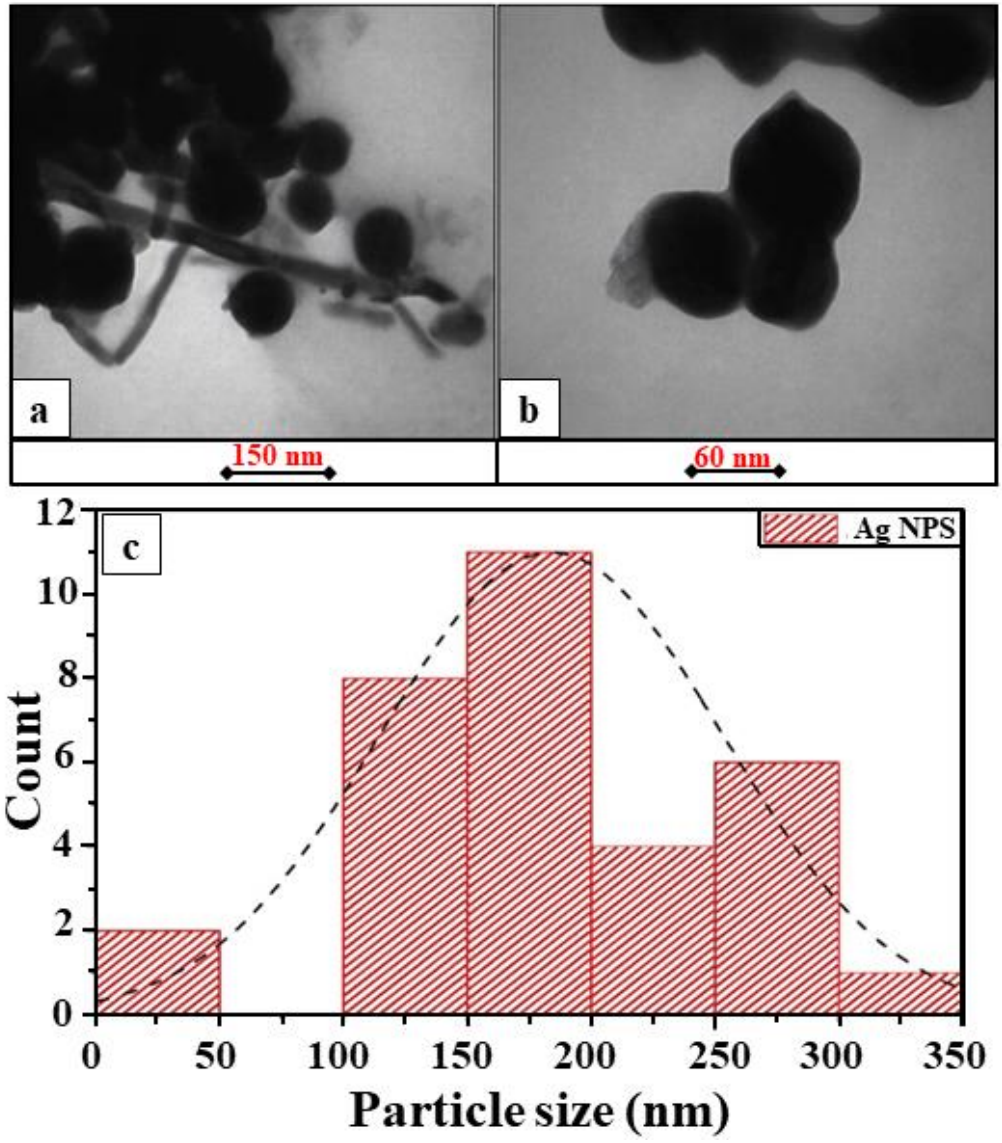

Fig (4-8). TEM Images showing the histogram size distribution and (a, b) different magnifications of Ag/Ago NPs made using the biosynthetic process

4.2.4. Atomic Force Microscope (AFM) analysis

The roughness and surface morphology of Ago/Ag NPs and Se NPs , as shown in the AFM pictures, and Figure (4_9) (A, B). Version 3.10.0.28 of the NaioNanosurf software was used to create this image (Goodarzi et al., 2014). The findings demonstrate that Se NPs have an average square roughness of 7.02 nm and a surface roughness of 4.505 nm, as shown in the Figure (4-9) .

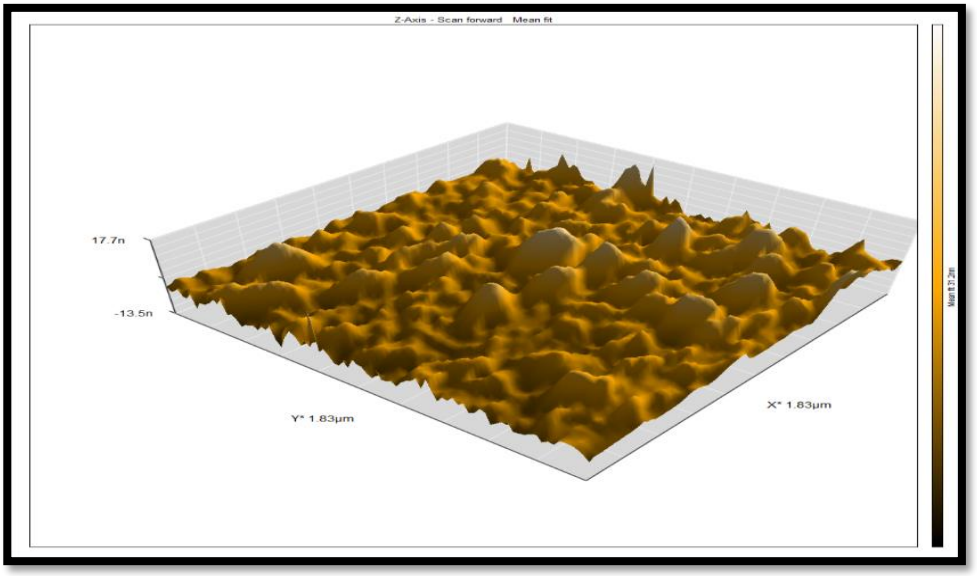

Fig (4-9). AFM images of Se NPs

While The results show that the surface roughness of Ago/Ag NPs was 9.32 nm with an average square roughness of 21.19 nm, as shown in Figure (4-10) .

The current findings agree with those of the TEM analysis, and proved that the aggregate in Se NPs less than aggregate in Ago/Ag NPs. This could be attributed to the effect of ascorbic acid as a source of vitamin C and its role in reducing the sizes of NPs.

4.2.5. Dynamic light scattering (DLS) analysis

The results of Se NPs confirm that the size distribution of the Se NPs was no more than 3 nm, as shown in Figure (4_11) (A). As for the distribution of Se NPs by intensity, the results showed that the nanoparticles were distributed in three regions, the first in the region less than 3 nm, the second region between 60 nm to 150 nm, and the last region in the size distribution greater than 1000 nm, as shown in Figure (4_11) (B). The results of the TEM Analysis and the current findings are closely aligned.

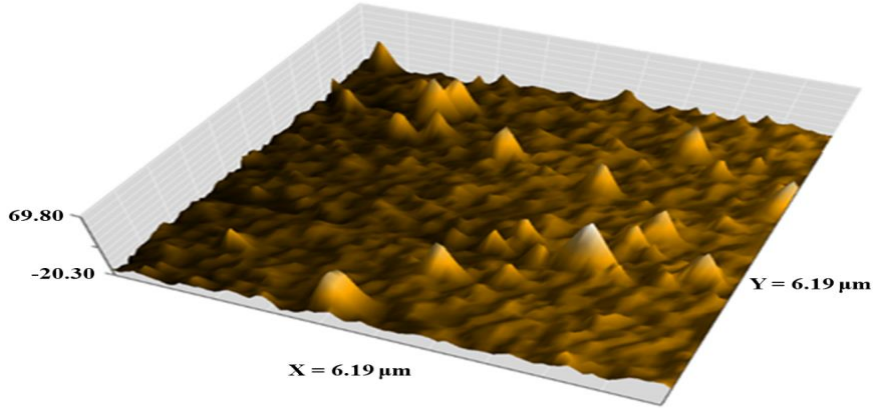

Fig (4-10). AFM images of AgO/Ag NPs

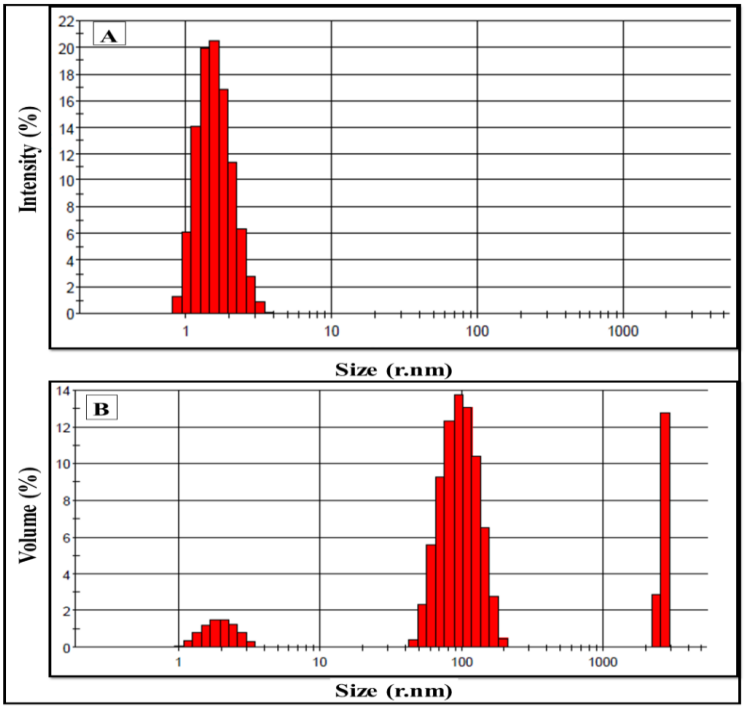

Fig (4-11). Size Distribution of Se NPs by Volume and Intensity. At 25 °C and a 60 s time period

While, Figure (4_12) demonstrates the size distribution of the Ago/Ag NPs produced by the plant extract (by volume and intensity). According to the figure, the distribution of Ago/Ag NPs had its largest peaks between 95 nm and 310 nm.

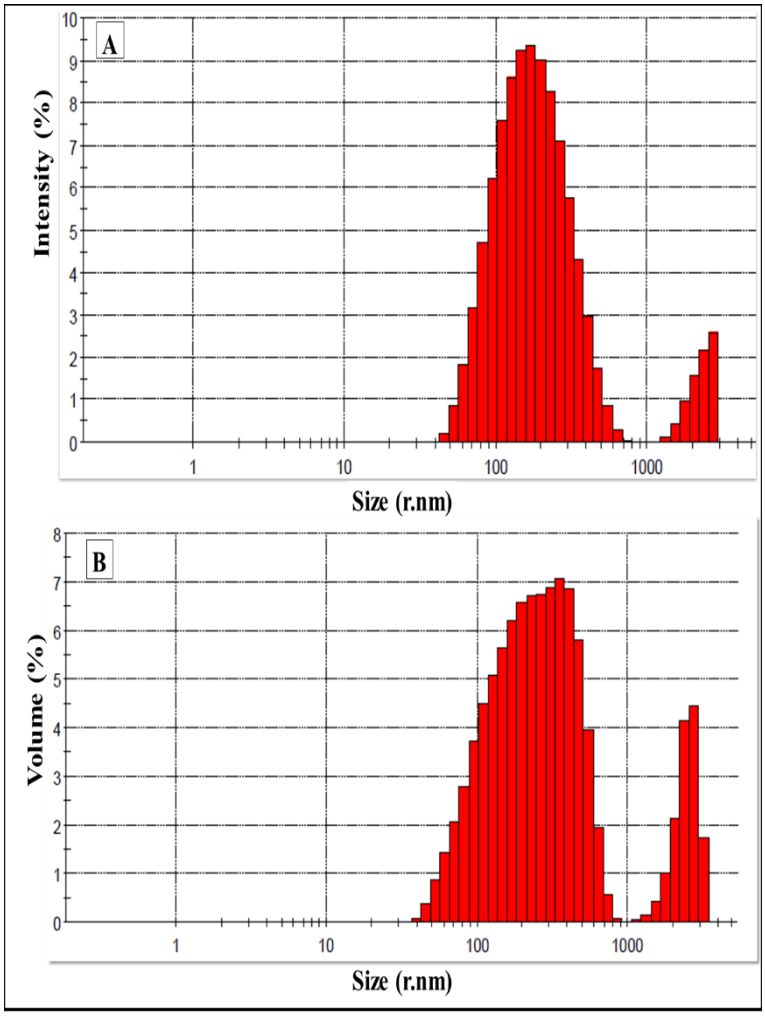

Fig (4-12). Ag/Ago NP Size Distribution by (A) Intensity and (B) Volume. At 25 °C and a 60 s time period

4.2.6. Zeta potential measurement

Figure (4_13) shows the surface charge measurements of both Se NPs and Ago/Ag NPs. The results confirm the dispersion of Se NPs have a zeta potential of -14.4 (mV) and a mobility of -1.132 (µmcm/Vs). The dispersion of Ago/Ag NPs, which have a zeta potential of -19.5 (mV) and a mobility of -1.532 (µmcm/Vs). The present results show a good dispersion state of nanoparticles in liquids(Balamanikandan et al., 2015).

The negative value in this test confirms the occurrence of repulsion between the silver nanoparticles and proves that they are very stable.

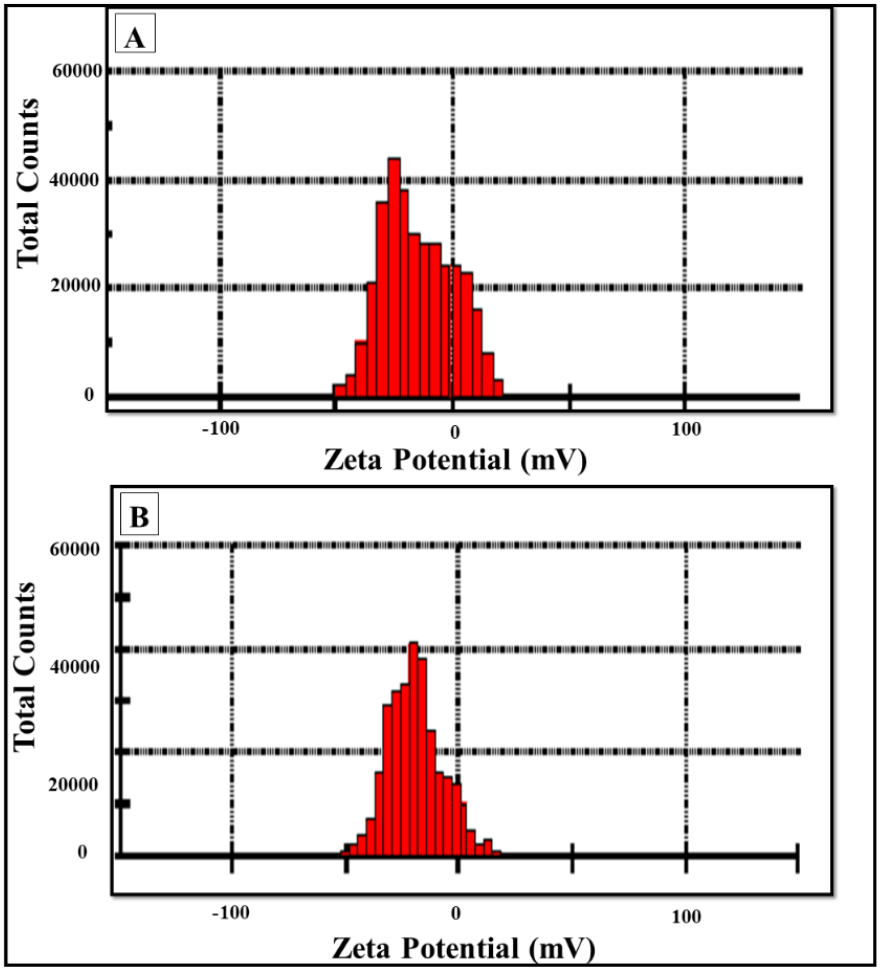

Fig (4-13). Zeta potential values of (A) Se NPs and (B) Ago/Ag NPs dispersion

4.2.7. Optical properties

UV-Visible absorption spectrum displayed in Figure (4_14) demonstrate the electromagnetic energy that Se NPs absorbed. The findings support the existence of two absorption bands with centers at wavelengths of 458 nm and 622 nm, respectively. The strong band centered at 2 = 622 nm can be attributed to surface plasmonic resonance and the small size of the nanoparticles created during the synthesis process, while the intermediate band, centered at 1=458 nm, is associated to selenium nanoparticles. Our outcome is in line with the research's findings (Habubi et al., 2013; Al-Otibi et al., 2021).

Figure (4-15) shows the optical absorption spectrum of Ago/Ag NPs prepared using garlic extract. The results show that there is an absorption peak at the wavelength 420

nm that can be attributed to the presence of the surface plasmon resonance (it is the result of the collective movement of free electrons in the silver when light falls on it),

hich is a characteristic of Ag NPs. This result is close to the source (Panchal & Chauhan, 2019). The present results are consistent with the results of the work (Sosa et al., 2003; Rasmagin & Apresyan, 2020)

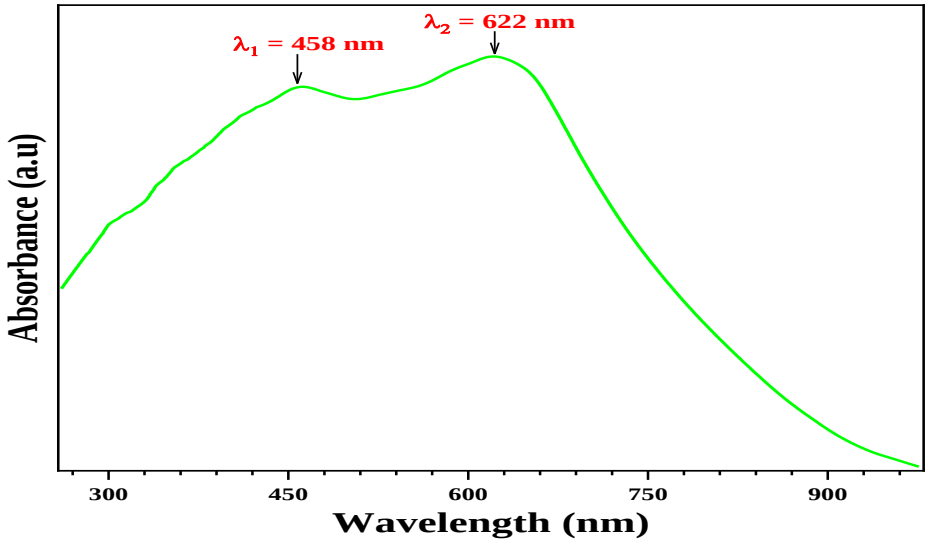

Fig (4-14). Se NPs' UV-visible absorption spectrum

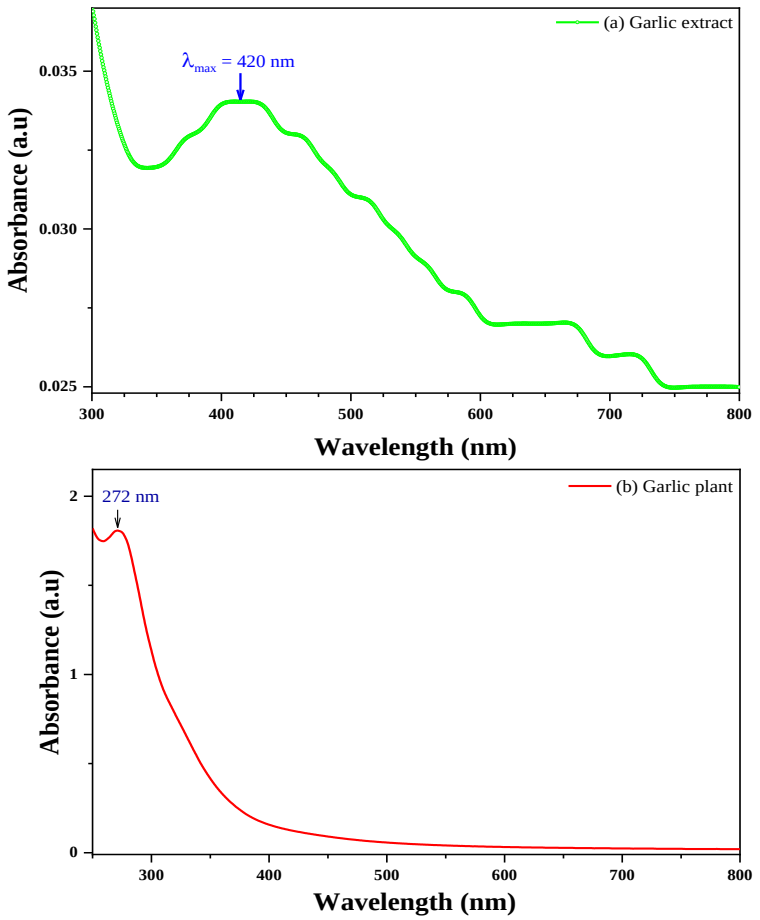

Fig (4-15). UV-visible absorption spectra of Ago/Ag NPs (Garlic plant and Garlic extract)

Optical absorption coefficient. The attenuation of light intensity as it passes through a substance is described by the absorption coefficient (α). It may be thought of as the total of a material's absorption cross-sections for an optical process per unit volume. The optical absorption coefficient (α) can be calculated by the following equation (Al-Mudhaffer et al., 2012).

$$\alpha(\lambda) = \frac{\mathrm{A}}{d} \times ln(10) \qquad (4.2)$$

Where, A =is absorption, d is thickness, ln (10) = 2.30.

Figure (4-16) shows the relationship between the wavelength of Se NPs made using the green method's optical absorption coefficient. The outcomes demonstrate that the sample exhibits strong absorption coefficient values in the visible range, peaking at a

wavelength of 2 = 622 nm. The recent findings support the findings of the works (Gates et al., 2002; Jiang et al., 2017)

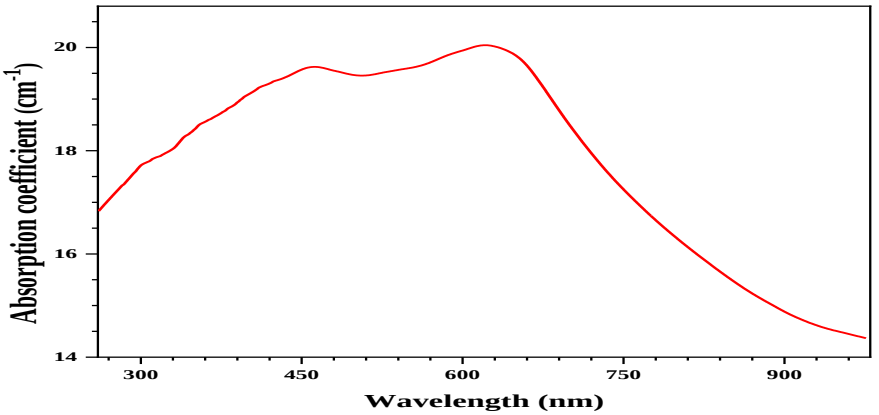

Fig (4-16). Absorption coefficient as function of wavelength of synthesized Se NPs

Figure (4-17) shows the relation between the optical absorption coefficient (α) and the wavelength of Ago/Ag NPs prepared by *garlic* plant extract. The results indicate a peak absorption coefficient at the wavelength of 420 nm with a high absorption edge close in the ultraviolet region. This curve represents the optical absorption coefficient (α) behavior of Ag NPs (Das et al., 2016; Abdelghani et al., 2022).

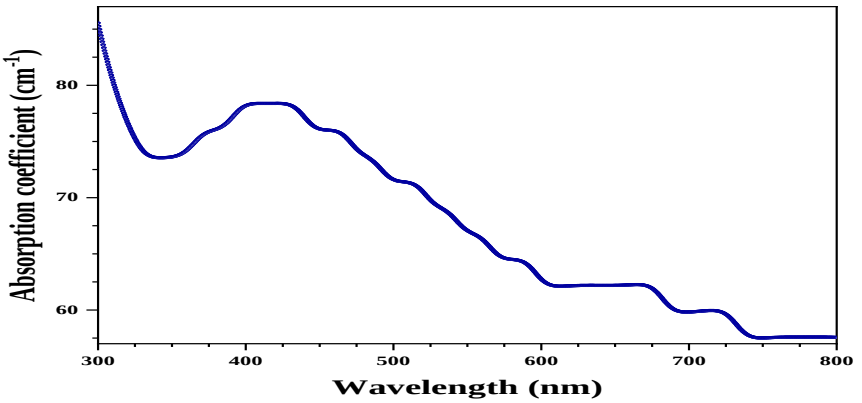

Fig (4-17). Absorption coefficient changes as a function of wavelength for Ago/Ag NPs

Urbach energy. Figure (4-18,19) shows the Ln (α) versus hν plots obtained for the Se and Ag nanoparticles thin film sample. This plot can be divided into three regions for analysis. The first region belongs to the weak absorption (WAT Region). It represents the transitions that take place from a tail state located above the valence band to another tail state located below the conduction band, and/or from a tail state located below the

conduction band to another tail state located above the valence band. In this WAT region, α follows hν according to the following relationship (Abdelghani et al., 2022):

$$\alpha(h\nu) = \alpha_0 e^{\left(\frac{h\nu}{E_{WAT}}\right)} \quad (4.3)$$

Where, α_0 is a constant, hν is the photon energy, E_{WAT} represents the weak absorption tail energy.

The Urbach region (U region) Figure (4-18, 19) represents the electronic transitions that take place from an extended valence band state to another tail state below the conduction band and/or d from a conduction band state extended to another tail state above the valence band. The E_u can be calculated by the following equation (Abdelghani et al., 2022):

$$\alpha(h\nu) = \alpha_0 e^{\left(\frac{h\nu}{E_u}\right)} \quad (4.4)$$

where, α_0 is a constant, h is the photon energy, E_u is the Urbach energy.

$$Ln(\alpha) = \frac{1}{E_u} h\nu + Ln(\alpha_0) \quad (4.5)$$

The Urbach energy was calculated by the inverse of slope to the curve.

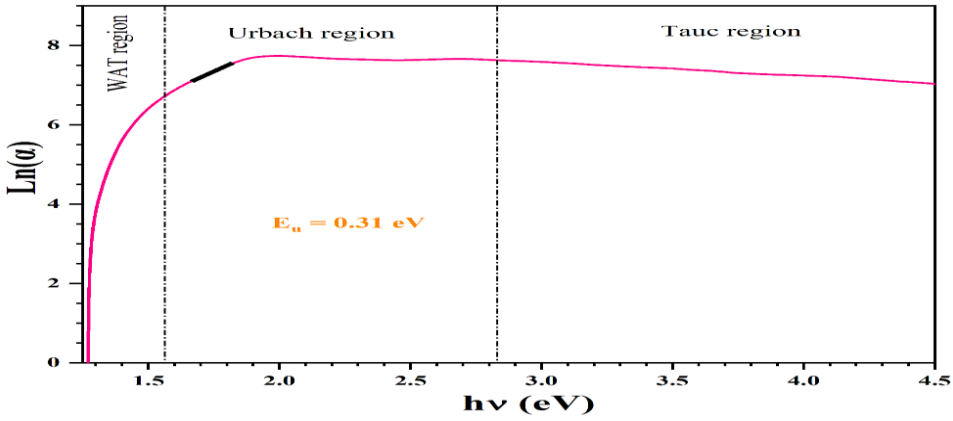

Fig (4-18). Variations in Ln(α) as a function of the Se NPs' incident photon energy

In Figure (4-18) we have the Urbach energy (E_u = 0.31 eV) this low value indicates low density of localized states in the bandgap of Se nanoparticles thin film. So minimal impurities in our prepared Se NPs film.

In Figure (4-19) we have the Urbach energy (E_u = 0.25 eV) this low value indicates low density of localized states in the bandgap of Se nanoparticles thin film. So minimal impurities in our prepared Ag NPs film.

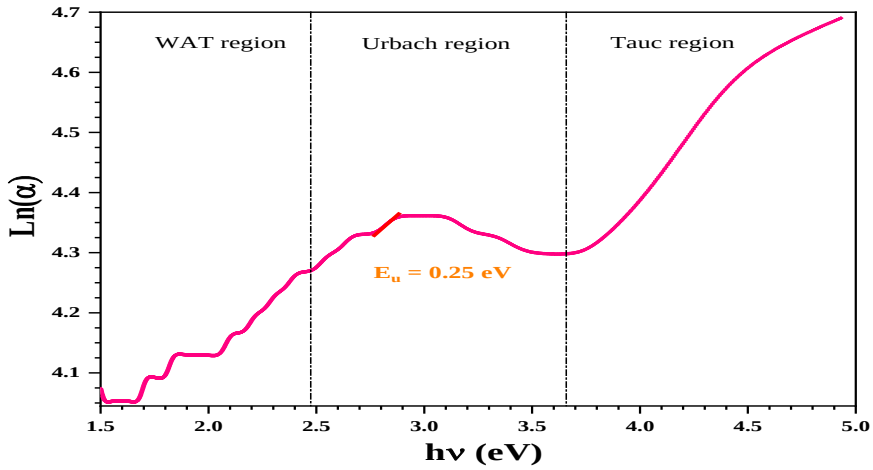

Fig (4-19). Variations of Ln(α) with incident photon energy of AgO/Ag NPs

The absorption coefficient at the threshold vs incident energy is demonstrated by the inter-band absorption theory to be as follows (Jiang et al., 2017; Al-Mudhaffer et al., 2012)

$$\alpha h\nu = B(h\nu - E_g)^n \qquad (4.6)$$

Where, B is the probability parameter for the transition, E_g the optical gap energy. The coefficient n is equal to $\frac{1}{2}$, for permitted direct transitions and to n = 2, for permitted indirect transitions. The substance under study possesses an absorption coefficient (α) that, for high photon energy, complies with the following relation because of the direct band gap ($h\nu$):

$$\alpha h\nu = B\left(h\nu - E_g\right)^{\frac{1}{2}} \qquad (4.7)$$

The E_g value corresponding to transitions in the direct band gap see Figure (4-20) can be calculated via the $(\alpha h\nu)^2$ versus $h\nu$ by applying the formula below:

$$(\alpha h\nu)^2 = B\left(h\nu - E_g\right) \qquad (4.8)$$

The values of E_g were estimated from the intersection of the extrapolated linear part of the $(\alpha h\nu)^2$ curves with the energy axis. Figure (4-20) shows the variation in $(\alpha h\nu)^2$ versus $h\nu$ for Se NPs. The findings show that the energy gap was about 1.6 eV. The current findings concur with the authors' findings (Gates et al., 2002; Das et al., 2016).

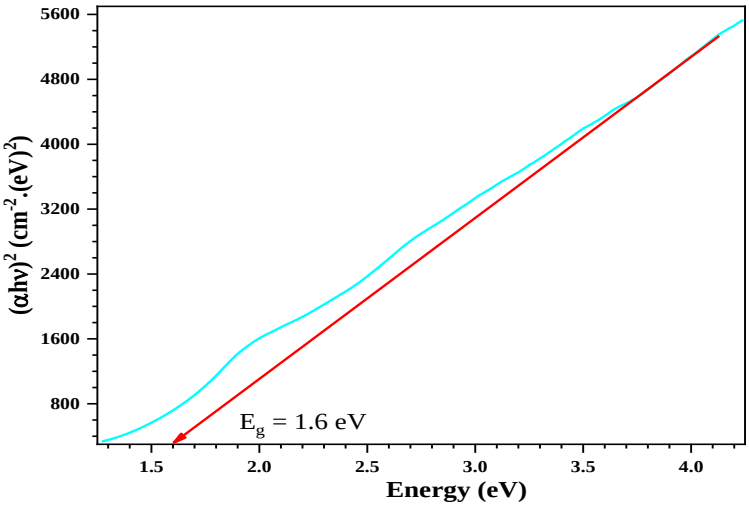

Fig (4-20). Tauc plot of prepared Se NPs

Optical bandgap analysis. The determination of the optical bandgap E_g was based on this Tauc formula:

$$(\alpha h\nu)^2 = \beta(h\nu - E_g) \qquad (4.9)$$

After plotting $(\alpha h\nu)^2$ in function of the photon energy ($h\nu$), the bandgap value could be determined using the extrapolating of the linear portion to $\alpha = 0$. As can be seen in Figure (4-21), the Tauc plot obtained for the Ag nanoparticles thin film sample. It was obtained from the T region in Figure (4-19) as it represents the longest transition. Figure (4-21) show the relation between the photon energy (eV) and $(\alpha h\nu)^2$ of Ago/Ag NPs, by drawing the tangent with the x-axis the direct optical energy gap can be calculated. From the Figure (4-21), the results confirm that the energy gap directly was 3.39 eV, this meaning the sample needs less energy to stimulate the electrons to move between the energy bands. The current results are in agreement with the results of work (Das et al., 2016).

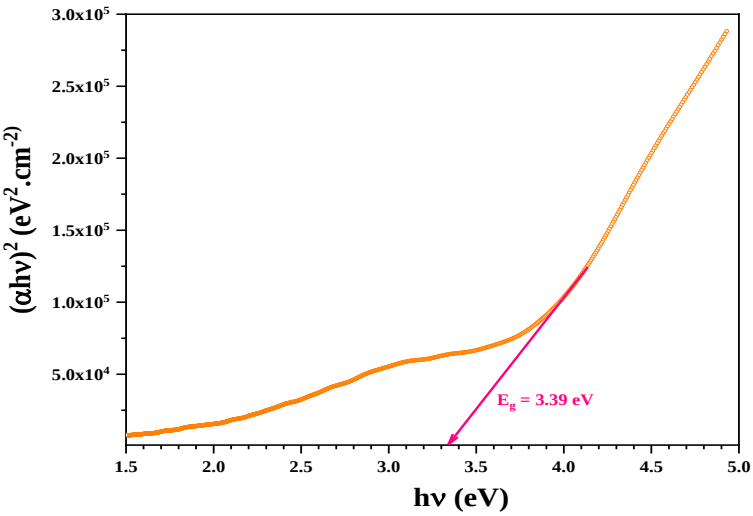

Fig (4-21). Tauc plot of Ago/Ag NPs prepared by *garlic* plant extract

Refractive index. It has been reported that, the refractive index n_r is a fundamental parameter of optical materials that plays a very important role in optical device designing. Thus, controlling the refractive index of optical nanomaterials makes them convenient for a wide range of applications in industrial and medical applications such as display devices, light-emitting diodes (OLEDs), optical communications, and antibacterial activities. The band gap values can be used to calculate a high frequency refractive index n_r according to the empirical relation applicable to different varieties of compounds:

$$n_r = \frac{1}{T_s} + \sqrt{\frac{1}{T_s - 1}} = \frac{1}{10^{-A} \times 100} + \sqrt{\frac{1}{10^{-A} \times 100 - 1}} \qquad (4.10)$$

Where, T_s is the percent transmittance, A is the absorbance.

As can be seen Figure (4-22), the value of the refractive index for the Se NPs in the range $0.1 - 0.4$.

As can be seen Figure (4-23), the value of the refractive index for the Ag-NPs in the range $0.113 - 0.116$. This is close to the usual value of silver (0.135). The difference is that our compound is formed by Ago nanoparticles in addition to Ag nanoparticles.

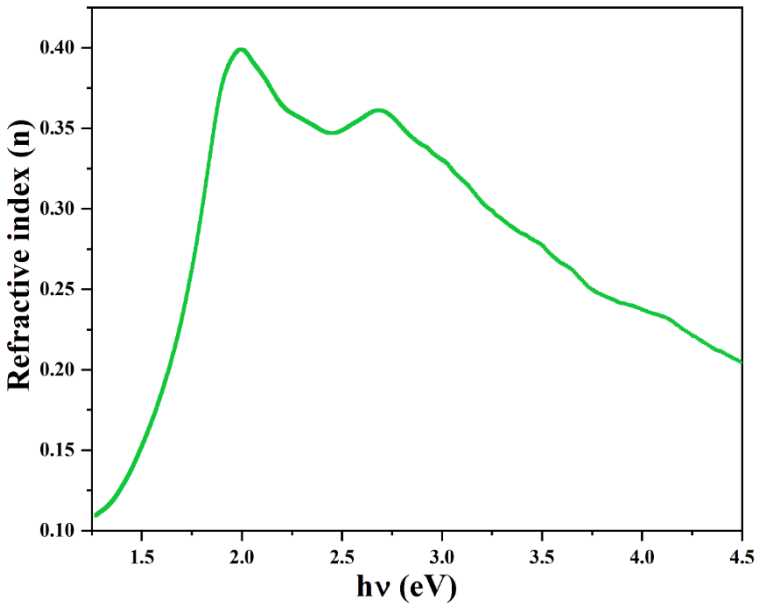

Fig (4-22). Plot of refractive index as function energy of Se NPs

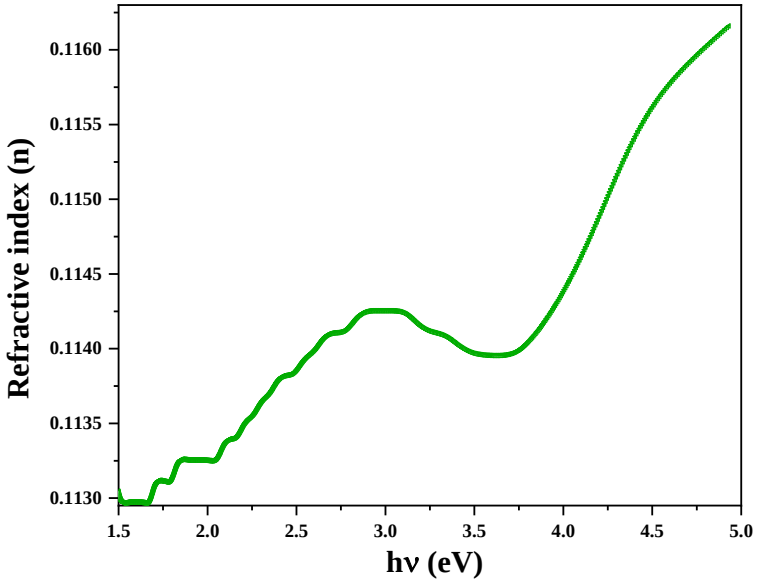

Fig (4-23). Plot of refractive index as function energy of Ago/Ag NPs

Optical conductivity. The optical conductivity (σ_{opt}) for this sample was calculated using the absorption coefficient α, and the refractive index n data using the following relation[180]:

$$\sigma_{opt} = \frac{\alpha n_r c}{4\pi} \qquad (4.11)$$

Where, c is the velocity of light in free space, α is the absorption coefficient, and n_r is the refractive index.

The optical conductivity of a material determines the relationship between the amplitude of the induced electric field and the density of the induced current in the material for any given frequency. This linear response function is a generalization of electrical conductivity, which is often considered in terms of static electric fields with slow or time-independent differences. It has to do with how conductive a material is, or how much electricity can flow through it. The conductivity of a particular material depends on the frequency of the electric field (that is, how fast it changes) (Gervais, 2002; Qiu, 2011).

Figure (4-24,25) It displays the relationship between photoconductivity and photon energy for Se and Ag nanoparticles, respectively.

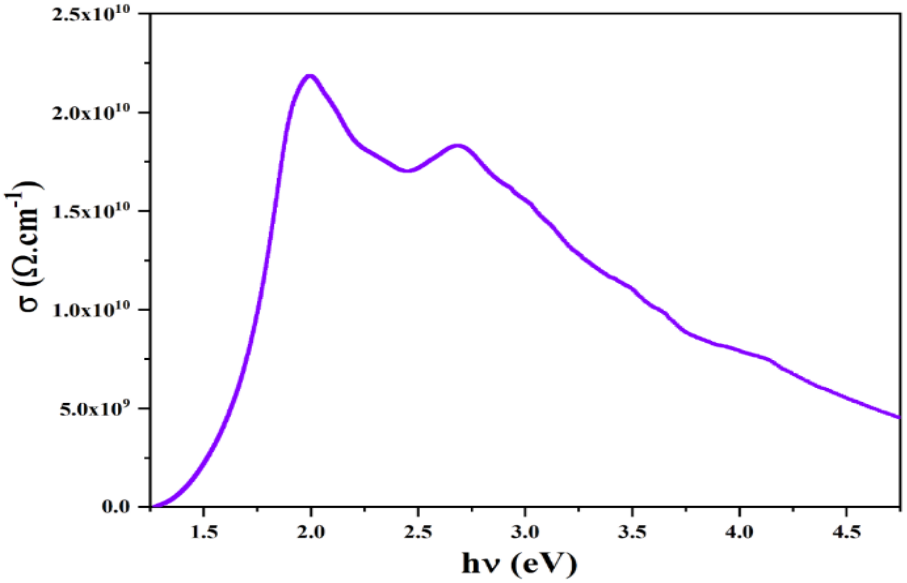

Fig (4-24). Se NPs' optical conductivity and energy relationship

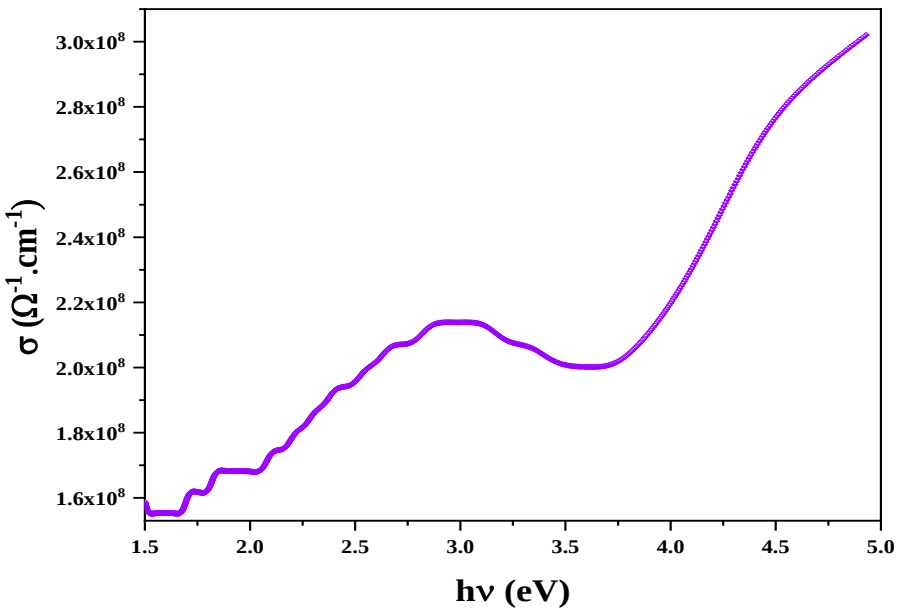

Fig (4-25). AgO/Ag NPs' optical conductivity and energy relationship

The findings demonstrate that the high energy of the photons, which causes the electrons to vibrate in the energy levels, is the cause of the conductivity, which rises with frequency.

4.3: Study of cytotoxic effect

4.3.1: Alkaline comet assay

The findings revealed a defense against the ensuing DNA degradation activities. Single-cell gel electrophoresis test results showed that NPs overcome cytotoxicity and cause reduced sperm cell death by reducing damage ratio when STZ-induced diabetes was used as a model. The results shown in Figure (4-26) indicate a statistic statistically significant variations between each group that received treatment and the most effective ones It reduces DNA damage rates and restores normal focus Sperm morphology in the testes of diabetic mice compared to the control group.

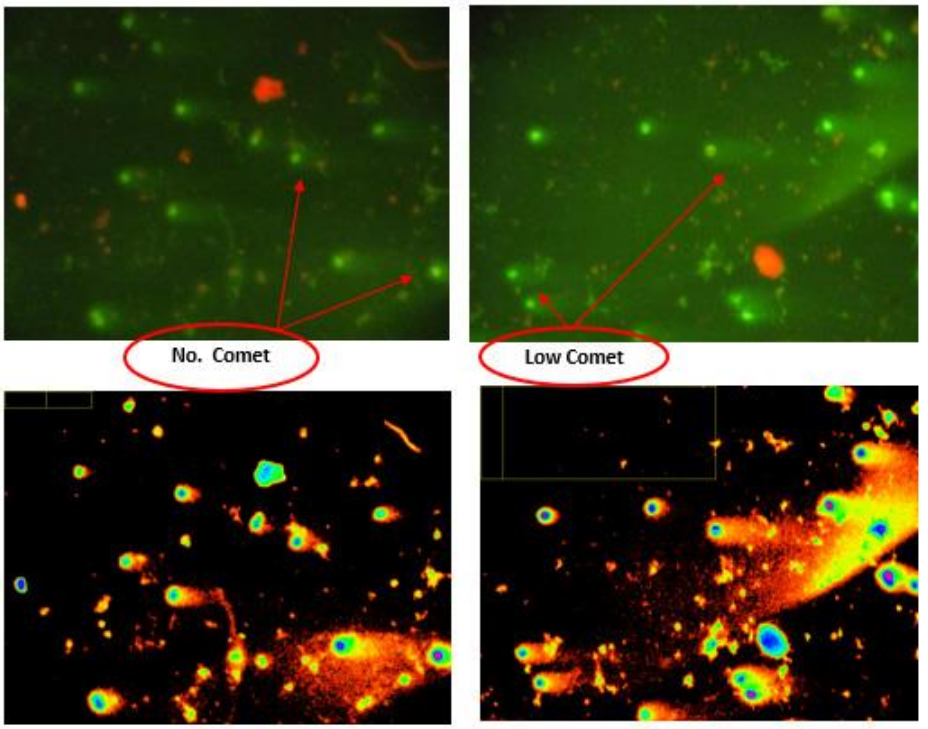

Fig (4-26) A. Se NPs were used to treat the group, which resulted in a high percentage of cells without comets and a poor comet score

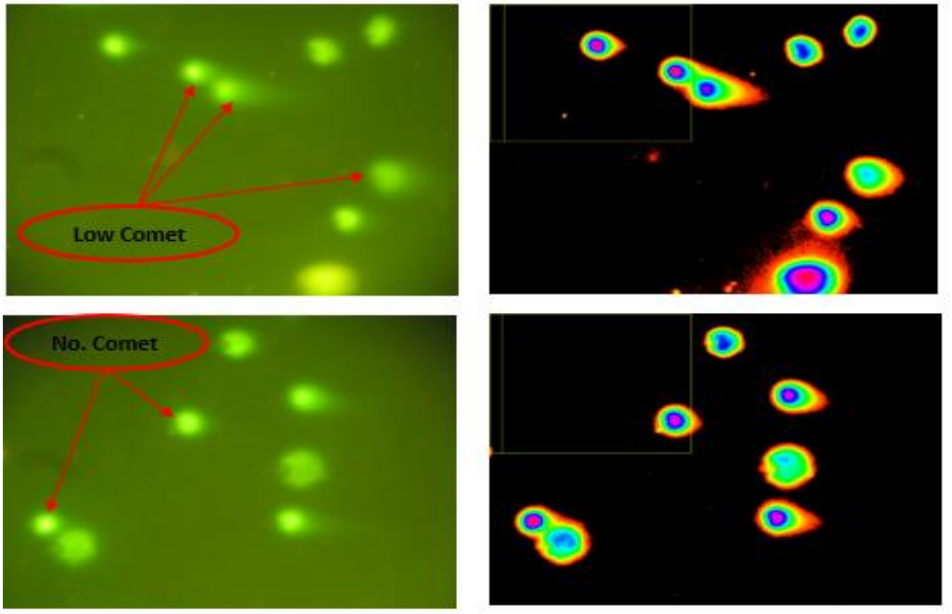

Fig (4-26) B. By employing the comet score program, the control group (negative) consists of a large number of cells with weak comets or no comets

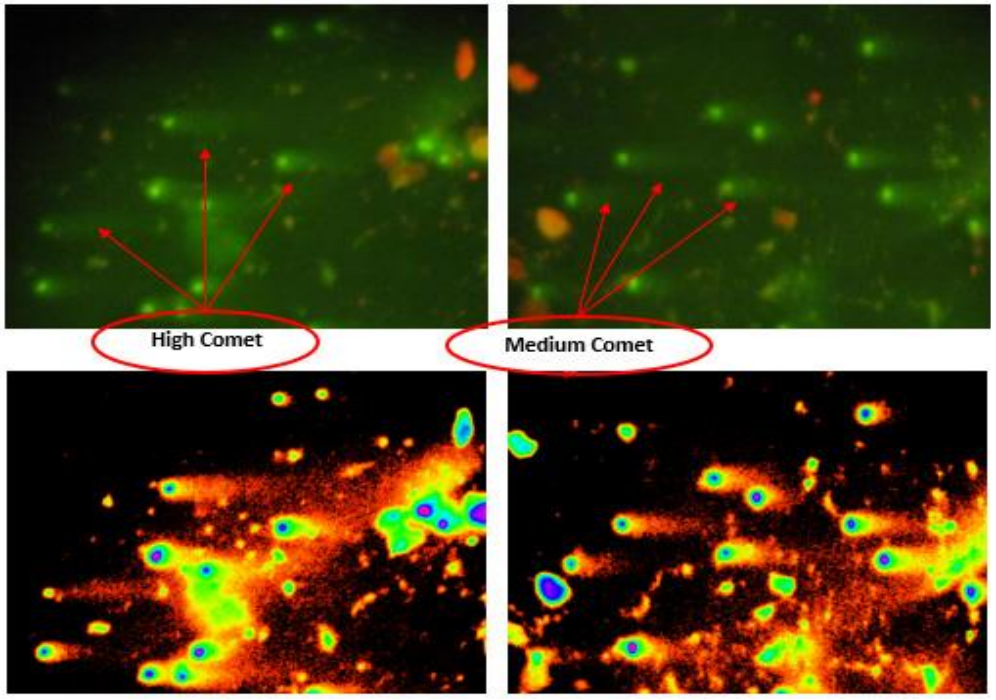

Fig (4-26) C. Positive control group (DM): a large percentage of cells utilizing the comet score program had high and medium comet values

Table (4-3) demonstrates that the value of medium and high damage decreased significantly ($P \leq 0.05$) following treatment with Se NPs compared to the streptozotocin group and became (8.347±1.314, 8.353±1.382) correspondingly, in terms of high damage, as well the treatment with Ag NPs led to an improvement in the value of medium and high damage, but with less effect than Se NPs, so the values became as follows (10.721±0.712, 9.487±0.605). Se NPs and Ag NPs with the letter D in their average specific value are not substantially different from the control sample. The particular mean values of STZ, however, varies. In addition, individuals denoted by the letter A differed significantly ($P \leq 0.05$) from the negative control group.

We conclude that the synthesis of Se NPs and Ag NPs In this approach, oxidative stress in the immune system is lessened or eliminated, which prevents ROS from promoting the lipid peroxidation that leads to eventual DNA damage. Hence, the energy metabolism is stable (Prasad & Selvaraj, 2014). and this result agrees with the previous study by (El-Nekeety et al., 2021; Artimani et al., 2018). Treatment with Se and Ag NPs was more successful than MET, Se or Ag usage alone.

Table (4-3). Alkaline Comet Assay

Parameters Groups	No Damage% (Mean ±SD)	Low Damage% (Mean ±SD)	Medium Damage% (Mean ±SD)	High Damage% (Mean ±SD)
Neg. control	A 42.478±0.975	A 43.410±0.553	E 7.066±0.942	D 7.045±0.599
STZ	D 33.189±1.565	E 33.698±0.878	A 15.025±0.554	A 18.088±1.072
STZ+ Met	BC 37.909±0.856	D 38.370±0.878	B 10.852±0.557	B 12.869±0.329
STZ+ Ag	C 37.746±0.755	CD 38.714±1.603	BC 10.604±1.300	B 12.936±0.974
STZ+ Se	BC 38.681±1.330	CD 38.487±0.939	BC 10.484±0.613	B 12.347±1.693
STZ+ Ag NPs	B 39.705±0.406	BC 40.087±0.724	CD 9.487±0.605	C 10.721±0.712
STZ+ Se NPs	A 41.65±2.31	B 41.654±1.790	DE 8.353±1.382	D 8.347±1.314
LSD	2.263	1.964	1.581	1.810
P-value	**0.00023**	**0.00001**	**0.0001**	**0.00031**

- STZ stands for streptozotocin diabetic mice.
- Different capital letters and small last names denote significant $p \leq 0.05$.
- Met for metformin.
- LSD is short for least significant difference.
- P stands for probability.

4.3.2. Sperm parameters

The results presented in Table (4-4) and Figure (4-27) sperm motility, dead sperms, abnormal sperm counts, and percentages in the treated and control groups. The results were measured to compare with the negative (uninfected) and positive (STZ-infected) control group. The mice were dosed with selenium, silver nanoparticles, silver selenium, and metformin. The effects of nanoparticles manufactured by the intact green method and metformin on the sperm parameters of healthy and streptozotocin-induced diabetic male mice are shown in the Table (4-4). When compared to the positive control group (infected with STZ), movement and vitality rose significantly and significantly ($P \leq 0.05$) in the groups treated with selenium nanoparticles. which appears in Figure (4-27) (85.00

±4.08, 88.50 ±3.11), respectively. While it was observed in the group treated with silver nanoparticles and metformin a significant increase ($P \leq 0.05$) in movement and vitality, but with less effect than the selenium nanoparticles group, as it became close to the negative control group, as shown (73.00 ±6.78, 80.00±4.08) respectively. At the time an increase in malformations and the number of significant deaths was recorded as a result of STZ-induced diabetes, where there was a decrease in the rate of malformations and the value of life increased significantly and significantly ($P \leq 0.05$) in the groups treated with selenium particles. The nanoparticles, which appear in the figure (14.25±6.40) and (19.50 ±2.65) when compared with the positive control group (infected with STZ), which are (25.75±3.86) and (38.75±5.19). Malformations and deaths decreased in the groups treated with silver nanoparticles and metformin, but with less significance than nanoparticle selenium. The treatment with silver and selenium did not record an important qualitative effect on movement and vitality, reducing deformities and thus increasing the value of life compared to the positive control group. (infected with STZ).

Table (4-4). Sperm motility, dead sperm, abnormal sperm, and count percentages in the treatment and control groups

Parameters Groups	Motility % (Mean ±SD)	Dead % (Mean ±SD)	Abnormalities % (Mean ±SD)	Count $\times 10^7$ (Mean ±SD)
Neg. control	A 88.50±3.11	E 12.25±2.22	C 14.50±3.00	A 28.00±2.94
STZ	D 61.75±3.59	A 38.75±5.19	A 25.75±3.86	E 17.250±1.708
STZ+ Met	B 80.00±4.08	CD 23.00±3.65	B 20.000±1.826	DE 19.75±2.22
STZ+ Ag	C 72.00±6.06	BC 25.50±3.87	AB 22.25±2.50	CD 20.50±2.08
STZ+ Se	D 61.00±2.94	B 29.75±3.86	A 25.75±2.75	DE 19.50±2.38
STZ+ Ag NPs	C 73.00±6.78	BC 27.25±3.30	AB 20.75±2.22	BC 23.50±2.08
STZ+ Se NPs	AB 85.00±4.08	D 19.50±2.65	C 14.25±6.40	B 24.000±1.826
LSD	7.936	6.307	6.097	3.822
P-value	**0.0001**	**0.0023**	**0.0004**	**0.0002**

- STZ stands for streptozotocin diabetic mice.

- Different capital letters and small last names denote significant p ≤0.05.
- Met for metformin.
- LSD is short for least significant difference.
- P stands for probability.

The nanoparticles prepared by the environmentally friendly green method protect plants beneficial to the body's immunity and the sperm environment via boosting immune system oxidative activity and reducing reactive oxygen species from promoting the lipid peroxidation that leads to eventual sperm destruction. The findings show that, thanks to nanoparticles' tiny size and high surface area, they had an effective impact on sperm parameters, have a large interaction with their surface, and thus increase the energy in the mitochondria and the energy of sperm movement, so they were used in medical applications and to improve male reproduction Fertility system as in the results of other previous studies (Goodarzi et al., 2014; Torabian et al., 2022; Zhu et al., 2023).

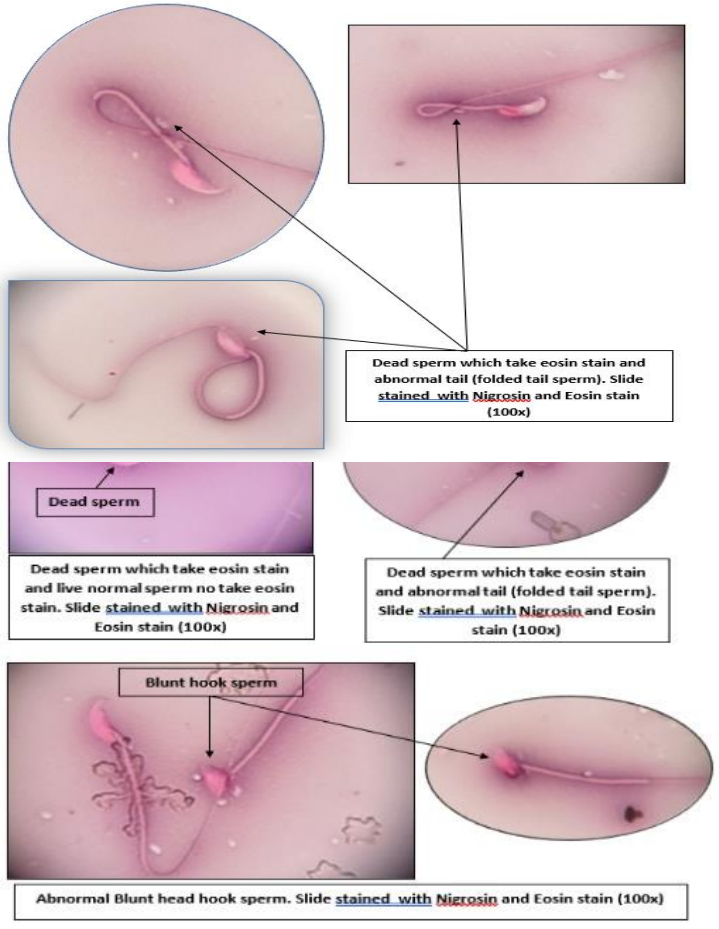

Dead sperm which take eosin stain and live normal sperm no take eosin stain. Slide stained with Nigrosin and Eosin stain (100x)	Dead sperm which take eosin stain and abnormal tail (Bent tail sperm). Slide stained with Nigrosin and Eosin stain (100x)

Fig (4-27) sperm parameters

4.3.3. Luteinizing hormone, follicle-stimulating hormone and testosterone level

Table (4-5) shows the effects of treatment with nanoparticles manufactured by the healthy green method on the one hand, and treatment with metformin, silver and selenium on the other hand, on the level of Luteinizing hormone, follicle-stimulating

hormone and testosterone in male mice with diabetes induced by STZ. Diabetes induced by STZ causes an increase in the level of LH, and this leads to damage to the testicles, as shown in Table (4-5).

The results showed a significant increase ($P \leq 0.05$) compared to the negative control. This increase causes significant testicular failure and may occur as a result of abnormalities in the sex chromosomes. Compared to the positive control group, the selenium nanoparticle-treated group's LH hormone level dropped. No clear effect was observed in the groups treated with silver nanoparticles, silver, selenium, and metformin, (3.021±0.426, 3.229±0.281, 2.899±0.373 and 3.403±0.413) respectively, while testosterone level did not have significant changes in all groups. Table (4-5) shows the results of the FSH test. The results indicate a significant increase ($P \leq 0.05$) in the percentage of FSH hormone in the positive control group (with STZ). We notice a decrease in the percentage of FSH hormone compared to the control group in all treatment groups.

Table (4-5). Luteinizing hormone, follicle-stimulating hormone and testosterone level

Parameters **Groups**	**Testosterone ng/ml** **(Mean ±SD)**	**FSH mIU/ml** **(Mean ±SD)**	**LH mIu/ml** **(Mean ±SD)**
Neg. control	AB 4.367±0.301	C 3.374±0.573	BC 2.847±0.510
STZ	D 3.709±0.269	A 5.405±0.540	A 3.941±0.709
STZ+ Met	BC 4.105±0.132	BC 3.870±0.513	AB 3.403±0.413
STZ+ Ag	ABC 4.193±0.126	C 3.434±0.189	BC 3.229±0.281
STZ+ Se	ABC 4.225±0.184	C 3.169±0.286	BC 2.899±0.373
STZ+ Ag NPs	C 4.024±0.117	B 4.567±0.834	BC 3.021±0.426
STZ+ Se NPs	A 4.500±0.276	C 3.665±0.448	C 2.691±0.496
LSD	0.370	0.900	0.821
P-value	**0.0011**	**0.0002**	**0.022**

- STZ stands for streptozotocin diabetic mice.
- Different capital letters and small last names denote significant $p \leq 0.05$.
- Met for metformin.

- LSD is short for least significant difference.
- P stands for probability.

The results showed the effect of nanoparticles and other substances on the level of testosterone, the results were positive and decreased LH and FSH hormone and not significantly in testosterone level. These results were also observed in [45] . Some studies using high concentrations of silver nanoparticles showed a change in the rate of LH, FSH and testosterone hormones, and this led to interference in the metabolism process and hepatic renal failure, as shown [190, 191].

4.3.4. Super Oxide Dismutase level on control and treated groups (SOD)and the Malondialdehyde (MDA)

From the outcomes displayed in Table (4-6) SOD levels were (4.763±0.480 units / ml) in the control group, and they considerably ($P \leq 0.05$) dropped in the streptozotocin group, as can be shown (1.673±0.205 units / ml) while the group increased The treatment with nano-selenium, which was prepared using the environmentally friendly green method, was (4.495±0.544 units / ml)[192]. The results shown in the table also showed an increase in each of the groups treated with metformin, silver, selenium, and nano-silver, but at a less significant level than the nano-selenium group, where the results were (2.224±0.399, 2.224±0.176, 2.128±0.166, and 2.917±0.234 units/ml), respectively. These findings demonstrated a substantial ($P \leq 0.05$) rise in SOD levels when compared to DM. It was significantly different from the other groups (DM, Met, Ag, Se, Ag NPs), while there are no significant differences between the green Se NPs group and the negative control group These results have been matched with other studies and as shown[193]. On the other hand, it was noted in the results presented in the Table (4-6) that the value of the MDA level was (6.031±0.739 units / ml) in the control group, and in the streptozotocin group, this value considerably rose ($P \leq 0.05$), (12.827±1.908 units / ml) while The MDA value returned and decreased in the group treated with selenium nanoparticles prepared by the environmentally friendly green method and it was (7.224±0.737 units / ml). The results shown in the table also showed a decrease in each of the groups treated with metformin, silver, selenium and silver nanoparticles, but at a less significant level than the group of nanoparticles selenium, where the results were (9.675±0.777, 9.844±0.487, 9.788 ±0.694, 8.748 ±0.651 units / ml), respectively. According to these findings, the amount of SOD decreased significantly ($P \leq 0.05$) when compared to DM. These results are in agreement with the study's findings [193].

On the other hand, it was noted in the results presented in the Table (4-6) that the value of the MDA level was (6.031±0.739 units / ml) This value was significantly higher (12.827±1.908 units / ml) in the streptozotocin group than it was in the control group (P

≤0.05) while The MDA value returned and decreased in the group treated with selenium nanoparticles prepared by the environmentally friendly green method and it was (7.224±0.737 units / ml). The results shown in the table also showed a decrease in each of the groups treated with metformin, silver, selenium and silver nanoparticles, but at a less significant level than the group of nanoparticles selenium, where the results were (9.675±0.777, 9.844±0.487, 9.788±0.694, 8.748±0.651 units / ml), respectively. According to these findings, the amount of SOD decreased significantly (P ≤0.05) when compared to DM. These results are in agreement with the study's findings [193]. They were significantly different from the other groups (DM, Met, Ag, Se, Ag NPs), while there are few significant differences between the green Se NPs group and the negative control group These results have been matched with other studies and as shown [194].

Table (4-6). Super Oxide Dismutase level on control and treated groups (SOD) and the Malondialdehyde (MDA)

Parameters Groups	SOD U/mg (Mean ±SD)	MDA nmol/ml (Mean ±SD)
Neg. control	A 4.763±0.480	C 6.031±0.739
STZ	D 1.673±0.205	A 12.827±1.908
STZ+ Met	C 2.321±0.399	B 9.675±0.777
STZ+ Ag	C 2.224±0.176	B 9.844±0.487
STZ+ Se	CD 2.128±0.166	B 9.788±0.694
STZ+ Ag NPs	B 2.917±0.234	B 8.748±0.651
STZ+ Se NPs	A 4.495±0.544	C 7.224±0.737
LSD	0.599	1.664
P-value	**0.0003**	**0.0001**

- STZ stands for streptozotocin diabetic mice.
- Different capital letters and small last names denote significant p ≤0.05.
- Met for metformin.
- LSD is short for least significant difference.
- P stands for probability.

Examination of SOD and MDA is an important marker for measuring oxidative stress by measuring lipid peroxidation in cells, and that high levels of MDA can cause damage

to proteins, nucleic acids and phospholipids due to increased ROS, and this leads to cell death. DM injury increases oxidative stress, and the latter causes protein changes such as carbon proteins and lipid peroxides. These protein changes are associated with infertility diseases, as they can cause freezing in sperm and immobility. Oxidative enzymes are significantly affected by nanoparticles, and their enhanced activity is a sign of this. based on their presence and capacity to collect ROS, which contributes to the protective effect against oxidative stress, reducing free radicals generated during DM, and preventing further damage to membrane lipids. These results have been matched with other studies and as shown [194, 195].

4.3.5. Liver enzymes

In this assay, the activity of liver enzymes was measured to determine the hepatic function of diabetic white male mice induced by streptozotocin. The results shown in Table (4-7) showed a significant increase ($P \leq 0.05$) in the serum levels of ALT, AST, and ALP in the blood of mice in the STZ group when compared to the control group, and the results were as follows (89.28±3.20, 154.88±6.28 and 120.16±3.19), respectively. There was a significant decrease ($P \leq 0.05$) in the serum levels of ALT, AST, and ALP in the blood of mice depending on the type of treatment Se NPs as shown (66.97±3.25, 109.84±6.42 and 75.81±3.08) on the other hand, no significant change was observed in the levels of ALT, AST, and ALP in the groups treated with MET, Ag, Se, and Ag NPs when compared to the positive control group, and no other significant negative signs or symptoms were recorded.

Table (4-7). Liver Enzymes

Parameters Groups	**ALT U/L (Mean ±SD)**	**AST U/L (Mean ±SD)**	**Alp U/L (Mean ±SD)**
Neg. control	E 60.09±3.16	E 87.64±4.03	D 78.48±2.77
STZ	B 89.28±3.20	A 154.88±6.28	A 120.16±3.19
STZ+ Met	C 80.00±3.97	C 120.56±3.53	C 88.57±4.75
STZ+ Ag	B 93.10±3.52	B 129.71±3.66	BC 94.66±7.00
STZ+ Se	A 101.06±7.60	B 134.24±4.66	B 101.12±6.46
STZ+ Ag NPs	C 77.29±4.44	C 120.08±5.41	D 79.54±2.94
STZ+ Se NPs	D 66.97±3.25	D 109.84±6.42	D 75.81±3.08
LSD	7.638	8.620	7.989
P-value	**0.0002**	**0.000**	**0.00060**

- STZ stands for streptozotocin diabetic mice.
- Different capital letters and small last names denote significant p ≤0.05.
- Met for metformin.
- LSD is short for least significant difference.
- P stands for probability.

The increase that appeared in the percentage of liver enzymes means that the liver was exposed to damage or weakness that led to an increase in the levels of liver enzymes, as many studies showed, including [196] that diabetes causes a decrease in immunity and antioxidant enzyme activity, as a result free radicals are formed, which in turn cause Tissue damage and these results are consistent with the study (Gutiérrez et al., 2022). The decrease that appeared in the percentage of ALT, AST and ALP in the group treated with Se NPs indicates that the nanoparticles in this group played the role of nutritional supplements that enhance activities and stimulate the immune response, which leads to get rid of oxidative stress through the elimination of free radicals. This study is consistent with the following study (Jha et al., 2022; Hashim et al., 2022).

4.3.6. Kidney enzymes

Kidney function was evaluated based on measuring the levels of urea, albumin and creatine in the kidneys in the positive control group (with STZ) and the groups treated with MT, Ag, Se, Ag NPs and Se NPs, and compared them with the negative control group.

The results in Table (4-8) indicate an increase in the levels of urea and creatinine in the group with STZ-induced diabetes when compared with the negative control group (P ≤0.05) and as shown (47.80±2.36, 186.51±5.58) respectively, with a decrease in Albumin levels in the same group, as shown in (2.842±0.514). Treatment with Se NPs prepared by the correct green method and concentration (2 mg/kg body weight/day) led to a decrease in urea and creatinine levels, as shown in the results (32.34±2.75, 155.66±5.23), respectively. And an increase in albumin levels, as shown (4.052±0.144), and these results are consistent with the study [200], which showed that treatment using Se NPs leads to the elimination of endothelial dysfunction and vascular disorders, through the regulation of antioxidants and the release of nitric oxide. After 35 days of therapy, there were no statistically significant variations in the parameters MT, Ag, and Se between the experimental groups and the control groups, while treatment using Ag NPs showed a decrease in urea and creatinine levels by a small percentage when compared with the control group, as shown in the results (33.87±2.62, 166.31±4.33), respectively. This has been observed in previous studies, with doses (100 mg / kg), where

urea and creatinine levels were significantly restored, which led to a reduction in toxicity caused by STZ in male mice, as shown (Hendi, 2011).

Table (4-8). Kidney enzymes

Parameters Groups	Urea mg/dl (Mean ±SD)	Albumin mg/dl (Mean ±SD)	Creatinine mg/dl (Mean ±SD)
Neg. control	E 29.34±3.34	A 4.790±0.229	F 148.64±4.13
STZ	A 47.80±2.36	F 2.842±0.514	A 186.51±5.58
STZ+ Met	C 38.57±3.69	EF 3.038±0.206	C 174.76±5.14
STZ+ Ag	BC 41.50±2.88	CD 3.4700±0.1643	BC 180.050±1.971
STZ+ Se	B 43.285±1.759	BC 3.7800±0.171	AB 182.44±2.95
STZ+ Ag NPs	D 33.87±2.62	DE 3.263±0.264	D 166.31±4.33
STZ+ Se NPs	DE 32.34±2.75	B 4.052±0.144	E 155.66±5.23
LSD	4.901	0.464	7.550
P-value	**0.00021**	**0.00068**	**0.0007**

- STZ stands for streptozotocin diabetic mice.
- Different capital letters and small last names denote significant $p \leq 0.05$.
- Met for metformin.
- LSD is short for least significant difference.
- P stands for probability.

The incidence of diabetes induced by STZ led to an increase in the concentration of urea and creatinine with a decrease in the concentration of albumin in the blood, and as the above results showed, this indicates a defect or disease in the kidneys as a result of diabetes. The treatment using Se NPs led to a reduction in the harmful effects of diabetes by improving the level of insulin in the blood. This in turn led to a decrease in diabetes and thus a decrease in urea and creatinine in the blood at the same time an increase in albumin in the blood, and this indicates the role of Se NPs This is consistent with [202]. who used selenium nanoparticles at a concentration of 0.1 mg/kg. It was also found that the treatment using low doses of AgNPs are made by the green environmentally friendly method at a concentration (2 mg/kg body weight/day), is effective in reviving all

parameters of the liver and kidneys without causing toxic effects and has an effective protective role for the body (Lotfy et al., 2023)

4.3.7. Concentration of glucose and insulin levels in the blood

The response of pancreatic beta cells to insulin was studied in STZ-induced diabetic male mice by measuring the concentration levels of glucose and insulin in the blood. The results were recorded for the groups treated with MET, Ag, Se, Ag NPs and Se NPs. The blood glucose levels were measured as shown in the Table (4-9). The glucose level in the serum of healthy mice increased significantly and clearly ($P \leq 0.05$) after being injected with STZ, so the glucose value became (291.50±9.26) when compared to the control group, which was (94.00±7.53). In the group treated with Se NPs showed a decrease in glucose levels when compared with the control group when the concentration (2 mg/kg body weight/day) and for a treatment period of 35 days reached (134.25±6.18). This result is consistent with the study shown (Gutiérrez et al., 2022). On the other hand, a significant decrease in glucose levels was not observed when diabetic groups were treated with Ag and Se. The group treated with concentration (2 mg/kg body weight/day) of Ag NPs reduced blood glucose levels as it became (180.00±12.99), but this decrease was less significant than the group treated with metformin, whose glucose reached (118.75±6.85) when compared with the group of diabetic mice left without treatment. These results are consistent with the study (Wahab et al., 2022), where treatment with Ag NPs at a concentration of (100 mg / kg) showed a better role for treating blood diabetes. The results showed in Table (4-9) that the value of insulin in the control group was (25.036±1.846), and when male mice were infected with STZ-induced diabetes, insulin levels decreased significantly ($P \leq 0.05$) and became (16.714±1.149). The results showed a significant increase in Insulin levels when treated with Se NPs became (21.143±1.807) when compared with the diabetic group, this result is consistent with the study (El-Borady et al., 2020). There are no significant differences that can be recorded when using the rest of the treatments when compared with the negative control group.

- STZ stands for streptozotocin diabetic mice.
- Different capital letters and small last names denote significant $p \leq 0.05$.
- Met for metformin.
- LSD is short for least significant difference.
- P stands for probability.

Table (4-9). Concentration of glucose and insulin levels in the blood

Parameters Groups	Glucose mg/dl (Mean ±SD)	Insulin IU/ml (Mean ±SD)
Neg. control	F 94.00±7.53	A 25.036±1.846
STZ	A 291.50±9.26	B 16.714±1.149
STZ+ Met	E 118.75±6.85	E 22.643±1.450
STZ+ Ag	B 235.25±7.50	DE 18.429±1.726
STZ+ Se	B 241.50±8.81	DE 17.714±0.508
STZ+ Ag NPs	C 180.00±12.99	CD 19.429±1.489
STZ+ Se NPs	D 134.25±6.18	BC 21.143±1.807
LSD	15.054	2.584
P-value	**0.0005**	**0.00023**

The STZ-induced diabetes led to the destruction of insulin-secreting cells in the pancreas and a decrease in the activity of enzymes associated with antioxidants, namely SOD. This decrease led to an increase in hydrogen peroxide radicals and ROS production. The increase in ROS production leads to the destruction of beta cells in the pancreas, which in turn increases blood glucose levels. Treatment with Se NPs restored antioxidant activity and enhanced metabolism, as Se particles are considered effective nutritional supplements that increase the body's immunity. Treatment with Se NPs leads to improvement of insulin receptors and beta cell regeneration, and thus a decrease in glucose. This is what was referred to in (Wang et al., 2017; Gutiérrez et al., 2022). so, it can be used as an anti-diabetic due to its natural activity as an antioxidant and an effective role as insulin. The effective activities of smaller Ag NPs can be attributed to better activity as antioxidants and inhibition of alpha amylase activity, as insulin sensitivity to glucose secretion can be enhanced by reducing oxidative stress as mentioned in (Kazmi et al., 2021).

Conclusions and Perspectives

Conclusions:

In this study, Se NPs and Ag NPs were successfully prepared utilizing a straightforward, secure biological approach at temperatures as high as 100 degrees Celsius. Their characteristics were examined, and their biological activities were assessed. The findings of this study can be summed up as follows:

- Using the leaves of the Withania somnifera and garlic plants, respectively, as a reducing and stabilizing agent, has been successful in reducing the size of Ag and Se particle.
- The biosynthesis produced crystalline Se NPs of high purity with an average crystal size of 25 nm and a spherical shape as shown in XRD and TEM, as well as crystalline Ag NPs of lower purity due to the presence of oxygen resulting from the presence of Ago compounds, which have a spherical shape with some agglomeration and an average crystal size of 30 nm.
- Se NPs and Ag NPs had antihyperglycemic and antioxidant benefits in metformin-induced diabetic mice by decreasing the production of free radicals and ROS brought on by high cholesterol, increasing blood insulin and SOD, and doing so with minimum toxicity and no negative side effects. mortality in a rat model, thereby stopping the spread of the illness.
- Nanoparticles with a high activity of 2 mg/kg body weight/day can effectively treat low sperm counts brought on by situations of high blood sugar and elevated ROS, as well as frailty that results in malformations and death.

Perspectives:

- The properties of Se NPs and Ag NPs when combined with organic materials, such as natural products, are still being researched and improved.
- More research should be done to determine how well Se NPs and Ag NPs perform in biological applications, particularly when utilized in vivo.
- Use more parameters used in manufacturing such as the effect of lowering the temperature on the morphology of the Se NPs and Ag NPs nanoparticles and study the variables that obtained the size and shape.
- Other techniques, such as the milling procedure with various concentrations, are used to synthesize Se NPs and Ag NPs

References

Abarikwu, S. O. (2013). Causes and risk factors for male-factor infertility in Nigeria: A review. African Journal of Reproductive Health, 17.

Abbas, R. H., Haleem, A. M., & Kadhim, A. (2023). The antimicrobial effect of simultaneously applying different diode lasers and silver nanoparticles synthesized by laser ablation on bacterial dental caries. Applied Nanoscience, 1-15.

Abdallah, A. B., El-Ghannam, M. A., Hasan, A. A., Mohammad, L. G., Mesalam, N. M., & Alsayed, R. M. (2023). Selenium nanoparticles modulate steroidogenesis-related genes and improve ovarian functions via regulating androgen receptors expression in polycystic ovary syndrome rat model. Biological Trace Element Research, 1-13.

Abdelghani, G. M., Ahmed, A. B., & Al-Zubaidi, A. B. (2022). Synthesis, characterization, and the influence of energy of irradiation on optical properties of ZnO nanostructures. Scientific Reports, 12, 20016.

Abdelghani, G. M., Ahmed, A. B., & Al-Zubaidi, A. B. (2022). Synthesis, characterization, and the influence of energy of irradiation on optical properties of ZnO nanostructures. Scientific Reports, 12, 20016.

Abdelkader, A. M., & Yeh, J. (2009). The potential use of intrauterine insemination as a basic option for infertility: A review for technology-limited medical settings. Obstetrics and Gynecology International.

Abid, N., Khan, A. M., Shujait, S., Chaudhary, K., Ikram, M., Imran, M., et al. (2021). Synthesis of nanomaterials using various top-down and bottom-up approaches, influencing factors, advantages, and disadvantages: A review. Advances in Colloid and Interface Science, 291, 102597.

Adil, S. F., Ashraf, M., Khan, M., Assal, M. E., Shaik, M. R., Kuniyil, M., et al. (2022). Advances in graphene/inorganic nanoparticle composites for catalytic applications. The Chemical Record, 22, e202100274.

Agbaje, A. O., Barker, A. R., Mitchell, G. F., & Tuomainen, T.-P. (2022). Effect of arterial stiffness and carotid intima-media thickness progression on the risk of dysglycemia, insulin resistance, and dyslipidemia: A temporal causal longitudinal study. Hypertension, 79, 667-678.

Ahmed, F., Dwivedi, S., Shaalan, N. M., Kumar, S., Arshi, N., Alshoaibi, A., et al. (2020). Development of selenium nanoparticle-based agriculture sensor for heavy metal toxicity detection. Agriculture, 10, 610.

Alagesan, V., & Venugopal, S. (2019). Green synthesis of selenium nanoparticle using leaves extract of Withania somnifera and its biological applications and photocatalytic activities. Bionanoscience, 9, 105-116.

Alahmar, T. A. (2019). Role of oxidative stress in male infertility: An updated review. Journal of Human Reproductive Sciences, 12, 4.

Alhazza, I. M., Ebaid, H., Omar, M. S., Hassan, I., Habila, M. A., Al-Tamimi, J., et al. (2022). Supplementation with selenium nanoparticles alleviates diabetic nephropathy during pregnancy in diabetic female rats. Environmental Science and Pollution Research, 29, 5517-5525.

Ali, I. A. M., Ahmed, A. B., & Al-Ahmed, H. I. (2023). Green synthesis and characterization of silver nanoparticles for reducing the damage to sperm parameters in diabetic compared to metformin. Scientific Reports, 13, 2256.

Allouche, J. (2013). Synthesis of organic and bioorganic nanoparticles: An overview of the preparation methods. Nanomaterials: A danger or a promise?, 27-74.

Al-Mudhaffer, M. F., Nattiq, M. A., & Jaber, M. A. (2012). Linear optical properties and energy loss function of Novolac: Epoxy blend film. Archives of Applied Science Research, 4, 1731-1740.

Al-Mudhaffer, M. F., Nattiq, M. A., & Jaber, M. A. (2012). Linear optical properties and energy loss function of Novolac: epoxy blend film. Archives of Applied Science Research, 4, 1731-7140.

Al-Otibi, F., Perveen, K., Al-Saif, N. A., Alharbi, R. I., Bokhari, N. A., Albasher, G., et al. (2021). Biosynthesis of silver nanoparticles using Malva parviflora and their antifungal activity. Saudi Journal of Biological Sciences, 28, 2229-2235.

Anderson, R., Moses, R., Lenherr, S., Hotaling, J. M., & Myers, J. (2018). Spinal cord injury and male infertility—a review of current literature, knowledge gaps, and future research. Translational Andrology and Urology, 7, S373.

Anjum, S., Abbasi, B. H., & Shinwari, Z. K. (2016). Plant-mediated green synthesis of silver nanoparticles for biomedical applications: Challenges and opportunities. Pak. J. Bot, 48, 1731-1760.

Artimani, T., Amiri, I., Soleimani Asl, S., Saidijam, M., Hasanvand, D., & Afshar, S. (2018). Amelioration of diabetes-induced testicular and sperm damage in rats by cerium oxide nanoparticle treatment. Andrologia, 50, e13089.

Astruc, D. (2020). Introduction: Nanoparticles in catalysis. ACS Publications, 120, 461-463.

Baig, N., Kammakakam, I., & Falath, W. (2021). Nanomaterials: A review of synthesis methods, properties, recent progress, and challenges. Materials Advances, 2, 1821-1871.

Balamanikandan, T., Balaji, S., & Pandirajan, J. (2015). Biological synthesis of silver nanoparticles by using onion (Allium cepa) extract and their antibacterial and antifungal activity. World Applied Science Journal, 33, 939-943.

Barron, E., Bakhai, C., Kar, P., Weaver, A., Bradley, D., Ismail, H., et al. (2020). Associations of type 1 and type 2 diabetes with COVID-19-related mortality in England: A whole-population study. The Lancet Diabetes & Endocrinology, 8, 813-822.

Bayda, S., Adeel, M., Tuccinardi, T., Cordani, M., & Rizzolio, F. (2019). The history of nanoscience and nanotechnology: From chemical–physical applications to nanomedicine. Molecules, 25, 112.

Birla, S., Singh, N., & Shukla, N. K. (2022). Nanotechnology: Device design and applications. CRC Press.

Bokov, D., Jalil, A. T., Chupradit, S., Suksatan, W., Ansari, M. J., Shewael, I. H., et al. (2021). Nanomaterial by sol-gel method: Synthesis and application. Advances in Materials Science and Engineering, 2021, 2021.

Bouqellah, N. A., Mohamed, M. M., & Ibrahim, Y. (2019). Synthesis of eco-friendly silver nanoparticles using Allium sp. and their antimicrobial potential on selected vaginal bacteria. Saudi Journal of Biological Sciences, 26, 1789-1794.

Bruna, T., Maldonado-Bravo, F., Jara, P., & Caro, N. (2021). Silver nanoparticles and their antibacterial applications. International Journal of Molecular Sciences, 22, 7202.

Burgner, A. M., & McCall, N. (2022). Pregnancy and diabetes. In Diabetes and Kidney Disease (pp. 401-416). Springer.

Burlinson, B. (2012). The in vitro and in vivo comet assays. In Genetic Toxicology: Principles and Methods (pp. 143-163).

Busatto, S., & de Mello Donega, C. (2022). Magic-Size Semiconductor Nanostructures: Where Does the Magic Come From? ACS Materials Au.

Buzea, C., Pacheco, I. I., & Robbie, K. (2007). Nanomaterials and nanoparticles: Sources and toxicity. Biointerphases, 2, MR17-MR71.

Castillo-Henríquez, L., Alfaro-Aguilar, K., Ugalde-Álvarez, J., Vega-Fernández, L., Montes de Oca-Vásquez, G., & Vega-Baudrit, J. R. (2020). Green synthesis of gold and silver nanoparticles from plant extracts and their possible applications as antimicrobial agents in the agricultural area. Nanomaterials, 10, 1763.

Chamoli, P., Banerjee, S., Raina, K., & Kar, K. K. (2020). Characteristics of graphene/reduced graphene oxide. Handbook of Nanocomposite Supercapacitor Materials I, 155-177.

Chulakham, Y. (2021). Heteroaggregation of lignin and zein nanoparticles: Effects of relative size and concentration. Louisiana State University and Agricultural & Mechanical College.

Cittrarasu, V., Kaliannan, D., Dharman, K., Maluventhen, V., Easwaran, M., Liu, W. C., et al. (2021). Green synthesis of selenium nanoparticles mediated from Ceropegia bulbosa Roxb extract and its cytotoxicity, antimicrobial, mosquitocidal, and photocatalytic activities. Scientific Reports, 11, 1032.

Damodharan, J. (2021). Nanomaterials in medicine–An overview. Materials Today: Proceedings, 37, 383-385.

Daraio, C., & Jin, S. (2012). Synthesis and patterning methods for nanostructures useful for biological applications. In Nanotechnology for Biology and Medicine (pp. 27-44). Springer.

Das, A., Kumar, R., Goutam, S., & Sagar, S. (2016). Sunlight irradiation-induced synthesis of silver nanoparticles using glycolipid bio-surfactant and exploring the antibacterial activity. Journal of Bioengineering & Biomedical Science, 6, 1-10.

Das, A., Kumar, R., Goutam, S., & Sagar, S. (2016). Sunlight irradiation induced synthesis of silver nanoparticles using glycolipid bio-surfactant and exploring the antibacterial activity. J. Bioeng. Biomed. Sci, 6.

Desai, D., Guerrero, Y. A., Balachandran, V., Morton, A., Lyon, L., Larkin, B., et al. (2021). Towards a microfluidics platform for the continuous manufacture of organic and inorganic nanoparticles. Nanomedicine: Nanotechnology, Biology and Medicine, 35, 102402.

Dessouky, A., Abdelhaleem, M., Halloull, N. M., Moustafa, M. M., & Askar, E. M. (2021). The Effect of Selenium Nanoparticles on Tramadol Induced Hepatotoxicity in a Rat Model. Egyptian Journal of Histology.

DiMeglio, L. A., Evans-Molina, C., & Oram, R. A. (2018). Type 1 diabetes. The Lancet, 391, 2449-2462.

Dolez, P. I. (2015). Nanomaterials definitions, classifications, and applications. In Nanoengineering (pp. 3-40). Elsevier.

Dosay-Akbulut, M. (2020). Determination of DNA damage caused by food additives using comet assay method. Progress in Nutrition, 22, 1-12.

Durgalakshmi, D., Balakumar, S., Rajendran, S., & Naushad, M. (2020). Functional nanomaterial in energy and environmental science. In Nanomaterials for Sustainable Energy and Environmental Remediation (pp. 1-23). Elsevier.

El-Borady, O. M., Othman, M. S., Atallah, H. H., & Moneim, A. E. A. (2020). Hypoglycemic potential of selenium nanoparticles capped with polyvinyl-pyrrolidone in streptozotocin-induced experimental diabetes in rats. Heliyon, 6, e04045.

El-Eskandarany, M. S., Al-Hazza, A., Al-Hajji, L. A., Ali, N., Al-Duweesh, A. A., Banyan, M., et al. (2021). Mechanical milling: A superior nanotechnological tool for fabrication of nanocrystalline and nanocomposite materials. Nanomaterials, 11, 2484.

El-Nekeety, A. A., Hassan, M. E., Hassan, R. R., Elshafey, O. I., Hamza, Z. K., Abdel-Aziem, S. H., et al. (2021). Nanoencapsulation of basil essential oil alleviates the oxidative stress, genotoxicity and DNA damage in rats exposed to biosynthesized iron nanoparticles. Heliyon, 7, e07537.

El-Ramady, H. R., Domokos-Szabolcsy, É., Shalaby, T. A., Prokisch, J., & Fári, M. (2015). Selenium in agriculture: Water, air, soil, plants, food, animals and nanoselenium. In CO2 Sequestration, Biofuels and Depollution (pp. 153-232).

El-Refai, A. A., Ghoniem, G. A., El-Khateeb, A. Y., & Hassaan, M. M. (2018). Eco-friendly synthesis of metal nanoparticles using ginger and garlic extracts as biocompatible novel antioxidant and antimicrobial agents. Journal of Nanostructure in Chemistry, 8, 71-81.

Ernst, M. (2021). Type 2 Diabetes. In A Guy's Guide: What Every Man Needs to Know About Their Health (pp. 100-120).

Fadl, M. S., Abdellateif, A.-E.-K. M., Khandel, A. A., & Aboella, A. A. (2023). Assessment of reproductive toxicity of silver nanoparticles on male albino mice. Egyptian Academic Journal of Biological Sciences, B. Zoology, 15, 53-67.

Falcone, M., Meier, J. J., Marini, M. G., Caccialanza, R., Aguado, J. M., Del Prato, S., et al. (2021). Diabetes and acute bacterial skin and skin structure infections. Diabetes Research and Clinical Practice, 174, 108732.

Feng, D., Zhang, R., Zhang, M., Fang, A., & Shi, F. (2022). Synthesis of eco-friendly silver nanoparticles using glycyrrhizin and evaluation of their antibacterial ability. Nanomaterials, 12, 2636.

Gál, E., Dolenšek, J., Stožer, A., Czakó, L., Ébert, A., & Venglovecz, V. (2021). Mechanisms of post-pancreatitis diabetes mellitus and cystic fibrosis-related diabetes: A review of preclinical studies. Frontiers in Endocrinology, 12, 1-20.

Galić, E., Radić, K., Golub, N., Vitali Čepo, D., Kalčec, N., Vrček, E., et al. (2022). Utilization of olive pomace in green synthesis of selenium nanoparticles: Physico-chemical characterization, bioaccessibility, and biocompatibility. International Journal of Molecular Sciences, 23, 9128.

Galicia-Garcia, U., Benito-Vicente, A., Jebari, S., Larrea-Sebal, A., Siddiqi, H., Uribe, K. B., et al. (2020). Pathophysiology of type 2 diabetes mellitus. International Journal of Molecular Sciences, 21, 6275.

Gates, B., Mayers, B., Cattle, B., & Xia, Y. (2002). Synthesis and characterization of uniform nanowires of trigonal selenium. Advanced Functional Materials, 12, 219-227.

Gates, B., Mayers, B., Cattle, B., & Xia, Y. (2002). Synthesis and characterization of uniform nanowires of trigonal selenium. Advanced Functional Materials, 12, 219-227.

Ge, J., Ngo, L. P., Kaushal, S., Tay, I. J., Thadhani, E., Kay, J. E., et al. (2021). CometChip enables parallel analysis of multiple DNA repair activities. DNA Repair, 106, 103176.

Georgakilas, V., Perman, J. A., Tucek, J., & Zboril, R. (2015). Broad family of carbon nanoallotropes: Classification, chemistry, and applications of fullerenes, carbon dots,

nanotubes, graphene, nanodiamonds, and combined superstructures. Chemical Reviews, 115, 4744-4822.

Gervais, F. (2002). Optical conductivity of oxides. Materials Science and Engineering: R: Reports, 39, 29-92.

Glazyrine, V., Stephens, D., Wentzell, E., Wallace-Young, K., & Nangia, A. K. (2022). Emotional consequences of male infertility. In Psychological and Medical Perspectives on Fertility Care and Sexual Health (pp. 23-44). Elsevier.

Göğebakan, K., & Şah, M. (2021). A review of recent advances for preventing, diagnosis, and treatment of diabetes mellitus using semantic web. In 2021 3rd International Congress on Human-Computer Interaction, Optimization and Robotic Applications (HORA) (pp. 1-6).

Goodarzi, V., Zamani, H., Bajuli, L., & Moradshahi, A. (2014). Evaluation of antioxidant potential and reduction capacity of some plant extracts in silver nanoparticles' synthesis. Molecular Biology Research Communications, 3, 165-170.

Gour, A., & Jain, N. K. (2019). Advances in green synthesis of nanoparticles. Artificial Cells, Nanomedicine, and Biotechnology, 47, 844-851.

Gul, R., Jan, H., Lalay, G., Andleeb, A., Usman, H., Zainab, R., et al. (2021). Medicinal plants and biogenic metal oxide nanoparticles: A paradigm shift to treat Alzheimer's disease. Coatings, 11, 717.

Gutiérrez, R. M. P., Gómez, J. T., Urby, R. B., Soto, J. G. C., & Parra, H. R. (2022). Evaluation of Diabetes Effects of Selenium Nanoparticles Synthesized from a Mixture of Luteolin and Diosmin on Streptozotocin-Induced Type 2 Diabetes in Mice. Molecules, 27, 5642.

Habubi, N. F., Bakr, N. A., & Salman, S. A. (2013). Optical parameters of amorphous selenium deposited by thermal evaporation technique. PCAIJ, 8, 54-58.

Hano, C., & Abbasi, B. H. (2021). Plant-based green synthesis of nanoparticles: Production, characterization, and applications. MDPI, 12, 31.

Hartmann, K., Möstl, K., Lloret, A., Thiry, E., Addie, D. D., Belák, S., et al. (2022). Vaccination of immunocompromised cats. Viruses, 14, 923.

Hasanuzzaman, M., Bhuyan, M. B., Raza, A., Hawrylak-Nowak, B., Matraszek-Gawron, R., Nahar, K., et al. (2020). Selenium toxicity in plants and environment: Biogeochemistry and remediation possibilities. Plants, 9, 1711.

Hashim, M., Mujahid, H., Hassan, S., Bukhari, S., Anjum, I., Hano, C., et al. (2022). Implication of Nanoparticles to Combat Chronic Liver and Kidney Diseases: Progress and Perspectives. Biomolecules, 12, 1337.

Hendi, A. (2011). Silver nanoparticles mediate differential responses in some of liver and kidney functions during skin wound healing. Journal of King Saud University-Science, 23, 47-52.

Hosnedlova, B., Kepinska, M., Skalickova, S., Fernandez, C., Ruttkay-Nedecky, B., Peng, Q., et al. (2018). Nano-selenium and its nanomedicine applications: A critical review. International Journal of Nanomedicine, 13, 2107-2138.

Hu, J., & Yang, Z. (2022). Layer-by-layer self-assembly preparation and desalination performance of graphene oxide membrane. Water Supply, 22, 126-136.

Ijaz, I., Gilani, E., Nazir, A., & Bukhari, A. (2020). Detail review on chemical, physical and green synthesis, classification, characterizations, and applications of nanoparticles. Green Chemistry Letters and Reviews, 13, 223-245.

Iketubosin, F. (2018). In vitro fertilization embryo transfer processes and pathway: A review from practice perspective. Tropical Journal of Obstetrics and Gynaecology, 35, 227-232.

Iqbal, S., Fakhar-e-Alam, M., Akbar, F., Shafiq, M., Atif, M., Amin, N., et al. (2019). Application of silver oxide nanoparticles for the treatment of cancer. Journal of Molecular Structure, 1189, 203-209.

Jadoun, S., Arif, R., Jangid, N. K., & Meena, R. K. (2021). Green synthesis of nanoparticles using plant extracts: A review. Environmental Chemistry Letters, 19, 355-374.

Jha, N., Annamalai, A., Essakiraj, P., Balamurugan, R., Lakra, A. K., Tilwani, Y. M., et al. (2022). Effects of polysaccharide-based silver and selenium nanoparticles on growth performance, biochemical parameters, and immune response of Cyprinus carpio. Fish and Shellfish Immunology Reports, 3, 100062.

Jiang, F., Cai, W., & Tan, G. (2017). Facile synthesis and optical properties of small selenium nanocrystals and nanorods. Nanoscale Research Letters, 12, 1-6.

Jiang, F., Cai, W., & Tan, G. (2017). Facile synthesis and optical properties of small selenium nanocrystals and nanorods. Nanoscale Research Letters, 12, 1-6.

Kalra, S., & Khandelwal, D. (2018). Thyrovigilance in diabetes; Glucovigilance in thyroidology. Primary Care Diabetes, 68, 966-967.

Karbaschi, M., Ji, Y., Abdulwahed, A. M. S., Alohaly, A., Bedoya, J. F., Burke, S. L., et al. (2019). Evaluation of the major steps in the conventional protocol for the alkaline comet assay. International Journal of Molecular Sciences, 20, 6072.

Kazmi, S. A. R., Qureshi, M. Z., Alhewairini, S. S., Ali, S., Khurshid, S., Saeed, M., et al. (2021). Minocycline-derived silver nanoparticles for assessment of their antidiabetic potential against alloxan-induced diabetic mice. Pharmaceutics, 13, 1678.

Kazmi, S. A. R., Qureshi, M. Z., Sadia, S., Alhewairini, S. S., Ali, S., Khurshid, S., et al. (2021). Minocycline-derived silver nanoparticles for assessment of their antidiabetic potential against alloxan-induced diabetic mice. Pharmaceutics, 13, 1678.

Khalid, K., Tan, X., Mohd Zaid, H. F., Tao, Y., Chew, C. L., Chu, D.-T., et al. (2020). Advances in developmental organic and inorganic nanomaterial: A review. Bioengineered, 11, 328-355.

Khan, F. A. (2020). Nanomaterials: Types, classifications, and sources. In Applications of Nanomaterials in Human Health (pp. 1-13). Springer.

Khan, I., Saeed, K., & Khan, I. (2019). Nanoparticles: Properties, applications, and toxicities. Arabian Journal of Chemistry, 12, 908-931.

Khan, S. A., Shahid, S., & Lee, C.-S. (2020). Green synthesis of gold and silver nanoparticles using leaf extract of Clerodendrum inerme; Characterization, antimicrobial, and antioxidant activities. Biomolecules, 10, 835.

Khanna, P. K., Bisht, N., & Phalswal, P. (2022). Selenium nanoparticles: A review on synthesis and biomedical applications. Materials Advances.

Khazaei, M. R., Gravandi, E., Ghanbari, E., Niromand, E., & Khazaei, M. (2022). Trifolium pratense extract increases testosterone and improves sperm characteristics and antioxidant status in diabetic rats. Biotechnic & Histochemistry, 1-8.

Kim, C. R., Noda, T., Okada, Y., Ikawa, M., & Baek, S. H. (2021). Protocol for isolation of spermatids from mouse testes. STAR Protocols, 2, 100254.

Kose, O., Mantecca, P., Costa, A., & Carrière, M. (2023). Putative adverse outcome pathways for silver nanoparticle toxicity on mammalian male reproductive system: a literature review. Particle and Fibre Toxicology, 20, 1-23.

Kuhn, R., Bryant, I. M., Jensch, R., & Böllmann, J. (2022). Applications of environmental nanotechnologies in remediation, wastewater treatment, drinking water treatment, and agriculture. Applied Nano, 3, 54-90.

Kumar, N., & Singh, A. K. (2015). Trends of male factor infertility, an important cause of infertility: A review of literature. Journal of Human Reproductive Sciences, 8, 191.

Kuznetsova, O. V., & Timerbaev, A. R. (2022). Magnetic nanoparticles for highly robust, facile, and efficient loading of metal-based drugs. Journal of Inorganic Biochemistry, 227, 111685.

Lawson, T. B. (2021). Nanoparticle sensors and lubricants for degenerative articular cartilage. Boston University.

Layden, E., & Bhaskar, S. (2022). Diabetes (Type 1 and 2) and gestational diabetes mellitus. In Handbook of Contraception and Sexual Reproductive Healthcare (p. 178).

Lenzen, S. (2008). The mechanisms of alloxan- and streptozotocin-induced diabetes. Diabetologia, 51, 216-226.

Li, R., Zhang, Y., Rasool, S., Geetha, T., & Babu, J. R. (2019). Effects and underlying mechanisms of bioactive compounds on type 2 diabetes mellitus and Alzheimer's disease. Oxidative Medicine and Cellular Longevity, 2019, 1-15.

Lobo, R. (2011). The optical conductivity of high-temperature superconductors. In High-Temperature Superconductors (pp. 103-146). Elsevier.

Lotfy, M. M., Dowidar, M. F., Ali, H. A., Ghonimi, W. A., Al-Farga, A., & Ahmed, A. I. (2023). Effect of Selenium Nanoparticles and/or Bee Venom against STZ-Induced Diabetic Cardiomyopathy and Nephropathy. Metabolites, 13, 400.

Lv, C., Zhang, X., Liu, Y., Zhang, T., Chen, H., Zang, J., et al. (2021). Redesign of protein nanocages: The way from 0D, 1D, 2D to 3D assembly. Chemical Society Reviews, 50, 3957-3989.

Mahmoud, A., AbdElMonem, H., & Abbas, M. (2022). The role of selenium and zinc oxide nanoparticles on mitigating side effects of obesity in rats. Brazilian Journal of Biology, 84.

Malik, M. A., Wani, M. Y., & Hashim, M. A. (2012). Microemulsion method: A novel route to synthesize organic and inorganic nanomaterials. Arabian Journal of Chemistry, 5, 397-417.

Manikandan, S., Subbaiya, R., Saravanan, M., Ponraj, M., Selvam, M., & Pugazhendhi, A. (2022). A critical review of advanced nanotechnology and hybrid membrane-based water recycling, reuse, and wastewater treatment processes. Chemosphere, 289, 132867.

Márquez-Pardo, R., Torres-Barea, I., Córdoba-Doña, J.-A., Cruzado-Begines, C., García-García-Doncel, L., Aguilar-Diosdado, M., et al. (2020). Continuous glucose monitoring and glycemic patterns in pregnant women with gestational diabetes mellitus. Diabetes Technology & Therapeutics, 22, 271-277.

Mauricio, M., Guerra-Ojeda, S., Marchio, P., Valles, S., Aldasoro, M., Escribano-Lopez, I., et al. (2018). Nanoparticles in medicine: A focus on vascular oxidative stress. Oxidative Medicine and Cellular Longevity, 2018, 1-12.

May, S., Hirsch, C., Rippl, A., Bürkle, A., & Wick, P. (2022). Assessing genotoxicity of ten different engineered nanomaterials by the novel semi-automated FADU assay and the alkaline comet assay. Nanomaterials, 12, 220.

Mazhir, S. N., Ali, I. A. M., Al-Ahmed, H. I., Bououdina, M., & Ali, F. A. M. (2020). Dependence of O. vulgare extract and cold plasma on the formation of silver nanoparticles: Anticancer activity against L20B cells. AIP Conference Proceedings, 020149.

McIntyre, H. D., Catalano, P., Zhang, C., Desoye, G., Mathiesen, E. R., & Damm, P. (2019). Gestational diabetes mellitus. Nature Reviews Disease Primers, 5, 1-19.

Mehmood, A., Murtaza, G., Bhatti, T. M., & Kausar, R. (2017). Phyto-mediated synthesis of silver nanoparticles from Melia azedarach L. leaf extract: Characterization and antibacterial activity. Arabian Journal of Chemistry, 10, S3048-S3053.

Modena, M. M., Rühle, B., Burg, T. P., & Wuttke, S. (2019). Nanoparticle characterization: What to measure? Advanced Materials, 31, 1901556.

Mohajerani, A., Burnett, L., Smith, J. V., Kurmus, H., Milas, J., Arulrajah, A., et al. (2019). Nanoparticles in construction materials and other applications, and implications of nanoparticle use. Materials, 12, 3052.

Mohammapdour, R., & Ghandehari, H. (2022). Mechanisms of immune response to inorganic nanoparticles and their degradation products. Advanced Drug Delivery Reviews, 180, 114022.

Mohammed Ali, I. A., AL-Ahmed, H. I., & Ben Ahmed, A. (2023). Evaluation of Green Synthesis (Withania somnifera) of Selenium Nanoparticles to Reduce Sperm DNA Fragmentation Diabetic Mice Induced with Streptozotocin. Applied Sciences, 13, 728.

Nasab, N. K., Sabouri, Z., Ghazal, S., & Darroudi, M. (2020). Green-based synthesis of mixed-phase silver nanoparticles as an effective photocatalyst and investigation of their antibacterial properties. Journal of Molecular Structure, 1203, 127411.

Neuberger, T., Schöpf, B., Hofmann, H., Hofmann, M., & Von Rechenberg, B. (2005). Superparamagnetic nanoparticles for biomedical applications: Possibilities and limitations of a new drug delivery system. Journal of Magnetism and Magnetic Materials, 293, 483-496.

Nile, S. H., Baskar, V., Selvaraj, D., Nile, A., Xiao, J., & Kai, G. (2020). Nanotechnologies in food science: Applications, recent trends, and future perspectives. Nano-Micro Letters, 12, 1-34.

Northcott, L. (2020). Improving patient education: Type 2 diabetes. Oklahoma City University.

Nzereogu, P., Omah, A., Ezema, F., Iwuoha, E., & Nwanya, A. (2022). Anode materials for lithium-ion batteries: A review. Applied Surface Science Advances, 9, 100233.

OKTAVIANI, O. (2021). Nanoparticles: Properties, applications, and toxicities. Jurnal Latihan, 1, 11-20.

Ombelet, W., & Van Robays, J. (2015). Artificial insemination history: Hurdles and milestones. Facts, Views & Vision in ObGyn, 7, 137.

Othman, M. S., Obeidat, S. T., Al-Bagawi, A. H., Fareid, M. A., Fehaid, A., & Moneim, A. E. A. (2022). Green-synthesized selenium nanoparticles using berberine as a promising anticancer agent. Journal of Integrative Medicine, 20, 65-72.

Panchal, S., & Chauhan, R. (2019). Variation in structural, electrical, and optical properties of selenium nanowires after irradiation with Ni^{6+} ions. Electronic Materials Letters, 15, 216-226.

Paradizo, R. N. V., Carriquiry, M., Viñoles, C., Meikle, A., & Astessiano, A. (2023). Uterine gene expression and follicular characteristics of pure and cross beef

multiparous cows grazing different herbage allowances of native grasslands. Available at SSRN 4420048.

Payton, E., Khubchandani, J., Thompson, A., & Price, J. H. (2017). Parents' expectations of high schools in firearm violence prevention. Journal of Community Health, 42, 1118-1126.

Poh, T. Y., Ali, N., Mac Aogáin, M., Kathawala, M. H., Setyawati, M. I., Ng, K. W., et al. (2018). Inhaled nanomaterials and the respiratory microbiome: Clinical, immunological, and toxicological perspectives. Particle and Fibre Toxicology, 15, 1-16.

Ponzano, M., Wiest, M. J., Coleman, A., Newton, E., Pakosh, M., Patsakos, E. M., et al. (2023). The use of alkaline phosphatase as a bone turnover marker after spinal cord injury: A scoping review of human and animal studies. The Journal of Spinal Cord Medicine, 46, 167-180.

Pouri, S., Motamedi, H., Honary, S., & Kazeminezhad, I. (2018). Biological synthesis of selenium nanoparticles and evaluation of their bioavailability. Brazilian Archives of Biology and Technology, 60, 1-12.

Prasad, K. S., & Selvaraj, K. (2014). Biogenic synthesis of selenium nanoparticles and their effect on As (III)-induced toxicity on human lymphocytes. Biological Trace Element Research, 157, 275-283.

Prasad, K. S., Patel, H., Patel, T., Patel, K., & Selvaraj, K. (2013). Biosynthesis of Se nanoparticles and its effect on UV-induced DNA damage. Colloids and Surfaces B: Biointerfaces, 103, 261-266.

Punab, M., Poolamets, O., Paju, P., Vihljajev, V., Pomm, K., Ladva, R., et al. (2017). Causes of male infertility: A 9-year prospective monocentre study on 1737 patients with reduced total sperm counts. Human Reproduction, 32, 18-31.

Pyrzynska, K., & Sentkowska, A. (2021). Biosynthesis of selenium nanoparticles using plant extracts. Journal of Nanostructure in Chemistry, 1-14.

Qiao, S., Alasmi, S., Wyatt, A., Wartenberg, P., Wang, H., Candlish, M., et al. (2023). Intra-pituitary follicle-stimulating hormone signaling regulates hepatic lipid metabolism in mice. Nature Communications, 14, 1098.

Qiu, X. G. (2011). High-temperature superconductors. Elsevier.

Rahmah, M. I., & Garallah, E. T. (2022). Preparation of copper oxides/polyvinyl alcohol nanocoatings with antibacterial activity. Chemical Data Collections, 39, 100869.

Rahmah, M. I., Sabry, R. S., & Aziz, W. J. (2021). Preparation of superhydrophobic Ag/Fe_2O_3/ZnO surfaces with photocatalytic activity. Surface Engineering, 37, 1320-1327.

Rai, M., Ingle, A. P., Trzcińska-Wencel, J., Wypij, M., Bonde, S., Yadav, A., et al. (2021). Biogenic silver nanoparticles: What we know and what do we need to know? Nanomaterials, 11, 2901.

Ramamurthy, C., Sampath, K., Arunkumar, P., Kumar, M. S., Sujatha, V., Premkumar, K., et al. (2013). Green synthesis and characterization of selenium nanoparticles and its augmented cytotoxicity with doxorubicin on cancer cells. Bioprocess and Biosystems Engineering, 36, 1131-1139.

Rashid, T. M., Nayef, U. M., & Jabir, M. S. (2021). Nano-ZnO decorated on gold nanoparticles as a core-shell via pulse laser ablation in liquid. Optik, 248, 168164.

Rasmagin, S., & Apresyan, L. (2020). Analysis of the optical properties of silver nanoparticles. Optics and Spectroscopy, 128, 327-330.

Rasmussen, M. K., Pedersen, J. N., & Marie, R. (2020). Size and surface charge characterization of nanoparticles with a salt gradient. Nature Communications, 11, 1-8.

Rezaei-Kelishadi, M., Ghasemi, A., Abdolyosefi, N. N., Zamani-Doabi, S., Ramezani, M., Changizi-Ashtiyani, S., et al. (2017). Effects of selenium nanoparticles on kidney and liver functional disorders in streptozotocin-induced diabetic rats. Physiology and Pharmacology, 21, 155-162.

Rezaei-Zarchi, S., Taghavi-Foumani, H., & Negahdary, M. (2013). Effect of silver nanoparticles on the LH, FSH and testosterone hormones in male rat. Journal of Babol University of Medical Sciences, 15, 25-29.

Richard, B., Lemyre, J.-L., & Ritcey, A. M. (2017). Nanoparticle size control in microemulsion synthesis. Langmuir, 33, 4748-4757.

Roep, B. O., Thomaidou, S., Van Tienhoven, R., & Zaldumbide, A. (2021). Type 1 diabetes mellitus as a disease of the β-cell (do not blame the immune system?). Nature Reviews Endocrinology, 17, 150-161.

Sabr, Z. A.-A., & Karim, A. P. Z. (2023). Effect of carbamazepine (Tegretol) on testicular parameters in adult male mice (Mus musculus). Annals of Forest Research, 66, 621-630.

Saleem, H., Zaidi, S. J., & Alnuaimi, N. A. (2021). Recent advancements in the nanomaterial application in concrete and its ecological impact. Materials, 14, 6387.

Saleh, T. A. (2022). Properties of nanoadsorbents and adsorption mechanisms. In Interface Science and Technology (Vol. 34, pp. 233-263). Elsevier.

Salem, S. S. (2022). Bio-fabrication of selenium nanoparticles using baker's yeast extract and its antimicrobial efficacy on food-borne pathogens. Applied Biochemistry and Biotechnology, 194, 1898-1910.

Salvioni, L., Morelli, L., Ochoa, E., Labra, M., Fiandra, L., Palugan, E., et al. (2021). The emerging role of nanotechnology in skincare. Advances in Colloid and Interface Science, 293, 102437.

Santhosh, G., & Nayaka, G. (2022). Nanoparticles in construction industry and their toxicity. In Ecological and Health Effects of Building Materials (pp. 133-146). Springer.

Sapra, A., Bhandari, P., & Wilhite Hughes, A. (2021). Diabetes Mellitus (Nursing).
Sengupta, P., Nwagha, U., Dutta, S., Krajewska-Kulak, E., & Izuka, E. (2017). Evidence for decreasing sperm count in African population from 1965 to 2015. African Health Sciences, 17, 418-427.
Shafiq, M., Anjum, S., Hano, C., Anjum, I., & Abbasi, B. H. (2020). An overview of the applications of nanomaterials and nanodevices in the food industry. Foods, 9, 148.
Shahabadi, N., Zendehcheshm, S., & Khademi, F. (2021). Selenium nanoparticles: Synthesis, in-vitro cytotoxicity, antioxidant activity, and interaction studies with ct-DNA and HSA, HHb, and Cyt c serum proteins. Biotechnology Reports, 30, e00615.
Shahbaz, M., Akram, A., Raja, N. I., Mukhtar, T., Mehak, A., Fatima, N., et al. (2023). Antifungal activity of green synthesized selenium nanoparticles and their effect on physiological, biochemical, and antioxidant defense system of mango under mango malformation disease. PLoS One, 18, e0274679.
Shantkriti, S., Pradeep, M., Unish, K., Das, V., Nidhin, S., Gugan, K., et al. (2023). Biosynthesis of silver nanoparticles using Dunaliella salina and its antibacterial applications. Applied Surface Science Advances, 13, 100377.
Shar, A., Lakhan, M., Wang, J., Ahmed, M., Alali, K., Ahmed, R., et al. (2019). Facile synthesis and characterization of selenium nanoparticles by the hydrothermal approach. Digest Journal of Nanomaterials and Biostructures, 14, 867-872.
Sharma, A. (2017). Male infertility; Evidences, risk factors, causes, diagnosis, and management in human. Annals of Clinical and Laboratory Research, 5, 0-0.
Sharma, V. K., Yngard, R. A., & Lin, Y. (2009). Silver nanoparticles: Green synthesis and their antimicrobial activities. Advances in Colloid and Interface Science, 145, 83-96.
She, L., Xiong, L., Li, L., Zhang, J., Sun, J., Wu, H., et al. (2023). Ginsenoside Rk3 ameliorates Aβ-induced neurotoxicity in APP/PS1 model mice via AMPK signaling pathway. Biomedicine & Pharmacotherapy, 158, 114192.
Shehata, A. M., Salem, F. M., El-Saied, E. M., Abd El-Rahman, S. S., Mahmoud, M. Y., & Noshy, P. A. (2021). Zinc nanoparticles ameliorate the reproductive toxicity induced by silver nanoparticles in male rats. International Journal of Nanomedicine, 16, 2555.
Shiragannavar, V. D., Gowda, N. G. S., Puttahanumantharayappa, L. D., Karunakara, S. H., Bhat, S., Prasad, S. K., et al. (2023). The ameliorating effect of withaferin A on high-fat diet-induced non-alcoholic fatty liver disease by acting as an LXR/FXR dual receptor activator. Frontiers in Pharmacology, 14, 352.
Shnoudeh, A. J., Hamad, I., Abdo, R. W., Qadumii, L., Jaber, A. Y., Surchi, H. S., et al. (2019). Synthesis, characterization, and applications of metal nanoparticles. In Biomaterials and Bionanotechnology (pp. 527-612). Elsevier.

Singh, A., Dubey, S., & Dubey, H. K. (2019). Nanotechnology: The future engineering. Nanotechnology, 6, 230-3.

Singh, A., Gautam, P. K., Verma, A., Singh, V., Shivapriya, P. M., Shivalkar, S., et al. (2020). Green synthesis of metallic nanoparticles as effective alternatives to treat antibiotics resistant bacterial infections: A review. Biotechnology Reports, 25, e00427.

Singh, J., Dutta, T., Kim, K.-H., Rawat, M., Samddar, P., & Kumar, P. (2018). 'Green' synthesis of metals and their oxide nanoparticles: Applications for environmental remediation. Journal of Nanobiotechnology, 16, 1-24.

Singh, V., Yadav, P., & Mishra, V. (2020). Recent advances on classification, properties, synthesis, and characterization of nanomaterials. In Green Synthesis of Nanomaterials for Bioenergy Applications (pp. 83-97).

Song, Y., Wang, B., Qiu, D., Xie, Z., Dai, S., Li, C., et al. (2021). Melatonin enhances metallic oxide nanoparticle stress tolerance in rice via inducing tetrapyrrole biosynthesis and amino acid metabolism. Environmental Science: Nano, 8, 2310-2323.

Songisepp, E., Stsepetova, J., Rätsep, M., Kuus, L., Piir, A., Kilk, K., et al. (2022). Polyfunctional metabolic properties of the human strain Lactiplantibacillus plantarum Inducia (DSM 21379): Experimental and clinical approaches. Journal of Functional Foods, 92, 105064.

Sosa, I. O., Noguez, C., & Barrera, R. G. (2003). Optical properties of metal nanoparticles with arbitrary shapes. The Journal of Physical Chemistry B, 107, 6269-6275.

Stodt, M. F., Liu, C., Li, S., Maedler, L., Fritsching, U., & Kiefer, J. (2021). Phase-selective laser–induced breakdown spectroscopy in flame spray pyrolysis for iron oxide nanoparticle synthesis. Proceedings of the Combustion Institute, 38, 1711-1718.

Stoimenov, P. K., Klinger, R. L., Marchin, G. L., & Klabunde, K. J. (2002). Metal oxide nanoparticles as bactericidal agents. Langmuir, 18, 6679-6686.

Subhan, M. A., Choudhury, K. P., & Neogi, N. (2021). Advances with molecular nanomaterials in industrial manufacturing applications. Nanomanufacturing, 1, 75-97.

Sun, L., Yuan, G., Gao, L., Yang, J., Chhowalla, M., Gharahcheshmeh, M. H., et al. (2021). Chemical vapour deposition. Nature Reviews Methods Primers, 1, 1-20.

Sweeting, A., Wong, J., Murphy, H. R., & Ross, G. P. (2022). A clinical update on gestational diabetes mellitus. Endocrine Reviews.

Syed, F. Z. (2022). Type 1 Diabetes Mellitus. Annals of Internal Medicine, 175, ITC33-ITC48.

Szabó, D. V., & Schlabach, S. (2014). Microwave plasma synthesis of materials—From physics and chemistry to nanoparticles: A materials scientist's viewpoint. Inorganics, 2, 468-507.

Tahir, M. B., Sagir, M., & Asiri, A. M. (2021). Nanomaterials: Synthesis, characterization, hazards and safety. Elsevier.

Tariq, M., Mohammad, K. N., Ahmed, B., Siddiqui, M. A., & Lee, J. (2022). Biological synthesis of silver nanoparticles and prospects in plant disease management. Molecules, 27, 4754.

Taufiq Musa, M., Shaari, N., & Kamarudin, S. K. (2021). Carbon nanotube, graphene oxide and montmorillonite as conductive fillers in polymer electrolyte membrane for fuel cell: An overview. International Journal of Energy Research, 45, 1309-1346.

Tice, R. R., Agurell, E., Anderson, D., Burlinson, B., Hartmann, A., Kobayashi, H., et al. (2000). Single cell gel/comet assay: Guidelines for in vitro and in vivo genetic toxicology testing. Environmental and Molecular Mutagenesis, 35, 206-221.

Torabian, F., Akhavan Rezayat, A., Ghasemi Nour, M., Ghorbanzadeh, A., Najafi, S., Sahebkar, A., et al. (2022). Administration of silver nanoparticles in diabetes mellitus: a systematic review and meta-analysis on animal studies. Biological Trace Element Research, 200, 1699-1709.

Umar, H., Kavaz, D., & Rizaner, N. (2019). Biosynthesis of zinc oxide nanoparticles using Albizia lebbeck stem bark, and evaluation of its antimicrobial, antioxidant, and cytotoxic activities on human breast cancer cell lines. International Journal of Nanomedicine, 14, 87.

Urbankova, L., Skalickova, S., Pribilova, M., Ridoskova, A., Pelcova, P., Skladanka, J., et al. (2021). Effects of Sub-Lethal Doses of Selenium Nanoparticles on the Health Status of Rats. Toxics, 9, 28.

Urbankova, L., Skalickova, S., Pribilova, M., Ridoskova, A., Pelcova, P., Skladanka, J., et al. (2021). Effects of sub-lethal doses of selenium nanoparticles on the health status of rats. Toxics, 9, 28.

Vahdati, M., & Tohidi Moghadam, T. (2020). Synthesis and characterization of selenium nanoparticles-lysozyme nanohybrid system with synergistic antibacterial properties. Scientific Reports, 10, 1-10.

Vickers, N. J. (2017). Animal communication: When I'm calling you, will you answer too? Current Biology, 27, R713-R715.

Vijayakumar, M., Surendhar, G., Natrayan, L., Patil, P. P., Ram, P., & Paramasivam, P. (2022). Evolution and recent scenario of nanotechnology in agriculture and food industries. Journal of Nanomaterials, 2022, 1-15.

Von White, G., Kerscher, P., Brown, R. M., Morella, J. D., McAllister, W., Dean, D., et al. (2012). Green synthesis of robust, biocompatible silver nanoparticles using garlic extract. Journal of Nanomaterials, 2012, 1-10.

Wahab, M., Bhatti, A., & John, P. (2022). Evaluation of Antidiabetic Activity of Biogenic Silver Nanoparticles Using Thymus serpyllum on Streptozotocin-Induced Diabetic BALB/c Mice. Polymers, 14, 3138.

Walsh, K. D., & Kato, T. A. (2022). Alkaline comet assay to detect DNA damage. In Chromosome Analysis: Methods and Protocols (pp. 65-72). Springer.

Wang, Y., Lin, M., Gao, X., Pedram, P., Du, J., Vikram, C., et al. (2017). High dietary selenium intake is associated with less insulin resistance in the Newfoundland population. PloS One, 12, e0174149.

Włodarczyk, R., & Kwarciak-Kozłowska, A. (2021). Nanoparticles from the cosmetics and medical industries in legal and environmental aspects. Sustainability, 13, 5805.

World Health Organization. (2021). WHO laboratory manual for the examination and processing of human semen.

Xue, W.-L., Li, X.-S., Zhang, J., Liu, Y.-H., Wang, Z.-L., & Zhang, R.-J. (2007). Effect of Trigonella foenum-graecum (fenugreek) extract on blood glucose, blood lipid, and hemorheological properties in streptozotocin-induced diabetic rats. Asia Pacific Journal of Clinical Nutrition, 16, 422-426.

Yadav, T. P., Yadav, R. M., & Singh, D. P. (2012). Mechanical milling: A top-down approach for the synthesis of nanomaterials and nanocomposites. Nanoscience and Nanotechnology, 2, 22-48.

Zhang, J., Zhu, X., Xu, W., Hu, J., Shen, Q., & Zhu, D. (2023). Exposure to acrylamide inhibits testosterone production in mice testes and Leydig cells by activating ERK1/2 phosphorylation. Food and Chemical Toxicology, 172, 113576.

Zhu, C., Li, L., Liu, Q., Li, J., Peng, G., Zhang, L., et al. (2023). Effect of selenium nanoparticles (SeNPs) supplementation on the sperm quality of fish after short-term storage. Aquaculture, 562, 738876.